Studies on the structural stability of tropomyosins from fish and marine invertebrates

(魚介類トロポミオシンの構造安定性に関する研究)

Hideo Ozawa

小澤　秀夫

Laboratory of Marine Biochemistry

The Graduate School of Agricultural and Life Sciences

The University of Tokyo

January, 2012

CONTENTS

Page

Acknowledgements

I would like to extend my sincere appreciation and gratitude to my graduate supervisor, Professor Shugo Watabe, The University of Tokyo. Thanks are also due to my co-supervisor Professor Yoshihiro Ochiai, Tokai University for his continual guidance, support throughout this project.

Thanks are also due to the other members of my thesis committee, Professor Shigeki Matsunaga, Professor Shuichi Asakawa, and Associate Professor Hideki Ushio. Their insistence on keeping the big picture visible, making the experimental framework of the results clear, and being precise in drawing conclusions, helped to make the thesis as it is.

I am grateful to the Japan Society for the Promotion of Science to award me Research Fellowships for young scientists (DC2). I would like to express my sincere thanks to the members in Laboratory of Marine Biochemistry and Laboratory of Aquatic Molecular Biology and Biotechnology.

Abstract

The amino acid sequences of tropomyosins (TMs) have been determined for many species: Atlantic salmon *Salmo salar* (Heeley et al., 1995), bluefin tuna *Tunnus tuna* (Huang et al., 2004; Ochiai et al., 2010), kuruma prawn *Marsupenaeus japonicas* (Motoyama et al., 2007), mussel *Mytilus edulis galloprovincialis* (Iwasaki et al., 1997), rabbit *Oryctolagus cuniculus* (Stone and Smillie, 1978; Mak et al., 1979), tokobushi abalone *Haliotis diversicolor* (Chu et al., 2000), torafugu *Takifugu rubripes* (Ikeda et al., 2003), white croaker *Pennahia argentata* (Ochiai et al., 2001), walleye pollack *Theragra chalcogramma* (Ochiai et al., 2003), Yesso scallop *Mizuhopecten yessoensis* (Hasegawa, 2001), and zebrafish *Danio rerio* (Ohara et al., 1989). Invertebrate TMs are known as allergens and show higher viscosity than fish TMs, but the basic characteristics, in view of the comparative biochemistry, have not been studied so much. Elucidation of the relationship between amino acid sequence and stability would contribute to ascertain above interesting invertebrate TM properties. But the stability of invertebrate TM has been rarely measured (Inoue et al., 2004).

The stability of TMs from fish (Huang and Ochiai, 2005) was estimated by differential scanning calorimetry (DSC) and it has been shown that fish TM, as rabbit TM (Potekhin and Privalov 1982), contains a few unfolding units. Thus, it would be adequate to measure the thermal stability of peptides or fragments.

In Chapter 1, the stability of invertebrate TMs was investigated. TMs from the tail muscle of kuruma prawn, mantle muscle of Japanese common squid *Todarodes pacificus*, foot muscle of tokobushi abalone, and striated and smooth adductor muscles of Yesso scallop were purified and these stabilities were determined by circular

dichroism (CD) spectrometry and DSC. The white croaker TM was used as control. In addition, three mRNAs encoding the smooth muscle TMs of the scallop have been sequenced (Hasegawa, 2001) and the major component was determined at the protein level. CD spectrometry and DSC have suggested that the thermal stability is in the order of prawn TM > abalone TM > squid TM ≒ white croaker TM > scallop smooth muscle TM > scallop striated muscle TM. The stability difference between scallop TMs and other TMs reflected the habitat temperature, but the stability difference between scallop striated and smooth muscle TMs could come from other physiological demands. The striated muscle expedites jet water propulsion for quick locomotion, while the smooth muscle can keep the shell closed by maintaining large tension with little energy expenditure for a long time (so-called catch condition). Therefore, the protein components are considered to have different profiles between the two muscles.

In Chapter 2, five synthetic peptides of 30mer were designed, based on the sequence of walleye pollack fast muscle TM: Peptide Nterm (Met1-Lys30) which consisted of N-terminal region, Peptide Var (Asp84-Leu113) which consisted of the variable region, Peptide Mid (Val128-Ala157) which consisted of the middle region of TM, Peptide Cys (Leu176-Lys205) which contained the conserved Cys190 residue, and Peptide Cterm (Asp255-Ile284) which consisted of C-terminal region. The thermal stabilities of these peptides were determined by CD spectrometry in the presence and absence of 40% 2, 2, 2-trifluoroethanol (TFE). In 40% TFE, the helical contents of these peptides were decreased, as temperature rose, though they showed no clear melting temperature, suggesting that the enthalpy necessary for transition from the highly α-helical conformation to the highly random coil containing conformation of each peptide was low. The calculation by AGADIR, α-helical content prediction software for the

monomeric peptides, showed good accordance with the measured α-helical contents of all peptides in the absence of TFE, except for Peptide Cterm. In addition, the α-helical contents did not show concentration dependence in 40% TFE. Thus, all peptides, except for Peptide Cterm, would not have coiled-coil interaction under these experimental conditions. These results suggested that the stability was in the order of Peptide Cterm > Peptide Var > Peptide Nterm ≒ Peptide Mid ≒ Peptide Cys. The higher stability of Peptide Cterm could be important for the head-to-tail interaction between N and C terminal regions.

In Chapter 3, white croaker TM was cleaved by 2-nitro-5-thiocyanatobenzoic acid (NTCB). At the 190th residue, fish TM has only one conserved cysteine residue, where NTCB cleaves the peptide bond. Fragments produced by NTCB were purified and measured by CD spectrometry. From CD data, C-terminal fragment (Cys190-Ile284) showed higher stability than N-terminal fragment (Met1-Lys189), regardless of its shorter length. It has been reported that the rabbit TM C-terminal fragment shows lower stability than the N-terminal fragment and low stability of the C-terminal fragment is discussed with the interaction with troponin. Thus, the present study suggests that such idea should be reconsidered.

In Chapter 4, molecular dynamics simulations for the rabbit and white croaker TM C-terminal fragments were performed by Amber10. These fragments (rabbit/white croaker) contain four amino acid substitutions (Ala/Ser191, Ser/Thr229, Thr/Ala247, and Ser/Thr252). The study in this chapter indicates that the substitution at the 229th residue stabilizes rabbit TM fragment, while the substitutions at the 247th and/or 252nd residue stabilize the white croaker TM fragment.

In Chapter 5, general discussion was performed, based on the results of the present study to make clear what was established for invertebrate and vertebrate TMs so far and to scope further investigations.

Parts of works described in this thesis have been or is published in the following journals.

1. Ozawa, H., Watabe S., Ochiai, Y., 2009. Thermal stability of the synthetic peptides with the sequence of fish fast skeletal muscle tropomyosin. Fish. Sci. 75, 1029-1037.

2. Ozawa H, Watabe S, Ochiai Y., 2010. Thermostability of striated and smooth adductor muscle tropomyosins from Yesso scallop *Mizuhopecten yessoensis*. J. Biochem. 147, 823-832.

3. Ozawa H, Watabe S, Ochiai Y., 2011. Thermodynamic characterization of muscle tropomyosins from marine invertebrates. Comp. Biochem. Physiol. B. 160, 64-71.

List of Notations

ΔC : Heat capacity

ε_n : Decrement of the α-helical fraction of the “n”th unfolding

ΔH : Enthalpy of unfolding

ΔH_n : Enthalpy of the “n”th unfolding

ΔH_{total} : The sum of unfolding enthalpy

ΔG_{app} : Apparent Gibbs free energy of unfolding

ΔG_{total} : The sum of Gibbs free energy of unfolding

$\Delta G_{([urea])}$: Gibbs free energy of unfolding in the presence of urea

$\Delta G_{([wat])}$: Gibbs free energy of unfolding in the absence of urea

ΔS : Entropy of unfolding

ΔS_n : Entropy of the “n”th unfolding

T_{Mapp} : Apparent midpoint temperature of unfolding

T_{Mn} : Midpoint temperature of the “n”th unfolding

List of Abbreviations

AEX : Anion exchange chromatography

BCA : Bicinchoninic acid

CBB : Coomassie brilliant blue

CD : Circular dichroism

CNBr : Cyanogen bromide

CV : Column volume(s)

DDA : Deviation of dihedral angle

DSC : Differential scanning calorimetry

DTT : Dithiothreitol

FDA : Fluctuation of dihedral angle

HBA : Helical bending angle

HD : Interhelical distance

HIC : Hydrophobic interaction chromatography

IgE : Immunoglobulin E

LBA : Local bending angle

LSA : Local staggering angle

LSD : Local staggering distance

MD : Molecular dynamics

NMR : Nuclear magnetic resonance

NTCB : 2-Nitro-5-thiocyanatobenzoic acid

PAGE : Polyacrylamide gel electrophoresis

RMSF : Root mean square fluctuation

RMSD : Root mean square deviation

SDS : Sodium dodecyl sulfate

TFE : 2, 2, 2-Trifluoroethanol

TM : Tropomyosin

Tn : Troponin

TnC : Troponin C

TnI : Troponin I

TnT : Troponin T

Tris : Tris(hydroxymethyl)aminomethane

General Introduction

Background

Tropomyosin (TM) was isolated from rabbit skeletal muscle for the first time (Bailey, 1946; 1948). Skeletal muscle TM consists of two parallel α-helical polypeptide chains of 284 residues (Crick, 1953; Fraser et al., 1965). TM plays a regulatory role in the contractile activities together with actin, troponin (Tn) and myosin (McKillop and Geeves, 1993; Maytum et al., 1999). Skeletal muscle TM is involved in the regulation of muscle contraction, interacting with one Tn complex and with seven actin molecules (Bailey, 1948; Perry, 2001; Robinson et al., 2007). TM polymerizes by head-to-tail interaction (Ooi et al., 1962; Sousa and Farah, 2002) through 9 amino acids of both termini, and the structures of the N- and C-termini are highly conserved (Coulton et al., 2008).

TM is widely distributed to all cell types, stabilizing actin filaments and modulating filament function (Perry, 2001; Grenklo et al., 2008). In rabbit, striated and smooth muscle α-TMs differ as a consequence of alternative splicing of exons 2 and 9 encoding amino acid residues 39-80 and 258-284, respectively, and the relationship between these spliced exons and function are studied (Cho and Hitchcock-DeGregori, 1991). In non-muscle cells, the precise role and structural dynamics of TM on actin are poorly understood (Lehman et al., 2000).

Thin filament proteins

Thin filaments consist of a double-helical arrangement of actin monomers together with the regulatory proteins, TM and Tn (Gordon et al., 2000; Perry, 2001). The atomic model of actin-TM shows strong electrostatic interactions between charged side-chains of TM residues and actin residues in the subdomains 3 and 4 (Lorenz et al., 1995). Tn is composed of TnI, TnC, TnT (Greaser and Gergely, 1971 and 1973). TnI and TnC have globular domains, while TnT has a rod-like domain (Flicker et al., 1982). The globular domain of Tn binds to TM near the residues 150-180. Rod-like domain of TnT binds to TM; 71-151 residues of TnT to 258-284 residues of TM (Hammell and Hitchcock-DeGregori, 1996) and the second half of period 4 of TM (152-165 residue) was shown to be a key region for inducing conformational changes of regulated thin filament required for its fully activated state (Sakuma et al., 2006).

Regulation of muscle contraction

The actomyosin complex rapidly dissociates, by binding of ATP to the ATPase site on the myosin crossbridge. Myosin then hydrolyzes ATP and forms ADP·Pi complex. Then myosin reattaches to a neighboring actin. Binding to actin causes a crossbridge to change its shape so as to move the actin approximately by 10 nm and release of the phosphate and then the ADP. This allows a new ATP molecule to bind to the myosin (Lymn and Taylor, 1971; Geeves and Holmes, 2005; Fig. 0-1).

The naked actin filament is unregulated and myosin crossbridges have full access to their binding sites on each actin monomer. In the presence of the TM and Tn Complex, three-state model of the thin filament has been proposed; a "blocked state" which is unable to bind S1, a "closed state" which can only bind S1 relatively weakly, and an

"open state" in which S1 can both bind and undergo an isomerization to a more strongly bound rigor-like conformation (McKillop and Geeves, 1993; Lehrer and Geeves, 1998; Poole et al., 2006; Fig. 0-2). TM moved on actin filament by Ca^{2+} changes: in the presence of Ca^{2+}, TM moved 25° away from its low Ca^{2+} position, exposing most of the myosin-binding sites and saturation of filaments with myosin heads produced a further 10° shift in TM position, thereby exposing the entire myosin-binding site (Vibert et al., 1997). Actually, TM oscillates dynamically between these positions on actin at all Ca^{2+} levels, and the concentration of Ca^{2+} controls equilibrium (Pirani et al., 2005). It has been suggested that end-to-end interactions of adjacent TM molecules are strengthened by the phosphorylation at Ser283, and that the phosphorylation is thus essential for long range cooperative activation along the thin filament (Rao et al., 2009).

Heptad repeat and coiled-coil

α-Helical coiled-coil structure is formed by the packing of two α-helices against one another (Crick, 1953). In this structure, characteristic heptad repeats formed by seven amino acids are found. The positions of each amino acid consisting one unit are labeled a*bcdefg*. The *a* and *d* positions are frequently occupied by hydrophobic amino acids and the *e* and *g* positions are with ionic amino acids, while other positions are with hydrophilic amino acids. It is likely that the relationship between residues at the *a*, *d*, *e*, and *g* positions are responsible for the stability of coiled-coil structure (Dong and Hartgerink, 2006). In the *a* and *d* positions, more than three consecutive stabilizing residues (leucine, methionine, isoleucine, valine, phenylalanine and tyrosine) would stabilize the coiled-coil (Lu and Hodges, 2004).

Alanine cluster and acidic core

In rabbit fast skeletal muscle TM, the six alanine clusters and two acidic cores have been identified as regions that may destabilize the structure (Brown et al., 2001, 2005; Minakata et al., 2008; Fig. 0-3). The alanine cluster, where a few alanine or small amino acids are consecutive at the *a* and *d* positions, is associated with decreased spacing together with an axial stagger between the two α-helices, whereas the two α-helices are displaced in the coiled-coil axis. It is hypothesized that alanine cluster would allow TM to bend at either end of the cluster so that TM could wrap around the actin filament. The acidic core, where one acidic amino acid positioned at the *a* or *d* position, destabilizes the structure because of the electric repulsion and exposure of the core region to the solvent.

TM fragment structure

The crystal structures of full length TM have been determined (Phillips et al., 1980 and 1986; Whitby and Phillips, 2000), but the resolution was not high enough. Thus, large and short TM fragments fused to yeast GCN4 transcription factor, which forms stable coiled-coil, have been used for the structure determination. Brown et al. (2001, 2005) have determined the crystal structure of deacetylated TM fragment (residues 1-81) and the crystal structure of mid region of TM (residues 89-208). The crystal structures of the C-terminal region of TM (residues 176-284, 176-273) have determined the structure of the mid region of TM (residues 176-273) (Nitanai et al., 2007; Minakata et al., 2008). From these structures, they have observed two types of bends have been observed: bends by the alanine cluster, where alanine or small residues are consecutive in the core region, and the bends around gaps in the core by isolated alanine, and the

bends around the acidic core, where aspartic acid or glutamic acid positions at the core region (Brown et al., 2001 and 2005; Minakata et al., 2008). Cys at the 190th residue is conserved for the vertebrate TMs. Although Cys is considered to be reduced *in vivo* because of the reduced atmosphere in the cell, the disulfide bond was formed in the crystal structure (Brown et al., 2005)

The structures of short TM fragments have been also determined. Greenfield et al. (1998) have determined the structure of acetylated N-terminal fragment TM (residues 1-14 of striated rabbit α-TM) by nuclear magnetic resonance (NMR). Li et al. (2002) have determined the crystal structure of the C-terminal 31 residues of rat striated muscle α-TM. They have found that the structure consists of two distinct domains: the N-terminal region of this fragment between the 254th and the 262nd residues showed a canonical two-stranded coiled-coil, whereas the C-terminal region between the 263rd and 284th residues consisted of α-helices (22 residues in length) that were separated from each other and are stabilized by crystal packing forces. The pairs of Gln263 and Tyr267 side chains did not display the usual symmetric knobs-into-holes packing pattern. Greenfield et al. (2003) have determined the structure of the 34 C-terminal residues of striated muscle α-TM. They have reported that the region between the 253rd and 269th residues forms a canonical coiled-coil and the region between the 270th and the 279th forms of parallel, linear helices, novel for TM, although the last five residues are nonhelical and flexible. From these studies, it has been suggested that two hydrophilic amino acids (Gln263 and Tyr267 at the *a* and *d* position of heptad repeat) perturbed the canonical coiled-coil, but not the α-helix. Greenfield et al. (2006) have determined the structure of the head-to-tail overlap region by NMR, and found the C-terminal coiled-coil spread apart to allow insertion of 11 residues of the N-terminal

coiled-coil into the resulting cleft, and claimed that the head-to-tail junction formed between TM molecules is flexible. Murakami et al. (2008) have determined the 2.9 Å resolution structure of crystals containing TM-N (1-24) and TM-C (254-284) together with a fragment of Tn-T (58-112). In this structure, 4-helix bundle, containing two TM-C chains and one chain each of TM-N and TnT was observed, and this could explain why the skeletal- and cardiac-muscle specific C-terminal region is required to bind TnT and why TM homodimer binds only single TnT.

N-terminal acetylation and head-to-tail interaction

It has been reported that N-terminal acetylation is essential for high viscosity, head-to-tail interaction and binding ability to actin of rabbit TM (Greenfield et al., 1994; Kluwe et al., 1995). In addition, the stronger head-to-tail interaction could result in lower flexibility on the actin filament and larger cooperativity in actomyosin ATPase (Chandy et al., 1999). The N-terminal acetylation is also essential for fish and scallop recombinant TMs (Jackman et al., 1996; Inoue et al., 2004). The additions of a few amino acids to the N-terminus of the recombinant TM resulted in the restoration of head-to-tail interaction of TM (Monterio et al., 1994; Coulton et al., 2006). The viscosity of invertebrate TM is higher than that of vertebrate TM. To the high viscosity of invertebrate TMs, the head-to-tail interaction should be mainly contributed, because the invertebrate TM with unacetylated N-terminus lost the viscosity (Inoue et al., 2004).

As nine residues at both of the N-terminus and C-terminus are generally regarded to form a head-to-tail interaction region, the residues at the N-terminus of molluscan and crustacean TMs show high sequence homology to vertebrate muscle TMs. However, those at the C-terminus show lower sequence homology than those of vertebrate TMs.

Therefore, the high viscosity of invertebrate TMs may be caused mainly by the amino acid substitutions in the C-terminal region.

Allergy by invertebrate TMs

TMs from invertebrate species are known as allergens (Leung et al., 1994; Miyazawa et al., 1996), while TMs from vertebrate species are considered non-allergenic. The reason why only invertebrate TMs are allergenic is not known, though Mikita and Padlan (2007) proposed that the larger invertebrate TM fragments, digested by Pepsin A, enter the blood stream, where the fragments can reconstruct a three dimensional structure whose stability approaches that of the intact molecule, and they elicit a specific antibody response. Immunoglobulin E (IgE)-binding epitopes of invertebrate TMs have been identified for some invertebrate TMs and are sometimes common to each other. Pacific oyster *Crassostrea gigas* allergens contain an IgE-binding epitope in the 92nd-105th residues (Ishikawa et al., 1998a), the turban shell *Turbo cornutus* allergen in the 256th-284th residues (Ishikawa et al., 1998b). In addition, Ishikawa et al. (1999) have showed that Yesso scallop and whelk *Neptunea arthritica* TM have the same epitope as Pacific oyster, but not with short-neck clam *Tapes japonica* and turban shell.

By the 46 synthetic peptides (15mer), the epitopes of brown shrimp *Penaeus aztecus* TM have been determined; the 43rd-55th, 88th-101st, 137th-141st, 144th-151st, 187th-197th, 249th-259th, 266th-273rd and 273rd-281st residues (Ayuso et al., 2002a; Ayuso et al., 2002b; Motoyama et al., 2007). The cross-reactivity among peptides from brown shrimp, American lobster *Homarus americanus*, American cockroach *Periplaneta americana*, and house dust *Dermatophagoides pteronyssinus* was evaluated

by using sera of shrimp-allergic subjects (Ayuso et al., 2002b). In addition, cross-reactivity between shrimp and molluscan exists, though these two groups belong to different phyla (Lehrer and McCants, 1987; Leung et al., 1996; Goetz et al., 2000). Cross-reactivity between different allergens occurs because of the similar or identical IgE-binding epitopes. The TM sequences of crustaceans showed high homology, which would lead to the cross-reactivity among crustacean TMs (Motoyama et al., 2007).

Chapter 1

Purification and thermostability of marine invertebrate tropomyosins

Invertebrate TMs have been intensively studied because they are the major allergens. However, their thermal stabilities have been rarely studied. Heterogeneity and tissue specificity of TM isoforms obtained from four species of bivalves, including ark shell *Scapharca broughtonii*, mussel *Mytilus galloprovincialis*, surf clam *Atrina pectinata* and Pacific oyster, were examined, and the mussel had only one TM and others had two isoforms (Fujinoki et al., 2006).

Yesso scallop *Mizuhopecten yessoensis* adductor muscle can be divided into three parts: the striated muscle, the translucent portion of smooth muscle, and opaque portion of smooth muscle. The striated muscle consists most of adductor muscle. The smooth muscle shows crescent form. The translucent portion positions inner edge, having contact with striated muscle, and the opaque potion positions outer edge. It was reported that each of striated muscle and the translucent portion (inner part) in the smooth muscle has only one TM species, though the opaque portion (outer part) in the smooth muscle has two TM species (Takahashi and Morita, 1986; Ishimoda-Takagi and Kobayashi, 1987; Ishimoda-Takagi et al., 1986). The sequence of TM from scallop striated muscle has been determined (accession number AB004636). Hasegawa (2001) have reported three cDNA sequences of Yesso scallop smooth muscle TM; e.g., sm TM-1, sm TM-2, and sm TM-3. Sm TM-1 is identical to the striated muscle TM. The deduced amino acid sequence of sm TM-1 is identical to those of sm TM-2 and sm

TM-3 in the range of the 1st–125th and 214th–284th residues (Fig. 1-1). In addition, the viscosity and solubility against ammonium sulfate solution was studied (Watabe and Hashimoto, 1980).

In the present chapter, TMs were purified from the tail muscle of kuruma prawn *Marsupenaeus japonicus*, mantle muscle of Japanese common squid *Todarodes pacificus*, foot muscle of tokobushi abalone *Haliotis diversicolor*, and striated muscle of Yesso scallop. In addition, their thermostability was evaluated by circular dichroism (CD) spectrometry and differential scanning calorimetry (DSC) measurement (Yang et al., 1986; Privalov et al., 1995). Then, major component of TMs in the scallop smooth muscle TM was identified.

Section 1

Purification of tropomyosin

Purifications of TMs have been performed for many invertebrate species. Some invertebrate muscles contain a few TM isoforms (Hasegawa, 2001; Fujinoki et al., 2006), although the determination of expressed TM(s) amino acid sequence was rarely performed.

In this section, purifications of TMs from the prawn, squid, abalone and scallop were carried out. In addition, discrimination of the scallop smooth adductor muscle TM was also performed.

Materials and Methods

Materials

Live specimens of the prawn, squid, abalone, and scallop were purchased at the Tokyo Central Wholesale Market.

Preparation of acetone powder

Tail muscle of the prawn, mantle muscle of the squid, foot muscle of the abalone, and striated and smooth adductor muscles of the scallop were minced. Then, they were washed with 10 volumes of ice-cold 50 mM KCl, 2 mM $NaHCO_3$ and left for 30 min. Ten volumes of water was added to the sediment, and left for 30 min. This procedure

was repeated once more. The precipitate was centrifuged at 4°C and 600×g for 5 min, and was washed with 10 volumes of acetone. Immediately, it was filtered through gauze, added with 10 volumes of acetone and left for 30 min. The sediment was further soaked in 10 volumes of acetone, left for 30 min, and filtrated through gauze.

Isolation of the prawn TM

The acetone dried powder of the prawn was extracted with 10 volumes (v/w) of 20 mM Tris-HCl (pH 7.5) containing 1 M KCl and 5 mM 2-mercaptoethanol overnight at 4°C. The mixture was centrifuged at 4°C and 10,000×g for 10 min. The supernatant was subjected to isoelectric precipitation at pH 4.5 with 1 N HCl. The pellet after centrifugation at 4°C and 10,000×g for 10 min was collected and dissolved in water. With 1 N NaOH, pH was adjusted to 7.6. Saturated ammonium sulfate solution was slowly added to the crude extract to 40% saturation under stirring, and the mixture was left for several hours. After centrifugation, the supernatant was applied to hydrophobic interaction chromatography (HIC).

HIC using a TSKgel BioAssist Phenyl column (0.78 × 5 cm) was carried out at a flow rate of 1 ml/min. The column was washed with 5 column volumes (CV) of 1.56 M (40% saturation) ammonium sulfate, containing 20 mM potassium phosphate buffer (pH 7.0). Protein was eluted by linearly decreasing the concentration of ammonium sulfate from 1.56 M to 0 M over 20 CV.

The fractions, containing TM as the major component, were dialyzed against 10 mM potassium phosphate buffer (pH 7.0) in the presence of 1 mM dithiothreitol (DTT). Anion exchange chromatography (AEX) using a Mono Q^{TM} 5/50 GL column (0.5 × 5 cm) was carried out at a flow rate of 0.5 ml/min. The column was washed with 10 CV

of the above buffer. The proteins were eluted by a linear gradient from 10 mM to 500 mM potassium phosphate buffer (pH 7.0) in the presence of 1 mM DTT over 20 CV.

Isolation of the squid TM

TM was extracted from the squid, and then KCl concentration of the extract was decreased to 0.1 M in order to precipitate contaminating paramyosin and centrifuged. Isoelectric precipitation was carried out. In ammonium sulfate fractionation, TM was obtained at 50-70% saturation. AEX was carried out as the prawn TM at a flow rate of 1 ml/min and eluted by a linear gradient from 150 mM to 490 mM KCl. Saturated ammonium sulfate solution (pH 7.0) was added to the fractions to 45% saturation (1.76 M) for the subsequent chromatography. HIC was carried out as in the case of the prawn TM, and proteins were eluted by linearly decreasing the concentration of ammonium sulfate from 1.76 M to 0 M for 20 CV.

Isolation of the abalone TM

Extraction and isoelectric precipitation were carried out. To optimize ammonium sulfate fractionation, the supernatant at pH 7.6 (0.4 ml) was dispensed to 1.5 ml tubes then added with distilled water and saturated ammonium sulfate (pH 7.0) to 1 ml. The tubes were put on ice for 1 hour and centrifuged at 4°C and 17,000×g for 10 min. The supernatants and the pellets were used for SDS-PAGE. Ammonium sulfate fractionation was carried out, and TM was obtained in 35-45% saturation fraction. Isoelectric precipitation and ammonium sulfate fractionation were repeated twice. AEX was carried out as the squid TM.

Isolation of the scallop striated adductor muscle TM

Extraction and isoelectric precipitation was carried out. Optimization of ammonium sulfate fluctuation was performed as the case of the abalone TM. Ammonium sulfate fractionation was carried out, and TM was obtained in 40-45% saturation fraction. AEX was carried out as in the case of the prawn TM, eluted by a linear gradient from 200 mM to 520 mM KCl, and washed with 1 M KCl.

Isolation of the scallop smooth adductor muscle TM

Extraction, dilution precipitation and isoelectric precipitation were carried out. Ammonium sulfate fractionation was carried out, and TM was obtained in 35-50% saturation fraction. HIC was carried out as in the case of the prawn TM. Protein was eluted by linearly decreasing the concentration of ammonium sulfate from 1.56 M to 0 M for 20 CV.

Discrimination of the scallop smooth adductor muscle TM

Smooth muscle TM was fragmented by endoproteinase Arg-C, which was purchased from Roche (Nonnenwald, Penzberg, Germany). TM, at a concentration of 2 mg/ml, was dissolved in 8.5 mM $CaCl_2$, 5 mM DTT, 0.5 mM EDTA, and 90 mM Tris(hydroxymethyl)aminomethane (Tris)-HCl (pH 7.6) with 5 μg/ml endoproteinase Arg-C and digested at 30°C. Digestion time was up to 1.5 hour. Digestion was stopped by addition of Tricine sodium dodecyl sulfate (SDS)-glycerol buffer and heated at 95°C

for 5 min. After the run, blotting to a polyvinylidene difluoride membrane was performed.

Three smooth muscle TMs (sm TM-1, sm TM-2, and sm TM-3) have methionine residue at the 1st, 8th, 11th and 25th positions, but only sm TM-2 has methionine residue at the 204th position. In order to confirm the isoform composition, smooth muscle TM was fragmented by cyanogen bromide (CNBr), which cleaves the peptide bond at N-terminus of methionine residue, as follows. TM was dissolved in 7 M urea and 0.1 M HCl at a concentration of 1 mg/ml (31 μM). CNBr (4.7 M in acetonitrile) was added at 500-fold molar excess over the TM, and the mixture was left in the dark at room temperature for 16 hours. White croaker TM was used as control.

Electrophoresis

SDS-polyacrylamide gel electrophoresis (SDS-PAGE) was performed according to Laemmli (1970), using 15% polyacrylamide slab gels. After the run, gels were stained with 0.05% Coomassie brilliant blue (CBB) R-250 (Wako) in methanol/acetic acid/water (5:1:4 v/v), and destained in methanol/acetic acid/water (25:7:68 v/v). Protein molecular weight markers were purchased from Sigma Chemicals (SDS-7, St. Louis, MO, USA)

The digested scallop smooth muscle TM was analyzed for purity by Tricine-SDS-PAGE (Schägger and Jagow, 1987). The samples were dissolved in 50 mM Tris-HCl (pH 6.8) containing 4% SDS, 1% 2-mercaptoethanol, 12% glycerol, and 0.01% bromophenol blue, and incubated at 40°C for 30 min. The stacking gel was 4% polyacrylamide gel containing 0.744 M Tris-HCl (pH 8.45) and 0.0744% SDS. The spacer gel (1.4 cm high) was 10% polyacrylamide gel containing 0.1 M Tris-HCl (pH

8.45) and 0.1% SDS. The separating gel (4.2 cm high) was 16% polyacrylamide gel containing 0.1 M Tris-HCl (pH 8.45), 0.1% SDS and 13.3% glycerol. The anodal buffer was 0.2 M Tris-HCl (pH 8.9) and the cathodic buffer was 0.1 M Tris, 0.1 M Tricine (pH 8.25) and 0.1% SDS. The electrophoresis was performed at 30 V for 1 hour until the sample completely entered the spacer gel, and then at 100 V for 3 hours. The protein bands were fixed in a solution containing 40% methanol and 10% acetic acid for 30 min, and then were stained with 0.025% CBB G 250 in 40% methanol and 10% acetic acid for 1 hour. The gel was destained in 10% acetic acid for 2 hours.

Protein concentration determination

Protein concentration was determined by bicinchoninic acid (BCA) method (Smith et al., 1985; Wiechelman et al., 1988) using bovine serum albumin as the standard.

Results

Preparation of acetone powder

From 113.1 g of the prawn tail muscle, 149.6 g of Japanese common squid mantle muscle, 126.9 g of the abalone foot muscle, 173.5 g of the scallop striated adductor muscle, and 24.4 g of the scallop smooth adductor muscle, 15.4 g, 7.3 g, 12.4 g, 18.8 g, and 3.4 g of acetone powder were obtained, respectively.

Isolation of TM

The prawn TM was prepared (Fig. 1-2) and purified by HIC and AEX (Fig. 1-3). The squid TM was prepared (Fig. 1-4) and purified by AEX and HIC (Fig. 1-5). TM of the abalone was prepared (Fig. 1-6) and purified by AEX (Fig. 1-7). The scallop striated muscle TM was prepared (Fig. 1-8) and purified by AEX (Fig. 1-9). The scallop smooth muscle TM was prepared and purified by HIC (Fig. 1-10). From 5 g of the prawn acetone powder, only 1.5 mg of TM was obtained. TM was lost at ammonium sulfate fractionation and AEX (Figs. 1-2 and 1-3).

In the ammonium sulfate precipitation, the prawn TM partially precipitated at 40 % saturation of ammonium sulfate unexpectedly (Fig. 1-2). It may be caused by low pH value of ammonium sulfate saturation solution. Thus, at the purification of other TMs, the pH of ammonium sulfate saturated solution was adjusted by ammonium. In AEX, the prawn TM was unexpectedly absorbed in column and not eluted by potassium phosphate gradient (Fig. 1-3). Thus, in AEXs of the other TMs, KCl gradient was adopted (Figs. 1-5, 1-6, and 1-9).

Discrimination of the scallop smooth adductor muscle TM

Smooth muscle TM was digested by endoproteinase Arg-C. Then, the fragments were separated by Tris-Tricine PAGE and blotted to PVDF membrane. The N-terminal amino acid sequences were determined by the Edman method. The sequences obtained were SLADDERIDA, which corresponded to the 134th-143rd residues of sm TM-2 and sm TM-3, and LEAADAKVHELEEEL, which corresponded to the 183rd-197th residues of sm TM-3. These results indicated that the mainly translated TM was sm TM-3 (Figs. 1-1 and 1-11).

In addition, smooth muscle TM was then cleaved by CNBr to verify the isoform composition. The cleavage position did not exist at the middle of the molecule (20 and 10 kDa fragments), but seemed to exist only in the N-terminal region (Figs. 1-1 and 1-11). White croaker TM was used as a positive control of this reaction. This TM has seven methionine residues at the 1st, 8th, 10th, 127th, 135th, 141st, and 281st positions. In the case of white croaker TM CNBr degradation, many small fragments of expected molecular sizes were observed, indicating the fragmentation was successful. Only one TM isoform (sm TM-2) contains methionine residue at the 204th position and is expected to produce the 20 kDa and 10 kDa fragments by CNBr degradation. However, no such fragment was obtained. This result supported the view that the mainly translated TM molecule in the smooth muscle is sm TM-3.

Section 2

Circular dichroism spectrometry, differential scanning calorimetry, and bioinformatics

As already well known, α-helical content was obtained by CD spectrometry (Yang et al., 1986) and enthalpy was calculated from temperature dependency of α-helical content (Greenfield and Hitchcock-DeGregori, 1995). Enthalpy required to unfolding was directly measured by DSC (Privalov et al., 1995). By these methods, thermostabilities of fish skeletal muscle TMs have been measured (Huang and Ochiai, 2005).

In this section, thermostability was measured for TMs from the prawn, squid, abalone and scallop by CD spectrometry and DSC. In addition, the amino acid substitutions, which would contribute to the stability difference, were estimated by secondary structure predication softwares (GOR IV and COILS)

Materials and Methods

Materials

The purifications of TMs of the prawn, Japanese common squid, the abalone, and striated and smooth adductor muscles of the scallop were performed as described in Section 1 of the present chapter. The purified TMs were subjected to freeze drying.

CD spectrometry

TM was dissolved in 10 mM sodium phosphate (pH 7.0), containing 0.1 M KCl, 0.1 mM DTT, and 0.001 % NaN_3. CD spectra were measured at 0.1 °C intervals using a spectropolarimeter (JASCO J-720) from 5°C to 80°C with the raising temperature at 1°C/min. While constant N_2 flux was employed, a cuvette of 10 mm optical path length was used. The temperature was controlled by PTC-343 (JASCO).

α-Helical contents were estimated by the mean residue ellipticity, $[\theta]_{222}$

α-Helical content (%) = 100 × $\{[\theta]_{222}$ /-36000$\}$

The unfoldings of TMs exhibited multiple transitions. To compare the overall stability of the proteins, two criteria were used: the temperature at the apparent midpoint temperature of unfolding (T_{Mapp}) and the apparent free energy of unfolding at 20°C (Greenfield and Hitchcock-DeGregori, 1995). The T_{Mapp} was defined here as the temperature at which the ellipticity at 222 nm was at the midpoint between the values found at 5°C and 80°C. The value of T_{Mapp} usually does not correspond to the midpoint of the major folding transition. To evaluate the free energy of unfolding at 20°C, it was assumed that the unfolding could be fit by two independent helix-coil transitions. The CD data, normalized to a scale of 0 to 1, was fit by the following equations:

$$\theta = \varepsilon_1\alpha_1+\varepsilon_2\alpha_2 \qquad (1)$$

where

$$\alpha_1 = K_1/(1 + K_1) \text{ and } \alpha_2 = K_2/(1 + K_2) \qquad (2)$$

ε_n is the decrement of the α-helical fraction of the "n"th unfolding.

$$K_1 = \exp((\Delta H_1/RT)((T/T_{M1}) - 1)\}, K_2 = \exp((\Delta H_2/RT)((T/T_{M2}) - 1)\} \qquad (3)$$

ΔH_n is the enthalpy of the "n"th unfolding. The first and second unfoldings are the transitions at the lower and higher temperatures, respectively. T_{Mn} is the midpoint

temperature of the "n"th unfolding. To calculate the values of ΔH_n and T_{Mn}, initial values of these parameters were estimated and the unfolding equations were fit using Excel 2007 (Microsoft). The ΔS_n was determined by the relationship of $\Delta S_n = \Delta H_n / T_{Mn}$. These values were then used to estimate the apparent Gibbs free energy of unfolding at 20°C (ΔG_{app}) using the relationship:

$$\Delta G_{app} = \varepsilon_1(\Delta H_1 - 293.15\Delta S_1) + \varepsilon_2(\Delta H_2 - 293.15\Delta S_2) \quad (4)$$

DSC

TM was analyzed by a differential scanning microcalorimeter (MicroCal model VP-DSC, Northampton, MA, USA) with the raising temperature at 1°C/min from 5°C to 90°C. Progress baseline mode was adopted, which reflected the extent of progress of the reaction. DSC data were analyzed for determination of ΔH_n and T_{Mn} of "n"th unfolding, using a software package Origin developed by MicroCal.

Bioinformatics

The amino acid sequences of TMs were cited from the NCBI database: BAE54431 for the squid, AAG08987 for the abalone, BAF47263 for the prawn, BAB20881 for white croaker, BAA20455 for the scallop striated muscle, and BAB17857 for the scallop smooth muscle.

Propensity for α-helix formation was used to estimate α-helix formation ability based on the amino acid sequence (Chou and Fasman, 1978). Hydrophobicity at the *a* and *d* positions on heptad repeat was estimated according to Kyte and Doolittle (1982). The secondary structure prediction was performed using the GOR IV program (Garnier

et al., 1996). In this program, the predicted secondary structure is basically one of the highest probabilities, compatible with a predicted α-helix segment of at least four residues and a predicted extended segment of at least two residues. The average probability score for α-helix at each amino acid position was also considered. The prediction of coiled-coil score was performed using the COILS program (Lupas et al., 1991), with a window width of 14, MTIDK as a matrix, and no weighting of position.

For the correlation among the values obtained by CD spectrometry, DSC and bioinformatics, the values from 0 to 0.2, from 0.2 to 0.4, from 0.4 to 0.7, from 0.7 to 0.9, and from 0.9 to 1.0 were regarded as very weak, weak, moderate, strong, and very strong, respectively.

Results

CD spectrometry and DSC

The concentrations of DTT, NaN_3 and EDTA were considered for the measurement of the CD spectrometry, because it was difficult to obtain clear data due to their high absorbance. Each absorbance at 222 nm was 2.77 for 10 mM sodium phosphate (pH 7.0) containing 0.1 M KCl, 1 mM DTT and 0.01 % NaN_3, 1.47 for 10 mM sodium phosphate (pH 7.0) containing 0.1 M KCl, 0.1 mM DTT and 0.001 % NaN_3, 2.25 for 10 mM sodium phosphate (pH 7.0) containing 0.5 M NaCl, 0.5 mM DTT and 1 mM EDTA, and 2.32 for 10 mM sodium phosphate (pH 7.0) containing 0.1 M KCl, 0.5 mM DTT and 1 mM EDTA.

The values of T_{Mapp} and ΔG_{app} by CD spectrometry and $\Delta G_{\mathrm{total}}$ by DSC were calculated for the prawn TM (Figs. 1-12 and 1-13; Tables 1-1 and 1-2), the squid TM (Figs. 1-14 and 1-15), the abalone TM (Figs. 1-16 and 1-17), and scallop striated muscle (Figs. 1-18 and 1-19), and scallop smooth muscle TMs (Figs. 1-20 and 1-21). The temperature with the maximum value of $-\mathrm{d}(\theta_{\mathrm{calculated}})/\mathrm{d}T$ by CD spectrometry was in good agreement with the maximum Cp value obtained by DSC. The values of $\Delta H_{\mathrm{total}}$ obtained by CD spectrometry and the 1st scan of the DSC showed strong correlation (correlation coefficient being 0.77). But, $\Delta H_{\mathrm{total}}$ values by DSC were much larger than those obtained by CD spectrometry, due to the difference in detectable numbers of transition unit: namely, two or three by CD spectrometry and more by DSC.

The thermostability of TM was determined by T_{Mapp}. The ΔG_{app} was used when T_{Mapp} was comparable. The T_{Mapp} values suggested that the squid and abalone TMs have

comparable stability, but slightly lower than that of the prawn TM (Table 1-2). The difference in ΔG_{app} has revealed that the abalone TM is more stable than the squid TM mainly due to the higher ΔH_2 value of the abalone TM. The stability was in the order of the prawn TM > abalone TM > white croaker TM > squid TM > scallop smooth muscle TM > scallop striated muscle TM. Based on ΔG_{total} in the 1st scan of the DSC, the stability is thought to be in the order of the prawn TM > abalone TM > white croaker TM > squid TM > the scallop smooth muscle > the scallop striated muscle TMs. The orders of the TM stability estimated by CD spectrometry and DSC did not show large discrepancy, partly because the values of ΔG_{total} by DSC also showed strong correlation with the values of T_{Mapp} and moderate one with ΔG_{app} obtained by CD spectrometry (Table 1-3). The stability difference between the squid and white croaker TMs was small. Thus, the stability orders by CD and DSC about these TMs were different.

Bioinformatics

Although the amino acid identity among vertebrate muscle TMs or among the scallop TM isoforms showed above 90% (Huang and Ochiai, 2005), the identity among TMs in the present experiment was low (60-80%; Fig. 1-22). To obtain the relationship between amino acid replacement and stability, the analysis was performed as described below.

Helix propensity showed marginal variance among the species, although it showed moderate correlation with ΔG_{total} and T_{Mapp}, but very weak one with ΔG_{app} (Table 1-3). Hydrophobicity per residue at the *a* and *d* positions of heptad repeat showed very weak reciprocal correlation with T_{Mapp} and moderate reciprocal correlation with ΔG_{app} and ΔG_{total} (Table 1-3), although it has been reported that the thermal stability can be

estimated by the hydrophobicity (Greenfield and Hitchcock-DeGregori, 1995). It may be because the residues at the *a* and *d* positions in invertebrate muscle TMs showed relatively high sequence homology or because the residues at the other positions have greatly affected the stability.

The helical scores (the full score being 1000) averaged for each amino acid by GOR IV (Table 1-2) showed strong correlation with ΔG_{app}, T_{Mapp}, and ΔG_{total} (Table 1-3). The coiled-coil formation (%) estimated by COILS showed very strong correlation with ΔG_{app} and moderate one with ΔG_{total}, but weak one with T_{Mapp} (Table 1-3). In addition, this value showed strong correlation with ΔH_{total} by CD spectrometry (0.88) and DSC (0.82).

From the correlations, helical scores by GOR IV and coiled-coil scores by COILS seemed to be good prediction parameters of thermal stability (Table 1-3). On the other hand, helix propensity and hydrophobicity were much less reliable, because helix propensity showed marginal variation and hydrophobicity showed reciprocal correlation with the set of thermostability index as obtained by CD spectrometry and DSC (Table 1-3).

Amino acid residues involved in structural stability

The amino acid residues involved in the thermostability difference of TMs among species were presumed (Fig. 1-22). The N- and C-termini regions and the region around the 130th residue of vertebrate and invertebrate TMs in this figure seemed to be unstable by GOR IV or COILS. At around the 50th residue, the helical score by GOR IV was low except for the prawn TM. This suggested that the high stability of the prawn TM was partly due to the sequence at around this residue. Furthermore, there are many

amino acid replacements around the 50th-53rd residues. In addition, the high stability of the prawn TM could have related with a higher coiled-coil score around the 165th and 215th residues compared to the squid or scallop striated muscle TMs and the other invertebrate TMs, respectively.

The region around the 200th residue of invertebrate TMs was in a random coil by GOR IV. This was partially due to the substitution of Thr by Gly at the 201st residue. The prawn TM showed a high coiled-coil score around the 215th residue, compared to the other invertebrate TMs. It has been, however, difficult to elucidate which substitutions would stabilize the prawn TM and be responsible for the stability difference among invertebrate TMs, because there are so many substitutions in this region among invertebrate TMs. Thus, mutagenesis study or molecular dynamics simulation should be performed to know the precise relationship between stability and amino acid substitutions.

Section 3

Discussion

TM preparation

The yield of the squid acetone powder was low, because the squid mantle muscle was very sticky and thus, it was difficult to mince it. In addition, the squid muscle was readily soluble in water compared to fish meat (Yoshimura, 1955). In HIC, high concentration of ammonium sulfate would weaken the ionic interaction, and the hydrophobic functional groups in the resin would weaken the hydrophobic interaction of proteins. Due to these effects, TM could be successfully separated by HIC and HIC could be a good option for the purification of TM.

The purified smooth muscle TM was a single component. Above the major TM band, weak band, which could be a minor isoform of TM, was observed (Fig. 1-8) and lost at 35% saturation of ammonium sulfate.

CD spectrometry and DSC

The α-helical contents at 5°C were estimated to be more than 80% for all TMs, although BCA method exhibits some degree of varying response toward different proteins. For example, compared to bovine serum albumin, bovine IgG shows higher absorbance (121%) and horse heart myoglobin shows lower absorbance (74%). Thus, the comparison of α-helical contents at 5°C between the different phyla must be meaningless because they show low amino acid identity of around 50%.

Ishida and Konno (1982) suggested that the squid TM easily lost Ca^{2+}-sensitivity and dissociated to subunits by urea. The squid TM showed lower thermostability,

compared to the prawn and abalone TMs, although it showed higher stability than the scallop TMs. Thus, further study should be performed for the stability of invertebrate TMs.

There was a large difference in thermostability between TMs from the scallop striated and smooth muscles as indicated by CD spectrometry. This result is in good agreement with the fact that striated muscle TM was more easily digested with trypsin than smooth muscle TM (Ishimoda-Takagi and Kobayashi, 1987).

Sequence and stability

Invertebrate TMs showed about 60% sequence identity with vertebrate TMs (Fig. 1-22). This homology is high, compared to the homology of Tn. The sequence of scallop TnC shows about 30% homology to vertebrate skeletal TnCs (Nishita et al., 1994). The sequence of akazara scallop *Chlamys nipponensis akazara*. TnT showed 26% homology to rabbit skeletal TnT (Inoue et al., 1996). Akazara scallop TnI has 100-133 amino acids insertion at the N-terminal region, compared to the vertebrate TnI, and the sequence of the C-terminal region (134th-292nd residues) showed 26-30% homology to vertebrate ones (Tanaka et al., 1998). The sequences corresponding to the critical region for actin-binding (1st-9th residues) and TnT-binding region (near residues 150-180) of rabbit α-TM are well conserved also in scallop TM (Inoue et al., 1999).

In most shellfish species, genus *Penaeus* is one of the most frequently reported causes of allergic reactions (Reese et al., 1999). Brown shrimp TM, which shows 100% amino acid sequence identity with kuruma prawn, has many epitopes; the 43rd-55th,

88th-101st, 137th-141st, 144th-151st, 187th-197th, 249th-259th, 266th-273rd and 273rd-281st residues (Ayuso et al., 2002a and 2002b; Motoyama et al., 2007). Japanese common squid TM was shown to be an allergen, but the epitope has not been shown. It has been shown that the abalone TM have the same epitopes as offshore greasyback prawn *Metapenaeus ensis* TM, but the epitope is unknown (Chu et al., 2000). TM of Pacific oyster contains an IgE-binding epitope in 92nd-105th residues and it has been shown that Yesso scallop TM have the same epitopes as the oyster ones (Ishikawa et al., 1998a and 1999). The region around these epitopes did not contain unstable region as examined by GOR IV and COILS, except for the C-terminus. These predictions support the idea that the structure of epitope is stable (Mikita and Padlan 2007).

The C-terminal region of vertebrate TMs showed the peculiar structure. The region between the 263rd and 284th residues showed α-helices that were separated from each other in the crystal structure (Li et al., 2002), and, in the solution, the region between the 270th and the 279th forms parallel, linear helices and the region between the 280th and 284th residues is nonhelical and flexible (Greenfield et al. 2003). It has been reported that Gln263 at the *a* position and Tyr267 at the *d* position, which do not display the usual symmetric knobs-into-holes packing pattern, would perturb the canonical coiled-coil, but not the α-helix. These two programs indicated that C-terminal amino acid sequence in vertebrate TMs was also unstable, but it was shown in Chapter 2 that this region is stable. Thus, GOR IV and COILS could not predict this region well. The C-terminal amino acid sequence in invertebrate TMs showed many substitutions compared with vertebrate TMs and the structures in invertebrate TMs have not been determined.

Chapter 2

Thermal stability of peptides synthesized based on the sequence of walleye pollack tropomyosin

Fish are mostly ectotherms, thus their TMs are expected to have clearly different thermal stabilities among species due to their habitat temperatures. The deduced amino acid sequences of fish TMs are available for several species (Ohara et al., 1989; Heeley et al., 1995; Ochiai et al., 2001; Ochiai et al., 2003; Ikeda et al., 2003; Huang et al., 2004). Huang and Ochiai (2005) have reported that fish TMs as well as rabbit TM are much alike in their amino acid sequence, with the identity higher than 93%. They also have measured the thermal stabilities of fast skeletal muscle TMs from white croaker *Pennahia argentata*, pufferfish *Takifugu rubripes*, walleye pollack *Theragra chalcogramma*, Atlantic salmon *Salmo salar*, bluefin tuna *Thunnus thynnus*, zebrafish *Danio rerio*, and rabbit *Oryctolagus cuniculus* by CD spectrometry and DSC. They have shown that denaturation temperature of walleye pollack TM is unexpectedly high as that of rabbit TM, though the habitat temperature of walleye pollack is 0-8 ºC.

In the present chapter, five peptides of 30mer were designed, based on the amino acid sequences of walleye pollack TM, to compare their regional stability difference.

Section 1

Peptide designing and circular dichroism spectrometry

The stabilities of fish TMs were highly varied, although fish TMs are much alike in their amino acid sequence, with the identity higher than 93% (Huang and Ochiai 2005). The regional stability difference of fish TM was rarely studied.

In this section, to evaluate their regional stability difference, the thermo stabilities of five synthesized peptides, based on the amino acid sequences of walleye pollack TM, were measured. In addition, the effect of N-terminal acetylation on the TM structure was estimated by secondary structure prediction software AGADIR.

Material and Methods

Peptide designing

Five synthetic peptides were designed based on the walleye pollack fast muscle TM sequences, namely, Peptide Nterm (MDAIKKKMQM LKVDKENALD RAEQAEGDKK, corresponding to Met1-Lys30), Peptide Var (DVASLNRRIQ LVEEVLDRAQ ERLATALTKL, corresponding to Asp84-Leu113), Peptide Mid (VIENRAMKDE EKMELQEIQL KEAKHIAEEA, corresponding to Val128-Ala157), Peptide Cys (LERTEERAEL SEGKCSELKE ELKTVTNNLK, corresponding to Leu176-Lys205), and Peptide Cterm (DLEDELYAQK LKYKAISEEL DHALNDMTSI, corresponding to Asp255-Ile284) (Fig. 2-1). Peptide Nterm and Peptide Cterm corresponded to the N-terminus and C-terminus of the walleye pollack TM, respectively.

Peptide Var contained one specific substitution at the center of this peptide; namely, other vertebrate TMs have Glu98 instead of valine. Peptide Mid was located in the center of molecule and Leu143 was replaced with Ile as in chicken and mammalian TMs. Peptide Cys contained Cys190 at the center of the peptide, and the residue is highly conserved in vertebrate TMs. The peptides were purchased from Thermo Fisher Scientific Co. (Ulm, Germany). The molecular weights of peptides have been checked by mass spectrometry and purities have been checked by HPLC as more than 90% by the producer.

CD spectrometry

These synthesized peptides were dissolved in 10 mM sodium phosphate (pH 7.0) containing 0.1 M KCl, 1 mM DTT, 0.01% NaN_3 at around 5°C with a spectropolarimeter (JASCO J-720, Tokyo, Japan). CD spectra were also measured in 10 mM sodium phosphate (pH 7.0) containing 0.1 M KCl, 1 mM DTT, 0.01% NaN_3 and 40% 2,2,2-trifluoroethanol (TFE) at various temperatures ranging from 2°C to 60°C.

While constant N_2 flux was employed, a jacketed cell of 0.2 mm optical path length was used. The temperature was controlled by circulating thermo-regulated water. Wavelength and protein concentration for measurement were in the range from 240 nm to 190 nm and 1 mg/ml, respectively.

α-Helical content was calculated as described in Section 2 of Chapter 1

Protein concentration determination

Protein concentration determination was performed as described in Section 1 of Chapter 1.

Secondary structure prediction

Secondary structure prediction was performed using AGADIR (Muñoz and Serrano, 1999). In AGADIR, the parameters were set at pH 7.0, 278 K, and 0.12 as ionic strength.

Results

α-Helical contents

The CD spectrometry of Peptide Nterm in the absence of TFE at 5.7°C is shown in Fig. 2-2A. The spectrometry of five peptides gave a high $[\theta]_{222}$ value and a low $[\theta]_{200}$ value, which are indicative of random coil spectrometry, but not of α-helix. In the absence of TFE, all peptides showed low α-helical contents (Table 2-1).

In 40% TFE, all peptides showed α-helical contents more than 40% (Figs. 2-2 and 2-3; Table 2-1). In 40% TFE, the $[\theta]_{222}/[\theta]_{208}$ values were in the range of 0.636-0.848, 0.684-0.877, 0.626-0.831, 0.646-0.859, and 0.728-0.920 for Peptides Nterm, Var, Mid, Cys, and Cterm, respectively. Since these values were lower than 1, it was suggested that these peptides did not form typical coiled-coil structures (Cooper and Woody, 1990; Greenfield and Hitchcock-DeGregori, 1993; Wallimann et al., 2003).

To determine the effect of peptide concentration on coiled-coil formation tendency, the CD spectrum of Peptide Cys was measured at several concentrations in the presence of 40% TFE. For 0.1 mg/ml, α-helical contents and $[\theta]_{222}/[\theta]_{208}$ ratio were 49.3-41.3% and 0.93-1.02 (4.2-16.9°C), respectively, although high noise was detected because the concentration of the peptide was low. For 1mg/ml, the α-helical contents and $[\theta]_{222}/[\theta]_{208}$ ratio were 48.4-38.5% and 0.85-0.80 (4.2-20.2°C), respectively. Since the solution of 10 mg/ml was slightly turbid, the solution was centrifuged at 4°C and 17,000×g for 10 min to reduce the turbidity and concentration was then determined to be 4.9 mg/ml. For this concentration, α-helical contents and $[\theta]_{222}/[\theta]_{208}$ ratio were 52.3-44.7% and 48.4-38.5% (4.4-19.4°C), respectively. By AGADIR, the helical

contents of peptides were predicted to be 2.6% for Peptide Nterm, 8.9% for Peptide Var, 6.7% for Peptide Mid, 1.7% for Peptide Cys, and 11.2% for Peptide Cterm at 5°C (Table 2-1). In addition, the helical content of the acetylated Peptide Nterm was also calculated as 6.8% by AGADIR.

Section 2

Discussion

In the absence of TFE, the five peptides were shown to have low α-helix contents and the α-helix contents roughly corresponded to the prediction by AGADIR, except for Peptide Cterm; the α-helical content of Peptide Cterm was much higher than the prediction by AGADIR. Peptide Cterm could show a dimeric interaction, because AGADIR predicts the helical behavior of monomeric peptides and only considers short range interactions.

The low α-helix contents may have come from the short sequence (30mer), because α-helix ends are weakened by missing backbone hydrogen bonds: the initial four NH groups and final four CO groups lack intrahelical hydrogen-bonding partners (Baldwin and Rose, 1999), although only a 14-amino-acid-residue peptide could form stable coiled-coil (Dong and Hartgerink, 2006). The low stability observed in the present experiment reflected the structural flexibility of TM to interact with actin and Tn.

It was thus necessary to measure the spectrometry of the peptides in the buffer including 40% TFE, which has been widely used as an α-helix stabilizing cosolvent (Nelson and Kallenbach, 1986; Jaravine et al., 2001). However, the five peptides did not form clear coiled-coil structures under these conditions, because $[\theta]_{222}/[\theta]_{208}$ ratio was lower than 1 for all of them (Cooper and Woody, 1990; Greenfield and Hitchcock-DeGregori, 1993; Wallimann et al., 2003). In addition, all five peptides in 40% TFE gradually unfolded, and this suggested that ΔH between folded and unfolded states was small.

It was expected that the effect of deacetylation on the α-helical content was small in the absence of TFE, because, in the crystal structure of deacetylated TM fragment, only the residues 1 and 2 turned out to be nonhelical (Brown et al., 2001). AGADIR supported this interpretation, because it predicted the α-helical content to be 2.6% for the unacetylated Peptide Nterm and 6.8% for the acetylated Nterm.

In the present study, five synthetic peptides (30mer) were analyzed to examine the regional stability difference in the TM molecule. Differences in stability between the peptides were recognized, suggesting that the structural stability is not equal throughout the entire molecule of TM. However, it was also suggested that the peptides do not always give clear reproduction for the structural aspects of native TM. Studies using longer peptides obtained by enzymatic or chemical cleavage of native TM should be carried out to reveal the regional structural characteristics of fish TMs.

Chapter 3

Thermal stability of white croaker tropomyosin fragments

Mammalian TMs have been discussed in relation with their regional stability intensively. There are many proteases and chemical reagents, which are useful to obtain fragments of TM. Trypsin, chymotrypsin, and endoproteinases Lys-C and Glu-C have been used as proteases for many biochemical experiments, and 2-nitro-5-thiocyanatobenzoic acid (NTCB) and CNBr are also used as cleavage regents (Inglis and Edman, 1970; Houmard and Drapeau, 1972). Although there are many sites to be cut by trypsin, chymotrypsin, Lys-C, and CNBr for TM, NTCB has only one site.

NTCB is commonly used to cyanylate and cleave proteins at Cys residues and its efficient reaction condition was studied (Degani and Patchornik, 1974; Tang and David, 2004; Fig. 3-1). Skeletal muscle TM has Cys at the 190th position, so it was expected that 22 and 11 kDa fragments were obtained by NTCB treatment. In the present chapter, attempts were made to purify and compare their regional stability difference by CD spectrometry.

Section 1

Purification and measurement of 2-nitro-5-thiocyanatobenzoic acid fragment

The stabilities of rabbit α-TM fragments obtained by NTCB treatment have been reported (Holtzer and Holtzer, 1990). This study supported that the C-terminal region of rabbit TM was unstable compared to the N-terminal region on crystal structure study (Phillips et al., 1980 and 1986; Whitby and Phillips, 2000).

In this section, thermostabilities of NTCB fragments of white croaker TM were measure by CD spectrometry. In addition, the secondary structure was evaluated by softwares GOR IV and COILS.

Materials and Methods

Preparation of white croaker acetone powder

Glycerinated muscle of white croaker fast skeletal muscle was used. Preparation of acetone powder was performed as described in Section 1 of Chapter 1.

Purification of white croaker TM

Extraction of TM, isoelectric precipitation, and ammonium sulfate fractionation were carried out as in the case of invertebrate TMs in Section 1 of Chapter 1. TM was obtained in 45-60% ammonium sulfate saturation fraction.

SDS-PAGE

SDS-PAGE was performed as described in Section 1 of Chapter 1.

Protein concentration determination

Protein concentration determination was performed as described in Section 1 of Chapter 1.

NTCB reaction

The purified TM was subjected to freeze drying after dialysis against 50 mM NH_4HCO_3. The lyophilized TM was dissolved in 1 M glycine containing 6 M guanidine-HCl (pH 9.0) at a concentration of 1 mg/ml (31 μM as monomer TM). NTCB (22 mM in the reaction mixture), was added to 20-fold molar excess (0.62 mM) over the total cysteine residue content, and the mixture was incubated at 37°C for 4 hours. The reaction was then terminated with 0.2 M 2-mercaptoethanol followed by incubation at 24°C for 15 min and desalted by ZipTip^{TM} (Millipore, Billerica, MA, USA) for SDS-PAGE or dialyzed against 50 mM NH_4HCO_3 for purification. One molar glycine or the mixture of 1 M glycine and 50 mM Tris were also used as reaction buffer instead of 1 M glycine containing 6 M guanidine-HCl.

Purification of NTCB fragment

TM fragmented with NTCB was dissolved in 50 mM potassium phosphate (pH 7.0) containing 4 M urea and 1 mM DTT before chromatography. AEX using a Mono Q^{TM} 5/50 GL column (0.5 × 5 cm) was carried out at a flow rate of 1 ml/min. About 7 mg of protein was loaded to the column, and the column was washed with 10 ml of the above buffer. Protein was eluted by linearly increasing the concentration of potassium phosphate from 50 mM to 400 mM in the presence of 4 M urea and 1 mM DTT. The fractions, containing the C-terminal fragment as the major component, were dialyzed against 50 mM NH_4HCO_3, and freeze-dried. This was dissolved in 50 mM potassium phosphate (pH 7.0) containing 1 mM DTT. The proteins were eluted by the linear gradient from 50 mM to 500 mM potassium phosphate buffer (pH 7.0) in the presence of 1 mM DTT, and the other conditions were the same as above. As a control of NTCB fragmentation, white croaker TM was treated with 1 M glycine, containing 6 M guanidine-HCl (pH 9.0), was purified as the first NTCB fragment purification chromatography.

CD spectrometry

CD spectrometry was performed as described in Section 2 of Chapter 1.

DSC

TM was analyzed by a differential scanning microcalorimeter (MicroCal model VP-DSC, Northampton, MA, USA) as described in Section 2 of Chapter 1.

Primary structure analysis

The analyses by GOR VI and COILS were performed as Section1 of Chapter 2.

Results

Reaction conditions

TM was fragmented only in 1 M glycine containing 6 M guanidine-HCl (pH 9.0) (Fig. 3-2). TM is a rod-like, not a globular, protein, so it was expected that this reaction could undergo without guanidine as the denaturing agent. Proteins were partly lost through desalting with ZipTip^{TM} (lanes 1-4 of Fig. 3-2B). Based on the densitometric analysis, about 52% of TM was cleaved (lane 5 of Fig. 3-2B).

Purification of NTCB fragments

In the first chromatography, C-terminal fragment (Cys190-Ile284) could not be isolated from the mixture of N-terminal fragment (Met1-Lys189) and uncleaved TM. The fragment was mainly eluted in the fractions 19-22 (Fig. 3-3). These fractions were used for the second chromatography and the C-terminal fragment was isolated (lanes 20 and 21 of Figs. 3-4 and 3-5).

CD spectrometry of NTCB fragments

By the guanidine treatment, the stability of white croaker TM was decreased (Figs. 3-6 to 3-9). The N- and C-terminal fragments showed lower stability than that of the guanidine treated TM, and the C-terminal fragment showed higher stability than the N-terminal fragment (Fig. 3-8; Table 3-1).

Primary structure analysis

GOR VI and COILS suggested the unstable region (Figs. 3-10 and 3-11; Table 3-1). From these analysis, the amino acid substitutions around the 170th and 250th residues resulted in the stability difference.

Section 2

Discussion

Fragmentation and stability

TM was not fragmented in 1 M glycine nor in 1 M glycine containing 50 mM Tris-HCl. Because Cys190 is at the core region (*a* position of heptad repeat), it may be difficult for NTCB to access and cyanylate the cysteine residue. In 4 M urea, TM is assumed to be present as a monomer. Small amount of trimer, consisting of a full length monomer and the N- and C-terminal fragments, was formed in the second chromatography (Fig. 3-4), and it was faintly observed at lane 23.

In the urea solution, the following relationship was formulated:

$$\Delta G_{([\text{urea}])} = \Delta G_{([\text{wat}])} - \text{m}[\text{urea}],$$

where $\Delta G_{([\text{urea}])}$ and $\Delta G_{([\text{wat}])}$ are Gibbs free energies for unfolding in the presence and absence of urea, respectively.

During dialysis, the urea concentration was decreased gradually, so it was expected that at a given concentration of urea, TM full-length dimer was thermodynamically favored, compared to the trimer.

CNBr reaction did not proceed efficiently (data not shown), though more than 90% efficiency were expected in this reaction. Because of the low efficiency, it was difficult to isolate CNBr fragments.

At around 50 °C, NTCB fragments Met1-Lys189 and Cys190-Ile284 were fully unfolded (Fig. 3-8C-F). From ΔG_{app} and T_{Mapp} (Table 2-1), the stability of α-helix in Cys190-Ile284 was higher than that of Met1-Lys189, though the length was shorter.

Comparison with TM fragment of rabbit

The stabilities of rabbit α-TM fragments by NTCB have been reported (Holtzer and Holtzer, 1990). The rabbit α-TM N-terminal fragment showed higher stability than its C-terminal fragment as observed by CD spectrometry; at the concentration of about 0.01 mg/ml, values of $T_{1/2}$, where helix contents are 50%, were 44°C and 27°C for the N- and C-terminal fragments, respectively (Holtzer and Holtzer, 1990). For white croaker TM, $T_{1/2}$ was 31°C for the N-terminal fragment and 33°C for the C-terminal fragment. From this comparison, the N-terminal fragment of white croaker TM showed much lower stability than the rabbit counterpart, and the C-terminal fragment of white croaker TM showed higher stability than the rabbit counterpart. The amino acid substitutions between rabbit and white croaker TMs are thirteen in the N-terminal fragments, and four in the C-terminal fragments. The sequence analysis by GOR IV (Garnier et al., 1996) or COILS (Lupas et al., 1991) suggested that, compared with the rabbit fragments, the substitutions (rabbit/white croaker) of Ala/Gly83, Ser/Gly174 and Ala/Thr179 would destabilize, and Ser/Ala247 and Ser/Thr252 would stabilize white croaker TM fragments.

Holtzer and Holtzer (1990) insisted that the region around the 127th-189th residues of the rabbit N-terminal fragment is unstable and unfolded below 20°C. This region of the white croaker N-terminal fragment seems to be unstable, judging from T_{M1} and ε_1. Based on these interpretations, decrement of $T_{1/2}$ by 13°C in the white croaker TM N-terminal fragment mainly resulted from the substitution of Ala/Gly83, because the region around the two substitutions [Ser/Gly174 and Ala/Thr179], predicted to destabilize the white croaker TM N-terminal fragment, would be unfolded below 20°C.

Compared with the rabbit TM C-terminal fragment, the increment of $T_{1/2}$ by 6°C in white croaker counterpart mainly resulted from the substitutions of Ser/Ala247, Ser/Thr252, or both of them.

It has been shown that the region from Lys152 to Val165 is essential for binding to the globular domain of Tn (Sakuma et al., 2006) and the region from Asp258 to Ile284(*d*) is essential for binding to a rod-like domain of Tn (Hammell and Hitchcock-DeGregori, 1996). The lower stability of C-terminal half of rabbit TM has been discussed in relation to the interaction with Tn (Lakkaraju and Hwang, 2009). However, in the present study, the C-terminal fragment, corresponding to the one-third of the entire white croaker TM, was found to show higher stability than the N-terminal fragment. Thus, the regional stability of C-terminal region of TM would be independent of Tn interaction.

Chapter 4

Molecular dynamics simulations of tropomyosin structure

It has been suggested, in Chapter 3, that the white croaker TM C-terminal fragment by NTCB cleavage would have higher stability than the rabbit TM fragment, although the amino acid substitutions (rabbit/white croaker) are only four: Ala/Ser191 at the *b* position, Ser/Thr229 at the *e* position, Thr/Ala247 at the *b* position, and Ser/Thr252 at the *g* position (Fig. 4-1). It is possible that the higher stability results in the higher myofibrillar ATPase cooperativity. In addition, the stability and the structure of TM would be important for the actin binding ability. Thus, further study for the flexibility should be performed.

In the present chapter, molecular dynamics (MD) simulation by the explicit water model was performed for the rabbit and white croaker TM C-terminal fragments. These fragments contain the sixth alanine cluster [Ala235(*d*)-Ala239(*a*)-Ala242(*d*)] and the second acidic core [Glu218(*a*)] (Fig. 4-1). The alanine cluster endows the stagger and curvature at each side of the cluster, and the acidic core endows the flexibility to TM. Thus, the effect of amino acid substitutions, alanine cluster, and acidic core, were focused in the present chapter.

In general, root mean square fluctuation (RMSF) and root mean square deviation (RMSD) are used for the analysis of MD simulation. RMSF is a good indicator for the flexibility and RMSD is used for the criteria for the conformational change or the adequacy of the simulation. The calculations of RMSF and RMSD need alignment by root mean square fitting, although the alignment for the whole structure is inappropriate for structural analysis of TM. Internal and overall motion could not be separated by root

means square fitting and this defect is unacceptable for the evaluation of flexible, rod-shaped proteins like TM. Thus, fluctuation of dihedral angle (FDA) and deviation of dihedral angle (DDA) by backbone dihedral angles [φ (C-N-C_α-C) and ψ (N-C_α-C-N)] were used.

Section 1

Regional flexibility difference of tropomyosin and its mutants

MD simulation can show the average structure and flexibility. This method would be adequate to show the effect of the amino acids substitutions on the structure and flexibility.

In this section, MD simulation was performed for the rabbit and white croaker TMs C-terminal fragments. In addition, the differences between these fragments were evaluated.

Materials and Methods

MD simulation

The crystal structure of C-terminal fragment of rabbit skeletal α-TM (PDB ID, 2D3E) was used as a template. The coordinate data of 190th-282nd residues of A and B chains were used. Since the PDB file lacks the positions of Ser283(*c*) and Ile284(*d*), the coordinates of main chains of these residues were added. His276(*c*) was regarded to take a δ-protonated state (HID). The side chains of Glu218(*a*)s could interact with each other, which could affect the p*K*a values. But the p*K*a value of each side chain was calculated to be lower than 7.0 by PROPKA 3.1 (http://propka.ki.ku.dk/). Thus, the carboxyl groups were regarded to take ionization state in this simulation.

To prepare for Amber simulation, xLEaP, which is a part of Amber suite (Case et al., 2005), was used. To solvate TM fragment structure, 23000 water molecules were added.

Then, 22 Na^+ were added to neutralize the solvated system, and 44 each of Na^+ and Cl^- were added to bring the salinity up to 0.1 M. There are four substitutions between the rabbit and white croaker TM C-terminal fragments, and to obtain the initial structure of the white croaker TM C-terminal fragment, the PDB file was edited.

The simulation was performed by AMBER10 (Case et al., 2005). To omit structural distortion, energy minimization was performed. Firstly, solvent energy minimization was performed at 500 steps of steepest descent minimization, followed by 500 steps of conjugate gradient minimization. In this energy minimization, the residues of these fragments were restrained to the initial structure with a 500 $kcal \cdot mol^{-1} \cdot Å^{-1}$ harmonic potential. Then, the whole system energy minimization was performed at 1000 steps of steepest descent minimization followed by 1500 steps of conjugate gradient minimization with no restraint.

For the following simulation, periodic boundary conditions and SHAKE method (Miyamoto and Kollman, 1992) for the bond involving hydrogen atom were used. The solvent equilibration for 20 ps (2 fs × 10000 steps) was performed at 278 K, using Langevin dynamics for the temperature control and constant volume condition (NVT). The residues of these fragments were restrained to the initial structure of equilibration with a 10 $kcal \cdot mol^{-1} \cdot Å^{-1}$ harmonic potential. Then, the whole system equilibration was performed for 100 ps (2 fs × 50000 steps) at 278K and 1 bar, using Berendsen dynamics for temperature control. The last equilibration was performed at 300 K in NVT with Berendsen dynamics for temperature control for 20 ps. Finally, productive simulation in NVT at 300 K was performed for 20 ns, using Berendsen dynamics for temperature control.

Calculation of RMSF, RMSD, FDA, and DDA.

Thousand snapshots (20 ps intervals) were used for the analysis, using ptraj of AMBER10 suite. Mass-weighted RMS fitting, using average structure of Cα, C, and N atoms of the main chains, were performed and RMSF was calculated.

To evaluate the flexibility for each residue, dihedral angles φ (C-N-C_α-C) and ψ (N-C_α-C-N) were used (Fig. 4-2 A). FDA of "n"th residue was calculated as follows:

$$\mathrm{FDA}(n) = \sqrt{\frac{1}{1000}\times\sum_{t=1}^{1000}[\{\varphi^{A}(t,n)-\overline{\varphi^{A}(n)}\}^2+\{\psi^{A}(t,n)-\overline{\psi^{A}(n)}\}^2+\{\varphi^{B}(t,n)-\overline{\varphi^{B}(n)}\}^2+\{\psi^{B}(t,n)-\overline{\psi^{B}(n)}\}^2]}$$

Superscripts A and B mean A and B chains, respectively.

Then, in order to calculate the time dependency, deviation of dihedral angles (DDAs) of "t"th snapshot was calculated as follows:

$$\mathrm{DDA}(t) = \sqrt{\frac{1}{82}\times\sum_{n=194}^{275}[\{\varphi^{A}(t,n)-\overline{\varphi^{A}(n)}\}^2+\{\psi^{A}(t,n)-\overline{\psi^{A}(n)}\}^2+\{\varphi^{B}(t,n)-\overline{\varphi^{B}(n)}\}^2+\{\psi^{B}(t,n)-\overline{\psi^{B}(n)}\}^2]}$$

Calculation of other criteria

TWISTER (Strelkov and Burkhard, 2002) computes the axes point [C_{helix1}(n), C_{helix2}(n)] of α-helices from C_α atoms of "n"th residue. Then, TWISTER calculates the axis point [C_{cc}(n)] of coiled-coil as average of the axis for each chain (Fig. 4-2B). In addition, the coiled-coil phase per residue are calculated as the average of dihedral angles C_{helix}(n-1)C_{cc}(n-1)C_{cc}(n)C_{helix}(n) and C_{helix}(n)C_{cc}(n)C_{cc}(n+1)C_{helix}(n+1) by TWISTER.

The structural analysis of TM obtained by crystal structure was proposed (Minakata et al., 2007). The interhelical distance (HD) is defined as $|C_{helix1}(n)C_{helix2}(n)|$. The local bending angle (LBA) was defined as the angle between v1 ($=\overrightarrow{C_{CC}(n-7)C_{CC}(n)}$) and v2 ($=\overrightarrow{C_{CC}(7)C_{CC}(n+7)}$) (Figs. 4-2C and 4-3). The local staggering angle (LSA) is defined as the angle between v3 ($=\frac{v1+v2}{2}$) and $\overrightarrow{C_{helix1}(n)C_{helix2}(n)}$ (Figs. 4-2C and 4-3).

In addition, some criteria were newly defined in the present study. Local staggering distance (LSD) was calculated as $C_{helix1}(n)C_{helix2}(n)\cos(LSA)$ (Fig. 4-2D). ΔLSD(n) was calculated as [LSD(n+3) – LSD(n-3)]/6. Then, helical bending angle (HBA) was calculated as the angle between v4 ($=\overrightarrow{C_{helix}(n-7)C_{helix}(n)}$) and v5 ($=\overrightarrow{C_{helix}(7)C_{helix}(n+7)}$). The α-helical hydrogen bond distance of "n"th residue was also measured as the distance between carbonyl oxygen of "n"th residue and nitrogen of "n+4"th residue.

Results

Comparison between RMSF and FDA

RMSF showed local minima around Glu208(*e*) and Ala262(*c*) (Fig. 4-4A and B). This was the root mean square fitting artifact (Fig. 4-4C). Thus, the RMSF and RMSD can not be used for the evaluation of TM fragment trajectory.

FDA was fluctuated around 20° for each fragment (Fig. 4-5). From FDA, the substitution (Ser/Thr229 at the *e* position) destabilized white croaker TM fragment between Glu222(*e*) and Lys231(*g*) for 24°, compared to rabbit counterpart. The substitutions of Thr/Ala247 at the *b* position and Ser/Thr252 at the *g* position stabilized white croaker TM fragment between Ala242(*d*) and Leu249(*d*) residue for 26°.

DDA did not show the large shift, which could reflect the considerable conformational change (Fig. 4-6). Thus, the whole trajectory would be used for the further analysis. The time-averaged value of DDA showed little difference between rabbit (19.8±1.4°) and white croaker (19.9±1.4°) TM fragments. Thus, it seemed to be difficult to discuss the relationship between thermostability and DDA.

Coiled-coil phase

Coiled-coil phases per residue, around Gln210(*g*) and the alanine cluster, were between -3° and -4° at and the values around other region were higher (Fig. 4-7A). The coiled-coil phases of rabbit and white croaker TM fragments showed little difference (Fig. 4-7A). White croaker TM fragment showed lower coiled-coil phase per residue and higher SD around Thr229(*e*), which would come from the substitution and from the difference of behaviors around the acidic core (Fig. 4-7B). On the other hand, the SD

around the two substitutions (Thr/Ala247 at the *b* position and Ser/Thr252 at the *g* position) of the rabbit TM fragment was higher, and this would come from the two substitutions. The sum of the coiled-coil phase per residues between Thr201(*e*) and Ile270(*d*) was -195°±18 and -195°±24 for the rabbit and white croaker TM fragments, respectively (Fig. 4-7A). The higher SD of white croaker TM fragment would reflect the SD of coiled-coil phase per residue around the acidic core (Fig. 4-7B).

HD change and its effects

At the alanine cluster, HD was narrowed (Fig. 4-7C). Decrement of HD initiated at Glu218(*a*) and increment of HD completed at Glu250(*e*) (Fig. 4-7C). Termination of HD increment from the alanine cluster toward adjacent regions was accomplished by changes in direction of α-helices around these residues. This change resulted in the curvatures of α-helices (Fig. 4-8), which was associated with the breakages of α-helical hydrogen bonds and higher fluctuation of backbone (Fig. 4-5). The HD of the white croaker TM fragment around Lys213(*c*) was larger than that of rabbit counterpart and the SD of white croaker TM fragment around this residue was higher than that of rabbit counterpart (Fig. 4-7C, D).

Flexible and curved regions

At the acidic core and in the regions around the substitutions of Thr/Ala247 at the *b* position and Ser/Thr252 at the *g* position, rabbit TM fragment was flexible (Fig. 4-5) and curved (Fig. 4-9). White croaker TM fragment was also flexible in these substitution regions but curved only around the acidic core. The coiled-coil structure around the acidic core, which was positioned at the N-terminal side of the alanine

cluster, was flexible and curved, compared to the structure around Glu250(*e*) (Figs. 4-5 and 4-9), because of the destabilization by Glu218(*a*) and the surrounding core residues [Ala211(*a*), Tyr214(*d*), and Tyr221(*d*)].

Rabbit TM fragment was curved around Val246(*a*) and staggered around the alanine cluster, compared to the white croaker counterpart (Figs. 4-9, 4-10, 4-11, and 4-12). In addition, around Glu250(*e*), only one chain of α-helix was curved for the rabbit TM fragment and the distance of main chain hydrogen bonds were increased (Fig. 4-8).

In the region around Val246(*a*), which was adjacent to the two substitutions (Thr/Ala247 at the *b* position and Ser/Thr252 at the *g* position), rabbit TM fragment showed larger FDA and coiled-coil curvature than the white croaker counterpart (Fig. 4-5). In addition, only the rabbit TM fragment (A chain and coiled-coil, but not B chain) was extremely curved around Val246(*a*) and this resulted in the coiled-coil curvature. The curvature was related to the staggers at the alanine cluster.

Compared to rabbit TM fragment, white croaker counterpart showed lower coiled-coil curvature around Leu246(*a*) (Fig. 4-9A) and FDA between the Ala242(*d*) and Leu249(*d*) (Fig. 4-5). At 10-13 and 17-19 ns, the stagger and coiled-coil curvature at Ala239(*a*) were observed for white croaker TM fragment (Fig. 4-12). These resulted in the high curvature flexibility at this residue in case of the white croaker TM fragment (Fig. 4-9B). On the contrary to the rabbit TM fragment, coiled-coil of white croaker TM fragment was slightly curved at Val246(*a*) (Fig. 4-9A). Additionally, the curvatures of two α-helices of white croaker TM were comparable at this residue (Fig. 4-8). The curvature of coiled-coil and α-helices of white croaker TM at this residue seemed to be independent from the stagger.

Ionic bonds around the alanine cluster

For rabbit TM fragment, the stagger conformation seemed to be stabilized by ionic bond between the side chains of Arg238(*g*) of A chain and Glu234(*c*) of A chain at 6-13 ns (data not shown). In addition, the ionic bond between the side chains of Arg238(*g*) of A chain and Glu236(*e*) of B chain could decrease the energetic barrier between staggered and unstaggered conformations in 3-6 and 13-17 ns (data not shown). In contrast, for the white croaker TM fragment, the interchain ionic bonds between the side chains of Arg238(*g*) and Glu234(*c*) were rarely observed, but the intrachain ionic bonds between the side chains of Arg238(*g*) of A chain and Glu236(*e*) of B chain were formed (data not shown). It was possible that side chain ionic bonds stabilized the stagger conformation in other alanine clusters. These results indicated that the acidic residues participate not only in the binding of actin filament, but also in the structural equilibrium between staggered and unstaggered conformations of TM.

Section 2 Discussion

It was shown that the region around Glu218(a) was unstable (Minakata et al., 2008). The hydrophobic core between Leu207(*d*) and Tyr221(*d*) was exposed to the water molecule, because of the electrical repulsion by side chains of Glu218(*a*) (Minakta et al., 2008). In addition, bulky side chains of Tyr214(*d*) and Tyr221(*d*) contributed to the increment of chain separation and the compact side chain of Ala211(*a*) left the hole at the core (Minakta et al., 2008). The unstability would come from not only the core packing around these region but also the HD change (Fig. 4-7C), resulted in the breakage of α-helical hydrogen bonds (Fig. 4-8)

It was hypothesized that alanine cluster resulted in the bending between the stagger and unstagger regions (Brown et al., 2001). At the N-terminal region of the alanine cluster [around Asp230(*f*)] did not show such curvature (Fig. 4-9A) as crystal structure study (Minakata et al., 2008). The C-terminal region of the alanine cluster [around Val246(*a*)] was curved for the rabbit TM fragment and was straight for the white croaker TM fragment (Fig. 4-9A). The curvature was observed for the crystal structure but it was regarded as the effect of the crystal packing (Minakata et al., 2008). The present study showed that TM could easily curve at this region and this curvature was affected by one or two amino acid substitution(s). The effects of amino acid substitutions on the structure, which have been shown by MD simulation, should be checked by atomic force microscope.

Chapter 5

General discussion and conclusion

Invertebrate tropomyosins

The present study showed that the stability was in the order of prawn TM > abalone TM > squid TM, white croaker TM > scallop smooth muscle TM > scallop striated muscle TM. The stability difference would reflect the acclimations: habitat temperature and other muscle contraction characteristics. The scallop TMs would be a good model to study the TM stability and their characteristics, because the discussion, where the temperature demand is ruled out, is possible.

Genus *Penaeus* is one of the most frequently reported causes of allergic reactions (Reese et al., 1999). Thus, the higher thermostability of crustacean TMs could result in the high allergenicity. The stability of TM in the human stomach would be higher than that in the present experiment because TM is an acidic protein, and under low pH condition like in the stomach, TM would show higher stability. The stability under acidic condition should be measured by CD or DSC and the pepsin treatment should be performed for the invertebrate TMs. In addition, the behavior of invertebrate TMs under acidic condition should be researched by MD simulation.

Vertebrate tropomyosins

The study, using five synthetic peptides of 30mer based on the sequence of walleye pollack fast muscle TM, showed that the thermal stability was in the order of Peptide Cterm (Asp255-Ile284) > Peptide Var (Asp84-Leu113) > Peptide Nterm (Met1-Lys30),

Peptide Mid (Val128-Ala157), and Peptide Cys (Leu176-Lys205). Our study suggested that the stability of C-terminal region was higher than that of N-terminal region and this could be important for the head to tail interaction of TM. The present study in peptides have confirmed that AGADIR is accurate in predicting the peptide fragment, designed from TM. Thus, this tool would be useful in the prediction of the stability of invertebrate TM fragment.

The stability of α-helix in Cys190-Ile284 was higher than that of Met1-Lys189. The lower stability of C-terminal half of rabbit TM has been discussed in relation to the interaction with Tn (Lakkaraju and Hwang, 2009). However, the C-terminal fragment was found to show higher stability than the N-terminal fragment. Thus, the relationship between Tn interaction and regional stability of TM should be reconsidered.

The study indicated that the region between 127th-189th residues was unstable in both rabbit and white croaker TMs. Thus, the stability of this region for other vertebrate TMs would also be low. This idea is coincident with the study by 30mer peptides, because Peptide Mid and Peptide Cys were not stable. In addition, Peptide Nterm showed low stability as these peptides. Thus, the N-terminal region could also be so unstable that it is unfolded at low temperatures, but there has been no such report so far.

The study by MD simulation showed that the small side chain of alanine cluster provides TM with stagger as reported (Brown et al., 2001). In addition, the cluster endows α-helical hydrogen bond breakage, concomitant to the HD alternation. The MD simulation showed the effect of the amino acid substitution on the structure and its flexibility. TM and Tn affect the cooperativity of contraction (Fujita et al., 1996). Thus, the effect of amino acid substitutions between vertebrate TMs on the cooperativity or other muscle characteristics should be studied.

References

Ayuso, R., Lehrer, S.B., Reese, G., 2002a. Identification of continuous, allergenic regions of the major shrimp allergen Pen a 1 (tropomyosin). Int. Arch. Allergy Immunol. 127, 27-37.

Ayuso, R., Reese, G., Leong-Kee, S., Plante, M., Lehrer, S.B., 2002b. Molecular basis of arthropod cross-reactivity: IgE-binding cross-reactive epitopes of shrimp, house dust mite and cockroach tropomyosins. Int. Arch. Allergy Immunol. 129, 38-48.

Bailey, K., 1946. Tropomyosin: a new asymmetric protein component of muscle. Nature 157, 368.

Bailey, K., 1948. Tropomyosin: a new asymmetric protein component of the muscle fibril. Biochem. J. 43, 271–279.

Baldwin, R.L., Rose, G.D., 1999. Is protein folding hierarchic? I. Local structure and peptide folding. Trends Biochem. Sci. 24, 26-33.

Brown, J.H., Kim, K.H., Jun, G., Greenfield, N.J., Dominguez, R., Volkmann, N., Hitchcock-DeGregori, S.E., Cohen, C., 2001. Deciphering the design of the tropomyosin molecule. Proc. Natl. Acad. Sci. U.S.A. 98, 8496-8501.

Brown, J.H., Zhou, Z., Reshetnikova, L., Robinson, H., Yammani, R.D., Tobacman, L.S., Cohen, C., 2005. Structure of the mid-region of tropomyosin: bending and binding sites for actin. Proc. Natl. Acad. Sci. U.S.A. 102, 18878-18883.

Case, D.A., Cheatham, T.E. 3rd, Darden, T, Gohlke, H., Luo, R., Merz, K.M., Jr, Onufriev., A, Simmerling, C., Wang, B., Woods, R.J., 2005. The Amber biomolecular simulation programs. J. Comput. Chem. 26, 1668-1688.

Chandy, I.K., Lo, J.C., Ludescher., R.D., 1999. Differential mobility of skeletal and cardiac tropomyosin on the surface of F-actin. Biochemistry 38, 9286–9294.

Cho, Y.J., Hitchcock-DeGregori, S.E., 1991. Relationship between alternatively spliced exons and functional domains in tropomyosin. Proc. Natl. Acad. Sci. U.S.A. 88, 10153-10157.

Chou, P.Y., Fasman, G.D., 1978. Prediction of the secondary structure of proteins from their amino acid sequence. Adv. Enzymol. Relat. Areas Mol. Biol. 47, 45-148.

Chu, K.H., Wong, S.H, Leung, P.S., 2000. Tropomyosin is the major mollusk allergen: reverse transcriptase polymerase chain reaction, expression and IgE reactivity. Mar. Biotechnol. 2, 499-509.

Cooper, T.M., Woody, R.W., 1990. The effect of conformation on the CD of interacting helices: a theoretical study of tropomyosin. Biopolymers. 30, 657-676.

Corrêa, F., Farah, C.S., 2007. Different effects of trifluoroethanol and glycerol on the stability of tropomyosin helices and the head-to-tail complex. Biophys. J. 92, 2463-2475.

Coulton, A., Lehrer, S.S., Geeves, M.A., 2006. Functional homodimers and heterodimers of recombinant smooth muscle tropomyosin. Biochemistry 45, 12853-12858.

Coulton, A.T., Koka, K., Lehrer, S.S., Geeves, M.A., 2008. Role of the head-to-tail overlap region in smooth and skeletal muscle β-tropomyosin. Biochemistry 47, 388-397.

Crick, F.H.C., 1953. The packing of α-helices: simple coiled-coil. Acta Crystallogr. 6, 689-697.

Degani, Y., Patchornik, A., 1974. Cyanylation of sulfhydryl groups by 2-nitro-5-thiocyanobenzoic acid. High-yield modification and cleavage of peptides at cysteine residues. Biochemistry 13, 1-11.

Dong, H., Hartgerink, J.D., 2006. Short homodimeric and heterodimeric coiled coils. Biomacromolecules 7, 691-695.

Flicker, P. F., Phillips G.N., Jr., Cohen, C., 1982. Troponin and its interactions with tropomyosin. An electron microscope study. J. Mol. Biol. 162, 495-501.

Fraser, R.D., MacRae, T.P., Miller, A., 1969. X-ray diffraction patterns of alpha-fibrous proteins. J. Mol. Biol. 41, 87-94.

Fujinoki, M., Ueda, M., Inoue, T., Yasukawa, N., Inoue, R., Ishimoda-Takagi, T. 2006. Heterogeneity and tissue specificity of tropomyosin isoforms from four species of bivalves. Comp. Biochem. Physiol. B. Biochem. Mol. Biol. 143, 500-506.

Fujita, H., Yasuda, K., Niitsu, S., Funatsu, T., Ishiwata, S., 1996. Structural and functional reconstitution of thin filaments in the contractile apparatus of cardiac muscle. Biophys J. 71, 2307-2318.

Garnier, J., Gibrat, J.F., Robson, B., 1996. GOR method for predicting protein secondary structure from amino acid sequence. Methods Enzymol. 266, 540-553.

Geeves, M.A., Holmes, K.C., 2005. The molecular mechanism of muscle contraction. Adv. Protein Chem. 71, 161-193.

Goetz, D.W., Whisman, B.A., 2000. Occupational asthma in a seafood restaurant worker: cross-reactivity of shrimp and scallops. Ann. Allergy Asthma Immunol. 85, 461-466.

Gordon, A.M., Homsher, E., Regnier, M., 2000. Regulation of contraction in striated muscle. Physiol. Rev. 80, 853-924.

Greaser, M.L., Gergely, J., 1971. Reconstitution of troponin activity from three protein components. J. Biol. Chem. 246, 4226-4233.

Greaser, M.L., Gergely, J., 1973. Purification and properties of the components of troponin. J. Biol. Chem. 248, 2125-2133.

Greenfield, N.J., Hitchcock-DeGregori, S.E., 1993. Conformational intermediates in the folding of a coiled-coil model peptide of the N-terminus of tropomyosin and αα-tropomyosin. Protein Sci. 2, 1263-1273.

Greenfield, N.J., Stafford, W.F., Hitchcock-DeGregori, S.E., 1994. The effect of N-terminal acetylation on the structure of an N-terminal tropomyosin peptide and αα-tropomyosin. Protein Sci. 3, 402-410.

Greenfield, N.J., Hitchcock-DeGregori, S.E., 1995. The stability of tropomyosin, a two-stranded coiled-coil protein, is primarily a function of the hydrophobicity of residues at the helix-helix interface. Biochemistry 34, 16797-16805.

Greenfield, N.J., Montelione, G.T., Farid, R.S., Hitchcock-DeGregori, S.E., 1998. The structure of the N-terminus of striated muscle α-tropomyosin in a chimeric peptide: nuclear magnetic resonance structure and circular dichroism studies. Biochemistry 37, 7834-7843.

Greenfield, N.J., Swapna, G.V., Huang, Y., Palm, T., Graboski, S., Montelione, G.T., Hitchcock-DeGregori, S.E., 2003. The structure of the carboxyl terminus of striated α-tropomyosin in solution reveals an unusual parallel arrangement of interacting α-helices. Biochemistry 42, 614-619.

Greenfield, N.J., Huang, Y.J., Swapna, G.V., Bhattacharya, A., Rapp, B., Singh, A., Montelione, G.T., Hitchcock-DeGregori, S.E., 2006. Solution NMR structure of the

junction between tropomyosin molecules: implications for actin binding and regulation. J. Mol. Biol. 364, 80-96.

Grenklo, S., Hillberg, L., Zhao Rathje, L. S., Pinaev, G., Schutt, C.E., Lindberg, U., 2008. Tropomyosin assembly intermediates in the control of microfilament system turnover. Eur. J. Cell Biol. 87, 905-920.

Hammell, R.L., Hitchcock-DeGregori, S.E., 1996. Mapping the functional domains within the carboxyl terminus of α-tropomyosin encoded by the alternatively spliced ninth exon. J. Biol. Chem. 271, 4236-4242.

Hasegawa, Y., 2001. Complete nucleotide sequences of cDNA encoding for tropomyosin isoforms from the catch muscle of scallop *Patinopecten yessoensis*. Fish. Sci. 67, 988-990.

Heeley, D.H., Bieger, T., Waddleton, D.M., Hong, C., Jackman, D.M., McGowan, C., Davidson, W.S., Beavis, R.C., 1995. Characterization of fast, slow and cardiac muscle tropomyosins from salmonid fish. Eur. J. Biochem. 232, 226-234.

Holtzer, M.E., Holtzer, A., 1990. α-Helix to random coil transitions of two-chain coiled coils: experiments on the thermal denaturation of isolated segments of αα-tropomyosin. Biopolymers 30, 985-993.

Houmard, J., Drapeau, G.R., 1972. Staphylococcal protease: a proteolytic enzyme specific for glutamoyl bonds. Proc. Natl. Acad. Sci. U.S.A. 69, 3506-3509.

Huang, M.C., Ochiai, Y., Watabe, S., 2004. Structural and thermodynamic characterization of tropomyosin from fast skeletal muscle of bluefin tuna. Fish. Sci. 70, 667-674.

Huang, M.C., Ochiai, Y., 2005. Fish fast skeletal muscle tropomyosins show species-specific thermal stability. Comp. Biochem. Physiol. B 141, 461-471.

Ikeda, D., Toramoto, T., Ochiai, Y., Suetake, H., Suzuki, Y., Minoshima, S., Shimizu, N., Watabe, S., 2003. Identification of novel tropomyosin 1 genes of pufferfish (*Fugu rubripes*) on genomic sequences and tissue distribution of their transcripts. Mol. Biol. Rep. 30. 83-90.

Inglis, A.S., Edman, P., 1970. Mechanism of cyanogen bromide reaction with methionine in peptides and proteins. I. Formation of imidate and methyl thiocyanate. Anal. Biochem. 37, 73-80.

Inoue, A., Ojima, T., Nishita, K., 1996. Cloning and sequencing of a cDNA for akazara scallop troponin T. J. Biochem. 120, 834-837.

Inoue, A., Ojima, T., Nishita, K., 1999. Cloning and sequencing of cDNA for akazara scallop tropomyosin. Fish. Sci. 65, 772-776.

Inoue, A., Ojima, T., Nishita, K., 2004. N-terminal modification and its effect on the biochemical characteristics of akazara scallop tropomyosins expressed in *Escherichia coli*. J. Biochem. 136, 107-114.

Ishida, K., Konno, K., 1982. Characteristic properties of native tropomyosin and of troponin from squid mantle muscle. Nippon Suisan Gakkaishi 48, 843-849.

Ishikawa, M., Ishida, M., Shimakura, K., Nagashima, Y., Shiomi, K., 1998a. Tropomyosin, the major oyster *Crassostrea gigas* allergen and its IgE-binding epitopes. J. Food Sci. 63, 44-47.

Ishikawa, M., Ishida, M., Shimakura, K., Nagashima, Y., Shiomi, K., 1998b. Purification and IgE-binding epitopes of a major allergen in the gastropod *Turbo cornutus*. Biosci. Biotechnol. Biochem. 62, 1337-1343.

Ishikawa, M., Nagashima, Y., Shiomi, K., 1999. Immunological comparison of shellfish allergens by competitive enzyme-linked immunosorbent assay. Fish. Sci. 65, 592-595.

Ishimoda-Takagi, T., Kobayashi, M., and Yaguchi, M., 1986. Polymorphism and tissue specificity of scallop tropomyosin. Comp. Biochem. Physiol. B 83, 515-521.

Ishimoda-Takagi, T., Kobayashi, M., 1987. Molecular heterogeneity and tissue specificity of tropomyosin obtained from various bivalves. Comp. Biochem. Physiol. B 88, 443-452.

Iwasaki, K., Kikuchi, K., Funabara, D., and Watabe, S. 1997. cDNA cloning of tropomyosin from the anterior byssus retractor muscle of mussel and its structural integrity from the deduced amino acid sequence. Fish. Sci. 63, 731-734

Jackman, D.M., Waddleton, D.M., Younghusband, B., Heeley, D.H., 1996. Further characterisation of fast, slow and cardiac muscle tropomyosins from salmonid fish. Eur. J. Biochem. 242, 363-371.

Jaravine, V.A., Alexandrescu, A.T., Grzesiek, S., 2001. Observation of the closing of individual hydrogen bonds during TFE-induced helix formation in a peptide. Protein Sci. 10, 943-950.

Kluwe, L., Maeda, K., Miegel, A., Fujita-Becker, S., Maéda, Y., Talbo, G., Houthaeve, T., Kellner, R., 1995. Rabbit skeletal muscle αα-tropomyosin expressed in baculovirus-infected insect cells possesses the authentic N-terminus structure and functions. J. Muscle Res. Cell Motil. 16, 103-110.

Kyte, J., Doolittle, R.F., 1982. A simple method for displaying the hydropathic character of a protein. J. Mol. Biol. 157, 105-132.

Laemmli, U.K., 1970. Cleavage of structural proteins during the assembly of the head of bacteriophage T4. Nature 227, 680-685.

Lakkaraju, S.K., Hwang, W., 2009. Modulation of elasticity in functionally distinct domains of the tropomyosin coiled-coil. Cell. Mol. Bioeng. 2, 57–65.

Lehman, W., Hatch, V., Korman, V., Rosol, M., Thomas, L., Maytum, R., Geeves, M. A., Van Eyk, J. E., Tobacman, L. S., Craig, R., 2000. Tropomyosin and actin isoforms modulate the localization of tropomyosin strands on actin filaments. J. Mol. Biol. 302, 593-606.

Lehrer, S.B., McCants, M.L., 1987. Reactivity of IgE antibodies with crustacea and oyster allergens: evidence for common antigenic structures. J. Allergy Clin. Immunol. 80, 133-139.

Lehrer, S.S., Geeves, M.A., 1998. The muscle thin filament as a classical cooperative/allosteric regulatory system. J. Mol. Biol. 277, 1081-1089.

Leung, P.S., Chu, K.H., Chow, W.K., Ansari, A., Bandea, C.I., Kwan, H.S., Nagy, S.M., Gershwin, M.E., 1994. Cloning, expression, and primary structure of *Metapenaeus ensis* tropomyosin, the major heat-stable shrimp allergen. J. Allergy Clin. Immunol. 94, 882-890.

Leung, P.S., Chow, W.K., Duffey, S., Kwan, H.S., Gershwin, M.E., Chu, K.H., 1996. IgE reactivity against a cross-reactive allergen in crustacea and mollusca: evidence for tropomyosin as the common allergen. J. Allergy Clin. Immunol. 98, 954-961.

Li, Y., Mui, S., Brown, J.H., Strand, J., Reshetnikova, L., Tobacman, L.S., Cohen, C., 2002. The crystal structure of the C-terminal fragment of striated-muscle alpha-tropomyosin reveals a key troponin T recognition site. Proc. Natl. Acad. Sci. U.S.A. 99, 7378-7383.

Lorenz, M., Poole, K.J., Popp, D., Rosenbaum, G., Holmes, K.C., 1995. An atomic model of the unregulated thin filament obtained by X-ray fiber diffraction on oriented actin-tropomyosin gels. J. Mol. Biol. 246, 108-119.

Lu, S.M., Hodges, R.S., 2004. Defining the minimum size of a hydrophobic cluster in two-stranded alpha-helical coiled-coils: effects on protein stability. Protein Sci. 13, 714-26.

Lupas, A., Van Dyke, M., and Stock, J., 1991. Predicting coiled coils from protein sequences. Science 252, 1162-1164.

Lymn, R. W., Taylor, E. W., 1971. Mechanism of adenosine triphosphate hydrolysis by actomyosin. Biochemistry 10, 4617-4624.

Mak, A.S., Lewis, W.G., Smillie, L.B., 1979 Amino acid sequences of rabbit skeletal beta- and cardiac tropomyosins. FEBS Lett. 105, 232-234.

Maytum, R., Lehrer, S.S., Geeves, M.A., 1999. Cooperativity and switching within the three-state model of muscle regulation. Biochemistry 38, 1102-1110.

McKillop, D.F., Geeves, M.A., 1993. Regulation of the interaction between actin and myosin subfragment 1: evidence for three states of the thin filament. Biophys. J. 65, 693-701.

Mikita, C.P., Padlan, E.A., 2007. Why is there a greater incidence of allergy to the tropomyosin of certain animals than to that of others? Med. Hypotheses 69, 1070-1073.

Minakata, S., Maeda, K., Oda, N., Wakabayashi, K., Nitanai, Y., Maéda, Y., 2008. Two-crystal structures of tropomyosin C-terminal fragment 176-273: exposure of the hydrophobic core to the solvent destabilizes the tropomyosin molecule. Biophys. J. 95, 710-719.

Miyamoto, S., Kollman, P.A., 1992. SETTLE: An analytical version of the SHAKE and RATTLE algorithm for rigid water models. J. Comput. Chem. 13, 952-962.

Miyazawa, H., Fukamachi, H., Inagaki, Y., Reese, G., Daul, C.B., Lehrer, S.B., Inouye, S., Sakaguchi, M., 1996. Identification of the first major allergen of a squid (*Todarodes pacificus*). J. Allergy Clin. Immunol. 98, 948-953.

Monteiro, P.B., Lataro, R.C., Ferro, J.A., Reinach, F.C., 1994. Functional α-tropomyosin produced in *Escherichia coli*. A dipeptide extension can substitute the amino-terminal acetyl group. J. Biol. Chem. 269, 10461-10466.

Motoyama, K., Suma, Y., Ishizaki, S., Nagashima, Y, Shiomi, K., 2007. Molecular cloning of tropomyosins identified as allergens in six species of crustaceans. J. Agric. Food Chem. 55, 985-991.

Muñoz, V., Serrano, L., 1999. Development of the multiple sequence approximation within the AGADIR model of α-helix formation: comparison with Zimm-Bragg and Lifson-Roig formalisms. Biopolymers 41, 495-509.

Murakami, K., Stewart, M., Nozawa, K., Tomii, K., Kudou, N., Igarashi, N., Shirakihara, Y., Wakatsuki, S., Yasunaga, T., Wakabayashi, T., 2008. Structural basis for tropomyosin overlap in thin (actin) filaments and the generation of a molecular swivel by troponin-T. Proc. Natl. Acad. Sci. U.S.A. 105, 7200-7205.

Nelson, J.W., Kallenbach, N.R., 1986. Stabilization of the ribonuclease S-peptide alpha-helix by trifluoroethanol. Proteins 1, 211-217.

Nishita, K., Tanaka H., Ojima, T., 1994. Amino acid sequence of troponin C from scallop striated adductor muscle. J. Biol. Chem. 269, 3464-3468.

Nitanai, Y., Minakata, S. Maeda, K. Oda, N. Maeda, Y., 2007 Crystal structures of tropomyosin: flexible coiled-coil. Adv. Exp. Med. Biol. 592, 137–151.

Ochiai, Y., Ahmed, K., Ahsan, M.N., Funabara, D., Nakaya, M., Watabe, S., 2001. cDNA cloning and deduced amino acid sequence of tropomyosin from fast skeletal muscle of white croaker *Pennahia argentata*. Fish. Sci. 67, 556-558.

Ochiai, Y., Huang, M.C., Fukushima, H., Watabe, S., 2003. cDNA cloning and thermodynamic properties of tropomyosin from walleye pollack *Theragra chalcogramma*. Fish. Sci. 69, 1031-1039.

Ochiai Y, Ozawa H, Huang MC, Watabe S., 2010. Characterization of two tropomyosin isoforms from the fast skeletal muscle of bluefin tuna *Thunnus thynnus orientalis*. Arch. Biochem. Biophys. 502, 96-103.

Ohara, O., Dorit, R.L., Gilbert, W., 1989. One-sided polymerase chain reaction: the amplification of cDNA. Proc. Natl. Acad. Sci. U.S.A. 86, 5673-5677.

Ooi, T., Mihashi, K., Kobayashi, H., 1962. On the polymerization of tropomyosin. Arch. Biochem. Biophys. 98, 1-11.

Perry, S.V., 2001. Vertebrate tropomyosin: distribution, properties and function. J. Muscle Res. Cell Motil. 22, 5-49.

Phillips, G.N., Jr., Fillers, J.P., Cohen, C. 1980. Motions of tropomyosin. Crystal as metaphor. Biophys. J. 32, 485-502.

Phillips, G.N., Jr., Fillers, J.P., Cohen, C., 1986. Tropomyosin crystal structure and muscle regulation. J. Mol. Biol. 192, 111-131.

Pirani, A., Xu, C., Hatch, V., Craig, R., Tobacman, L. S., Lehman, W., 2005. Single particle analysis of relaxed and activated muscle thin filaments. J. Mol. Biol. 346, 761-772.

Poole, K.J., Lorenz, M., Evans, G., Rosenbaum, G., Pirani, A., Craig, R., Tobacman, L.S., Lehman, W., Holmes, K.C., 2006. A comparison of muscle thin filament

models obtained from electron microscopy reconstructions and low-angle X-ray fibre diagrams from non-overlap muscle. J. Struct. Biol. 155, 273-284.

Potekhin, S.A., Privalov, P.L., 1982. Co-operative blocks in tropomyosin. J. Mol. Biol. 159, 519-535.

Privalov, G., Kavina, V., Freire, E., Privalov, P.L., 1995. Precise scanning calorimeter for studying thermal properties of biological macromolecules in dilute solution. Anal. Biochem. 232, 79-85.

Robinson, P., Lipscomb, S., Preston, L.C., Altin, E., Watkins, H., Ashley, C.C., Redwood, C.S., 2007. Mutations in fast skeletal troponin I, troponin T, and beta-tropomyosin that cause distal arthrogryposis all increase contractile function. FASEB J. 21, 896-905.

Rao, V.S., Marongelli, E.N., Guilford, W.H., 2009. Phosphorylation of tropomyosin extends cooperative binding of myosin beyond a single regulatory unit. Cell Motil. Cytoskeleton 66, 10-23.

Sakuma, A., Kimura-Sakiyama, C., Onoue, A., Shitaka, Y., Kusakabe, T., Miki, M., 2006. The second half of the fourth period of tropomyosin is a key region for Ca^{2+}-dependent regulation of striated muscle thin filaments. Biochemistry 45, 9550-9558.

Schägger, H., Jagow, V.J., 1987. Tricine-sodium dodecyl sulfate-polyacrylamide gel electrophoresis for the separation of proteins in the range from 1 to 100 kDa. Anal. Biochem. 166, 368-379.

Smith, P.K., Krohn, R.I., Hermanson, G.T., Mallia, A.K., Gartner, F.H., Provenzano, M.D., Fujimoto, E.K., Goeke, N.M., Olson, B.J., Klenk, D.C., 1985. Measurement of protein using bicinchoninic acid. Anal. Biochem. 150, 76-85.

Sousa, A.D., Farah, C.S., 2002. Quantitative analysis of tropomyosin linear polymerization equilibrium as a function of ionic strength. J. Biol. Chem. 277, 2081-2088.

Stone, D., Smillie, L.B., 1978. The amino acid sequence of rabbit skeletal α-tropomyosin. The NH_2-terminal half and complete sequence. J. Biol. Chem. 253, 1137-1148.

Strelkov, S.V., Burkhard, P., 2002. Analysis of α-helical coiled coils with the program TWISTER reveals a structural mechanism for stutter compensation. J. Struct. Biol. 137, 54-64.

Takahashi, M., Morita, F., 1986. An activating factor (tropomyosin) for the superprecipitation of actomyosin prepared from scallop adductor muscles. J. Biochem. 99, 339-347.

Tanaka, H., Ojima T. Nishita. K., 1998. Amino acid sequence of troponin-I from akazara scallop striated adductor muscle. J. Biochem. 124, 304-310.

Tang, H.Y., Speicher, D.W., 2004. Identification of alternative products and optimization of 2-nitro-5-thiocyanatobenzoic acid cyanylation and cleavage at cysteine residues. Anal. Biochem. 334, 48-61.

Vibert, P., Craig, R., Lehman, W., 1997. Steric-model for activation of muscle thin filaments. J. Mol. Biol. 266, 8-14.

Wallimann, P., Kennedy, R.J., Miller, J.S., Shalongo, W., Kemp, D.S., 2003. Dual wavelength parametric test of two-state models for circular dichroism spectra of helical polypeptides: anomalous dichroic properties of alanine-rich peptides. J. Am. Chem. Soc. 125, 1203-1220.

Watabe, S., and Hashimoto, K. (1980) Studies on adductor muscle proteins of the scallop. 4. Isolation and characterization of scallop smooth adductor tropomyosin. Nippon Suisan Gakkaishi 46, 1183-1188

Whitby, F.G., Phillips, G.N., Jr., 2000. Crystal structure of tropomyosin at 7 Ångstroms resolution. Proteins 38, 49-59.

Wiechelman, K.J., Braun, R.D., Fitzpatrick, J.D., 1988. Investigation of the bicinchoninic acid protein assay: identification of the groups responsible for color formation. Anal. Biochem. 175, 231-237.

Yang, J.T., Wu, C.C., Martinez, H.M., 1986. Calculation of protein conformation from circular dichroism. Method. Enzymol. 130, 208-268.

Yoshimura, K., 1955. Studies on the tropomyosin of squid. Mem. Fac. Fish., Hokkaido Univ. 3, 159-176.

Table 1-1.

Estimation of the thermodynamic parameters for the unfolding of TMs based on the ellipticity at 222 nm as a function of temperature

Species	ΔH_1	ΔH_2	T_{M1}	T_{M2}	ε_1	ε_2	ΔG_{app}	T_{Mapp}
Japanese common squid	103	272	38.5	53.1	0.610	0.390	14.5	43.5
Tokobushi abalone	126	751	40.1	58.4	0.799	0.201	23.9	43.0
Kuruma prawn	110	850	32.5	48.2	0.347	0.653	50.2	47.3
Yesso scallop (striated muscle)	146	545	29.3	30.7	0.395	0.605	13.4	30.5
Yesso scallop (smooth muscle)	136	808	28.3	36.4	0.281	0.719	31.9	36.0
White croaker (Fish)	84	640	37.3	41.7	0.506	0.494	24.1	41.2

ΔH_n is the enthalpy in kJ/mol of the "n"th unfolding. T_{Mn} is the midpoints temperature (°C) of corresponding unfolding. ε_n is the decrement of the α-helical fraction of corresponding unfolding. ΔG_{app} is the apparent Gibbs free energy of unfolding at 20°C and T_{Mapp} is the temperature (°C) at which the ellipticity, normalized to a scale of 0-1, is equal to 0.5.

Table 1-2.

The thermostability and secondary structure prediction of TMs

Species	ΔG_{app} (kJ/mol) by CD	T_{Mapp} (°C) by CD	ΔG_{total} (kJ/mol) by DSC	Helix propensity [a]	Hydrophobicity [b]	Helical score [c]	Coiled-coil scor (%) [d]
Kuruma prawn	50.2	47.3	271	1.16	2.01	755	89.2
Japanese common squid	14.5	43.5	129	1.16	2.06	702	83.8
Tokobushi abalone	23.9	43.0	253	1.17	1.97	728	86.6
Yesso scallop (striated muscle)*	13.4	30.5	72	1.14	2.05	678	85.6
Yesso scallop (smooth muscle)*	31.9	36.0	110	1.15	1.97	710	86.9
White croaker (Fish)*	24.1	41.2	139	1.18	2.06	753	86.9

[a] Chou and Fasman (1978). Per residue.

[b] Kyte and Doolittle (1982). At the *a* and *d* residues and per residue.

[c] Calculated by GOR IV.

[d] Estimated by COILS.

Table 1-3.

Correlation between the thermostability and secondary structure prediction of TMs

	ΔG_{app} (kJ/mol)	T_{Mapp} (°C)	ΔG_{total} (kJ/mol)	Helix propensity [a]	Hydrophobicity [b]	Helical score [c]
ΔG_{app} (kJ/mol) by CD						
T_{Mapp} (°C) by CD	0.55					
ΔG_{total} (kJ/mol) by DSC	0.68	0.82				
Helix propensity [a]	0.13	0.68	0.50			
Hydrophobicity [b]	-0.43	-0.06	-0.43	0.13		
Helical score [c]	0.71	0.76	0.71	0.78	-0.10	
Coiled-coil score (%) [d]	0.91	0.33	0.62	0.17	-0.42	0.71

[a] Chou and Fasman (1978). Per residue.

[b] Kyte and Doolittle (1982). At the *a* and *d* residues and per residue.

[c] Calculated by GOR IV.

[d] Estimated by COILS.

Table 2-1. The α-helical content for the peptides (%)

Conditions	Nterm	Var	Mid	Cys	Cterm
Prediction at 5°C [a]	2.6	8.9	6.7	1.7	11.2
5°C, -TFE	5.4	10.3	8.0	3.9	21.6
5°C, 40% TFE	47.1	65.3	46.0	48.4	71.6
60°C, 40% TFE	19.2	35.3	20.4	19.9	36.6

[a] Estimated by AGADIR (Muñoz and Serrano, 1999).

Table 3-1. Estimation of the thermodynamic parameters for the unfolding of TM and its fragments based on the ellipticity at 222 nm as a function of temperature

	ΔH_1	ΔH_2	T_{M1}	T_{M2}	ε_1	ε_2	ΔG_{app}	T_{mapp}
TM	93	702	38.4	41.7	0.535	0.465	25.4	41.3
TM treated with 6 M guanidine-HCl (pH9.0)	112	782	39.9	59.7	0.925	0.075	13.6	41.1
TM treated with 7 M urea, 0.1M HCl	117	544	40.2	60.7	0.847	0.153	16.5	42.7
N-terminus (Met1-Lys189)	198	245	16.8	34.7	0.348	0.652	6.9	31.0
C-terminus (Cys190-Ile284)	155	306	24.9	36.2	0.319	0.681	11.7	34.3

Table 3-2. Sequence analysis for TMs and their fragments

	GOR VI [a]	COILS [b]
White croaker TM	92.3%	86.9%
White croaker Met1-Lys189	90.0%	87.9%
White croaker Cys190-Ile284	88.4%	89.4%
Rabbit TM	94.5%	89.3%
Rabbit Met1-Lys190	95.2%	92.3%
Rabbit Cys190-Ile284	87.3%	82.9%

[a] Predicted α-helical contents. [b] Coiled-coil probability.

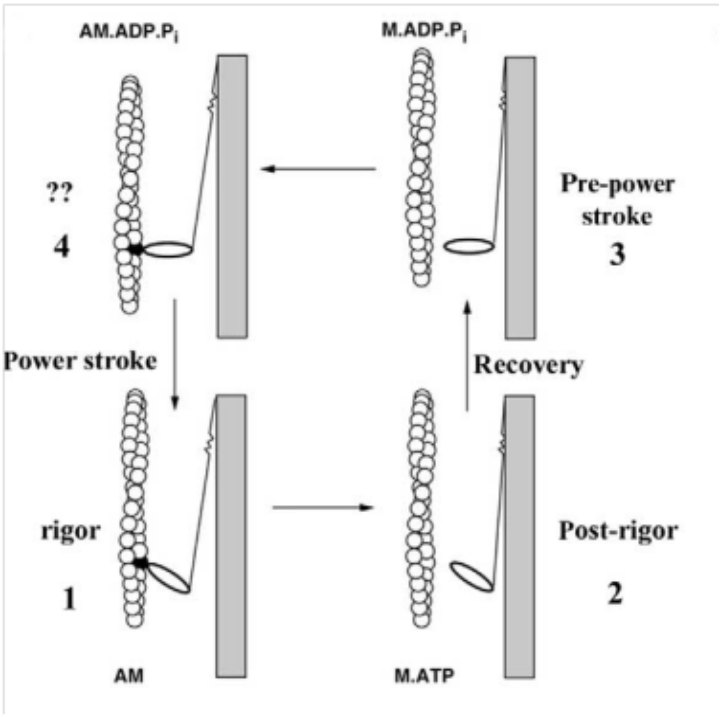

Fig. 0-1. The crossbridge cycle with annotation. The binding of ATP to the actin–myosin complex (1) leads to rapid dissociation of the crossbridge from actin, but without hydrolysis of ATP (2). The crossbridge then undergoes a conformational change (recovery stroke) that puts the lever arm in the prepowerstroke or ‘‘UP’’ conformation (3). This form is the ATPase. Subsequent rebinding to actin (4) leads to product release and the moving ‘‘DOWN’’ of the lever arm (powerstroke). Species 1, 2, and 3 have been named on the basis of three crystal structures. No crystal structure analogous to species 4 has been defined to date and its exact form is poorly defined. Cited from Geeves and Holmes (2005).

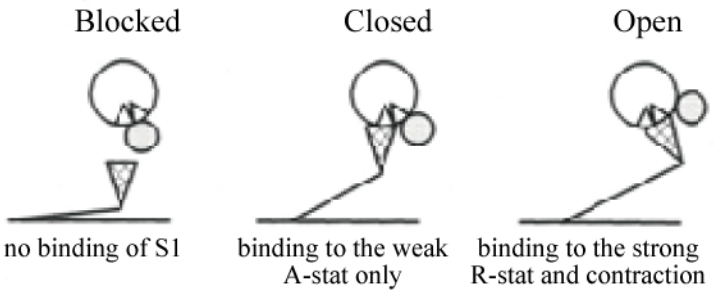

Fig. 0-2. A diagrammatic representation of a direct steric blocking version of the three-state model. Formally this is identical to the two-state model with the addition of the blocked state which does not bind S1. As shown here in the blocked state, TM prevents all binding of Sl to actin. In the closed state, Tn moves to uncover a binding site which allows S1 to form the relatively weakly bound A state. In the open state, the full interaction of S1 with actin is possible and the R state is occupied. Cited from McKillop and Geeves (1993).

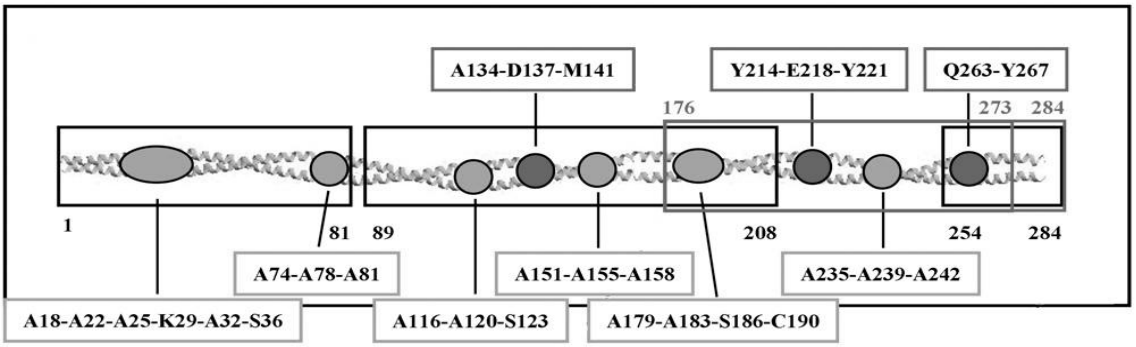

Fig. 0-3. Alanine clusters (Ala18-Ala22-Ala25-Lys29-Ala32-Ser36, Ala74-Ala78-Ala81, Ala116-Ala120-Ser123, Ala151-Ala155-Ala158, Ala179-Ala183-Ser186-Cys190, Ala235-Ala239-Ala242) and the breaks in hydrophobic core (Ala134-Asp137-Met141, Tyr214-Glu218-Tyr221, Gln263-Tyr267) are shown. The crystal structures of large TM fragments have been determined: the residues between the 1st and 81st (PDB ID: 1IC2) by Brown et al. (2001), the residues between the 89th and the 208th (PDB ID: 2B9C) by Brown et al. (2005), the residue between the 176th and 273rd (PDB ID: 2EFR and 2EFS) by Minakata et al. (2008), and the residues between the 176th and 284th (PDB ID: 2D3E) by Nitanai et al. (2007). Cited from Minakata et al. (2008).

```
                1       10        20        30        40        50        60
                ....|....|....|....|....|....|....|....|....|....|....|....|
heptad position abcdefgabcdefgabcdefgabcdefgabcdefgabcdefgabcdefgabcdefgabcd
sm TM-1         MDAIKKKMQAMKVDRENAQDLAEQMEQKLKDTETAKAKLEEDFNDLQKKLTTTENNFDVA
sm TM-2         ............................................................
sm TM-3         ............................................................

               61       70        80        90        100       110       120
                ....|....|....|....|....|....|....|....|....|....|....|....|
heptad position efgabcdefgabcdefgabcdefgabcdefgabcdefgabcdefgabcdefgabcdefga
sm TM-1         NEQLQEANVKLENSEKQITQLESGVGALQRRLQLLEEDFERSEEKLLTTTEKLEEASKAA
sm TM-2         ............................................................
sm TM-3         ............................................................

               121       130       140       150       160       170       180
                ....|....|....|....|....|....|....|....|....|....|....|....|
heptad position bcdefgabcdefgabcdefgabcdefgabcdefgabcdefgabcdefgabcdefgabcde
sm TM-1         DESERNRKVLEGRSNTSDERIDVLEKQLDSAKTVATDADTKFDEAARKLAITEVDLERAE
sm TM-2         .....G.....S..LAD.....A..A..KE..YI.E...R.Y..................
sm TM-3         .....G.....S..LAD.....A..A..KE..YI.E...R.Y..................

               181       190       200       210       220       230       240
                ....|....|....|....|....|....|....|....|....|....|....|....|
heptad position fgabcdefgabcdefgabcdefgabcdefgabcdefgabcdefgabcdefgabcdefgab
sm TM-1         TRLEAADAKVHELEEELTVVGANIKTLQVQNDQASQREDSYEETIRDLTKNLKDAENRAT
sm TM-2         ..........L......K...N.M.S.EISEQE...........................
sm TM-3         ............................................................

               241       250       260       270       280
                ....|....|....|....|....|....|....|....|....
heptad position cdefgabcdefgabcdefgabcdefgabcdefgabcdefgabcd
sm TM-1         EAERQVVKLQKEVDRLEDELLAEKERYKQISDELDQTFAEIAGY
sm TM-2         ............................................
sm TM-3         ............................................
```

Fig. 1-1. Sequence alignment of Yesso scallop *Mizuhopecten yessoensis* smooth muscle tropomyosins (TMs). Sm TM-1, sm TM-2 and sm TM-3 were reported by Hasegawa (2001).

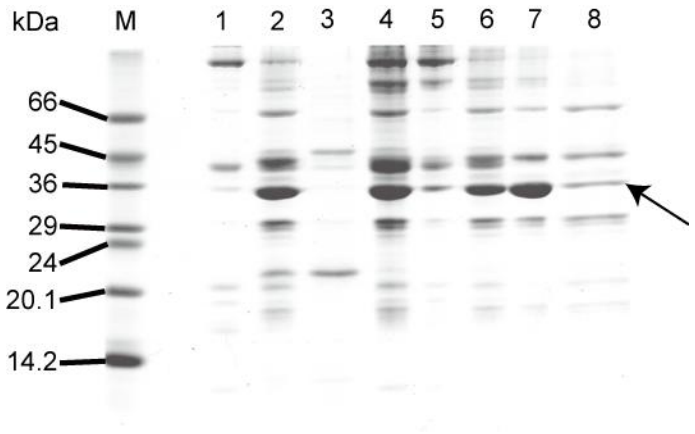

Fig. 1-2. SDS-PAGE patterns of each step of kuruma prawn (*Marsupenaeus japonicus*) TM preparation. M, marker (SDS-7); 1 and 2, the precipitate and supernatant of 20 mM Tris-HCl (pH 7.5) containing 1 M KCl and 5 mM 2-mercaptoethanol; 3 and 4, the supernatant and precipitate at pH 4.5; 5 and 6, the precipitate and supernatant at pH 7.6; 7 and 8, precipitate and supernatant at 40% saturation of ammonium sulfate. The arrow indicates tropomyosin (TM). 15% gel.

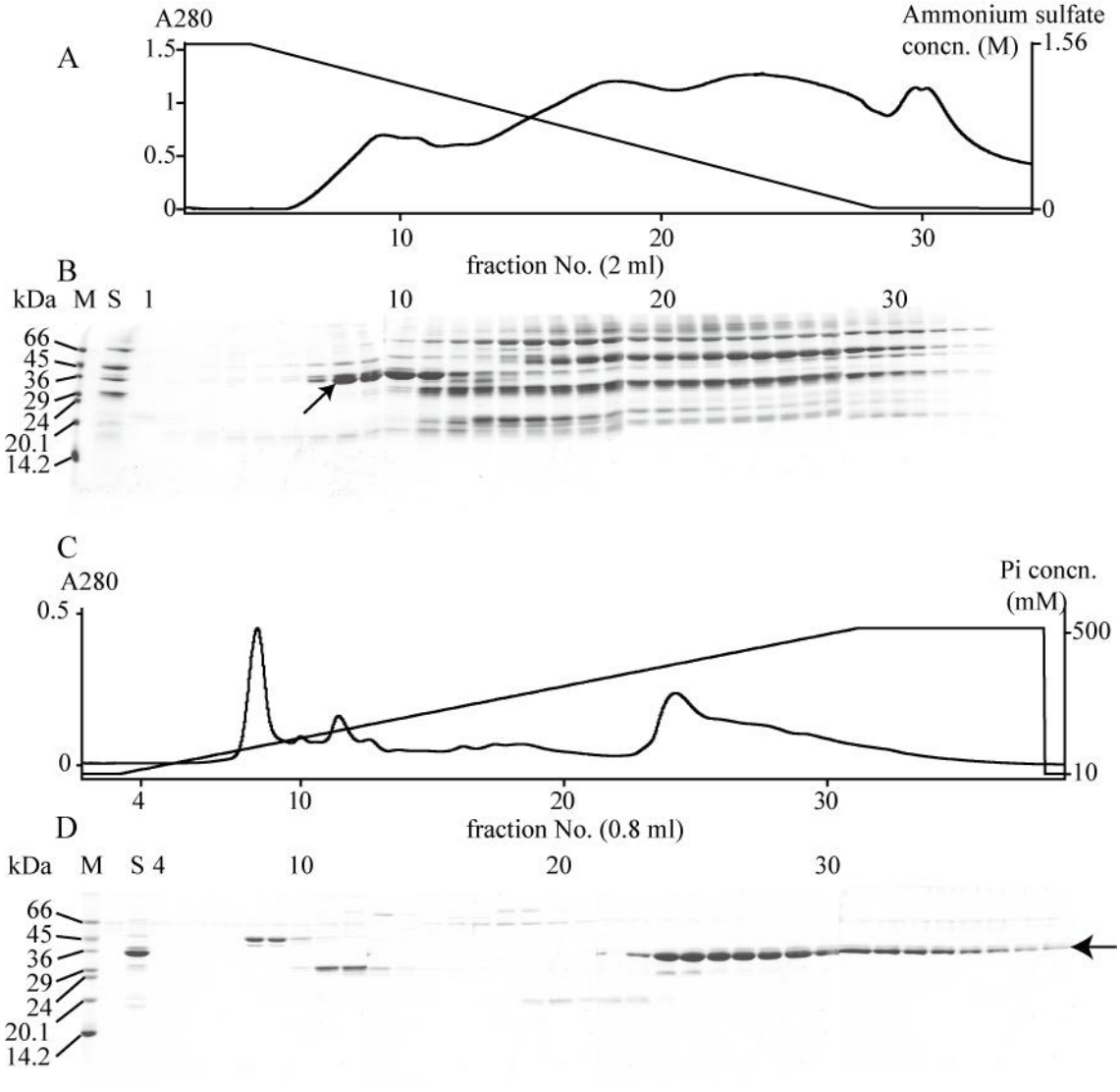

Fig. 1-3. Elution pattern of the prawn TM from a TSKgel BioAssist Phenyl column (0.78 × 5 cm) (A) and Mono Q^{TM} 5/50 GL column (0.5 × 5 cm) (C). The proteins were eluted by the linear gradient from 1.56 M to 0 M ammonium sulfate in the presence of 20 mM potassium phosphate buffer (pH 7.0) (A) and by the linear gradient from 10 mM to 500 mM potassium phosphate buffer (pH 7.0) in the presence of 1 mM DTT (C). (B, D) SDS-PAGE patterns of the fractions obtained by chromatography in (A, C). M, marker (SDS-7); S, the loaded sample. Each number on the top of gel corresponds to the fraction number in (A, C). The fractions 1-4 and 1-3 are the flow through fractions in (A) and (C), respectively. Fractions (8-11 in A) were further applied to the next chromatography. The arrow indicates TM. 15% gel. TM was eluted at 1.5.-1.2 M ammonium sulfate by HIC and 350-500 mM potassium phosphate buffer by AEX.

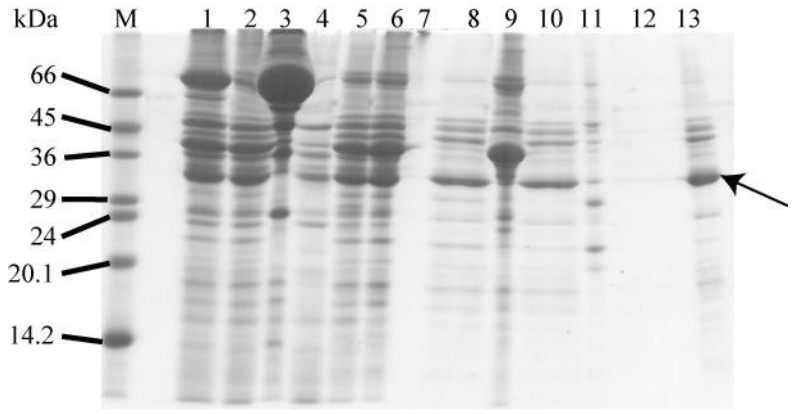

Fig. 1-4. SDS-PAGE patterns of each step of Japanese common squid TM preparation. M, marker (SDS-7); 1, crude extract of acetone powder; 2 and 3, the supernatant and precipitate at 0.1 M KCl; 4 and 5, the supernatant and precipitate at pH 4.5; 6 and 7, the supernatant and precipitate at pH 7.6; 8 and 9, supernatant and precipitate at 40% ammonium sulfate saturation; 10 and 11, supernatant and precipitate at 50% saturation; 12 and 13, supernatant and precipitate at 70% saturation. 15% gel. The arrow indicates TM.

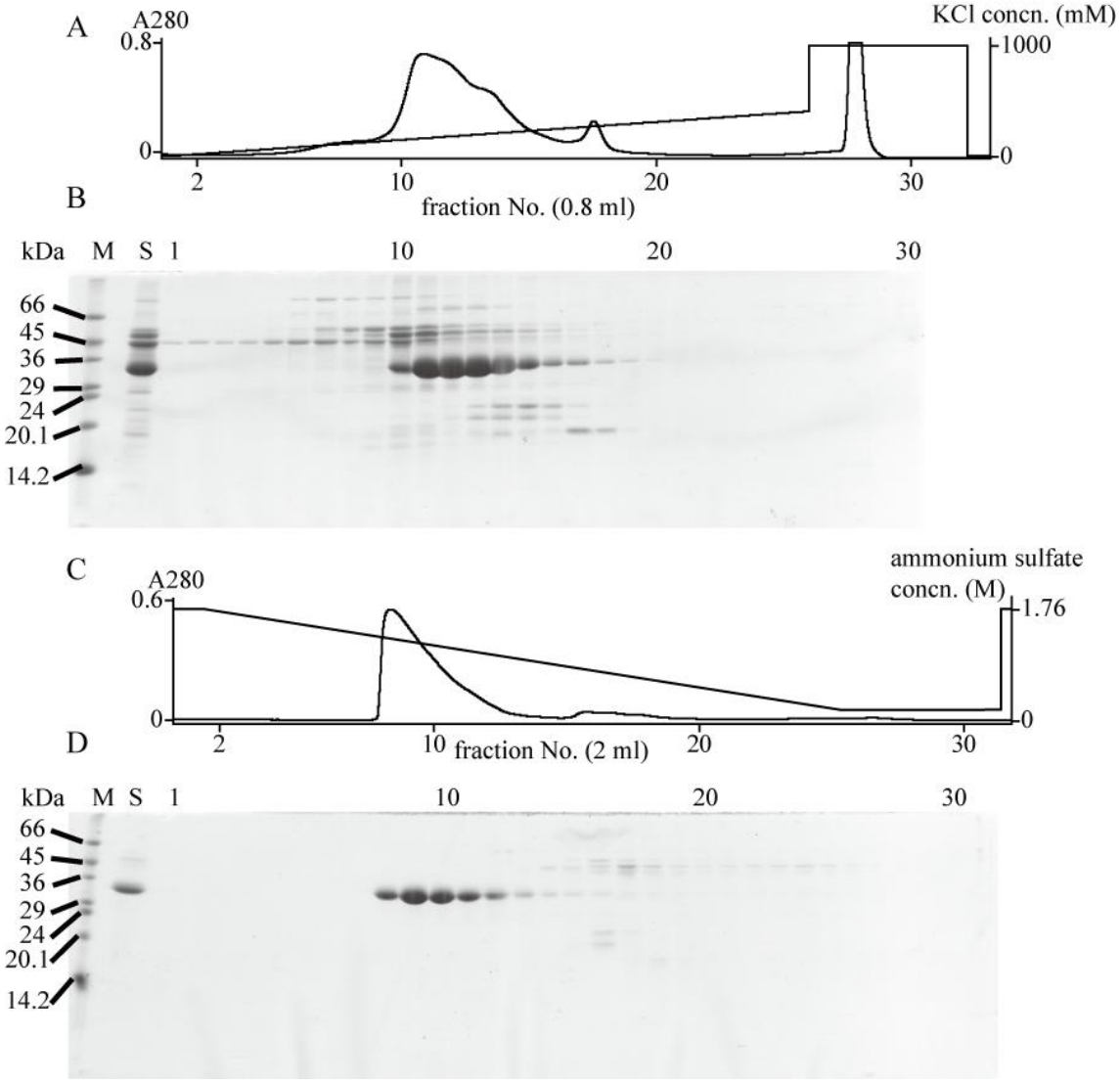

Fig. 1-5. Elution pattern of the squid TM from a Mono Q^{TM} 5/50 GL column (0.5 × 5 cm) (A) and a TSKgel BioAssist Phenyl column (0.78 × 5 cm) (C). The proteins were eluted by the linear gradient from 150 mM to 490 mM KCl in the presence 50 mM potassium phosphate buffer (pH 7.0) and 1 mM DTT (A) and by the linear gradient from 1.76 M to 0 M ammonium sulfate in the presence of 20 mM potassium phosphate buffer (pH 7.0) (C). (B, D) M, marker (SDS-7); S, the loaded sample. Each number on the top of the gel corresponds to the fraction number in (A, B). The fraction 1 is the flow through fraction. 15% gel. Fractions (11-14 in B) were further applied to the subsequent HIC. TM was eluted at 250-300 mM KCl by AEX and 1.3-1.1 M ammonium sulfate by HIC.

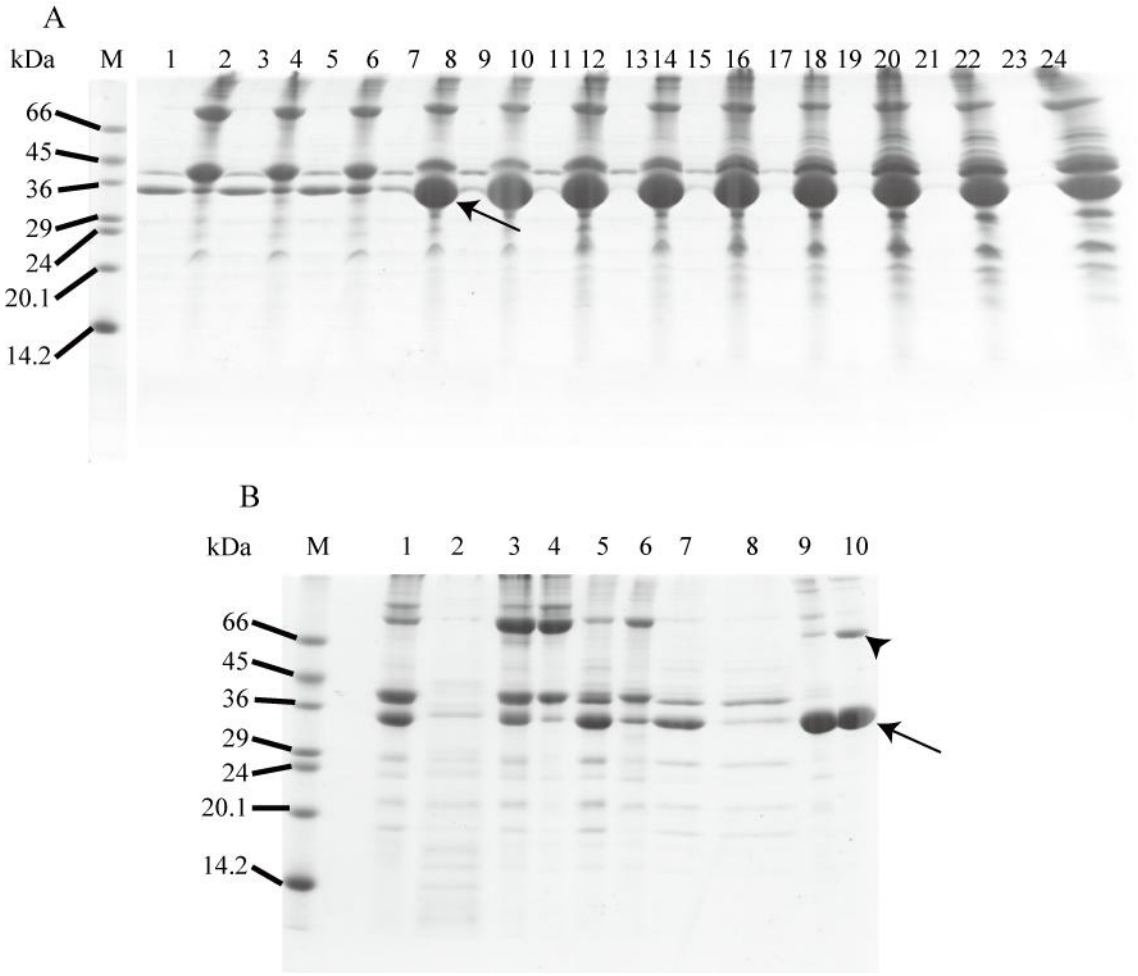

Fig. 1-6. (A) SDS-PAGE patterns of tokobushi abalone TM of ammonium sulfate saturation supernatants and precipitates. M, marker (SDS-7); lanes 1, 3, 5, 7, 9, 11, 13, 15, 17, 19, 21, and 23: supernatants at 32.5%, 35%, 37.5%, 40%, 42.5%, 45%, 47,5% 50%, 52.5%, 55%, 57.5%, and 60% ammonium sulfate saturation, respectively. Lanes 2, 4, 6, 8, 10, 12, 14, 16, 18, 20, 22, and 24: precipitates at 32.5%, 35%, 37.5%, 40%, 42.5%, 45%, 47.5% 50%, 52.5%, 55%, 57.5%, and 60% ammonium sulfate saturation, respectively. 15% gel. The arrow indicates TM. (B) SDS-PAGE patterns of each step of the abalone TM preparation. M, marker (SDS-7); 1, crude extract of acetone powder; 2 and 3, the supernatant and precipitate at pH 4.5; 4 and 5, the precipitate and supernatant at pH 7.6; 6 and 7, the precipitate and supernatant at 35% ammonium sulfate saturation; 8 and 9, supernatant and precipitate at 45% saturation; 10 after repeated isoelectric precipitation and ammonium sulfate fractionation. 15% gel. The arrow head and the arrow indicate dimer and monomer of TM.

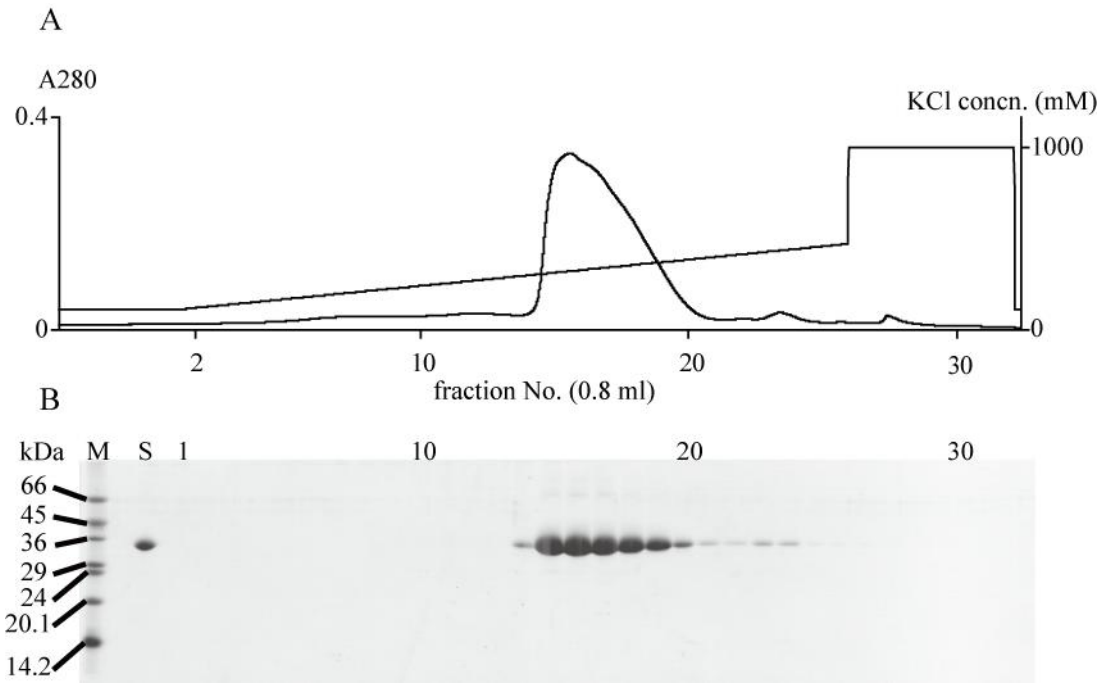

Fig. 1-7. Elution pattern of TM from a Mono Q^{TM} 5/50 GL column (0.5 × 5 cm) of the abalone TM. (A) The proteins were eluted by the linear gradient from 150 mM to 490 mM KCl in the presence of 50 mM potassium phosphate buffer (pH 7.0) and 1 mM DTT. (B) SDS-PAGE patterns of the fractions obtained by the chromatography in (A). M, marker (SDS-7); S, the loaded sample. Each number on the top of the gel corresponds to the fraction number in (A). The fraction 1 is the flow through fraction. 15% gel. TM was mainly eluted in the fractions 14-20, namely at around 300 mM KCl.

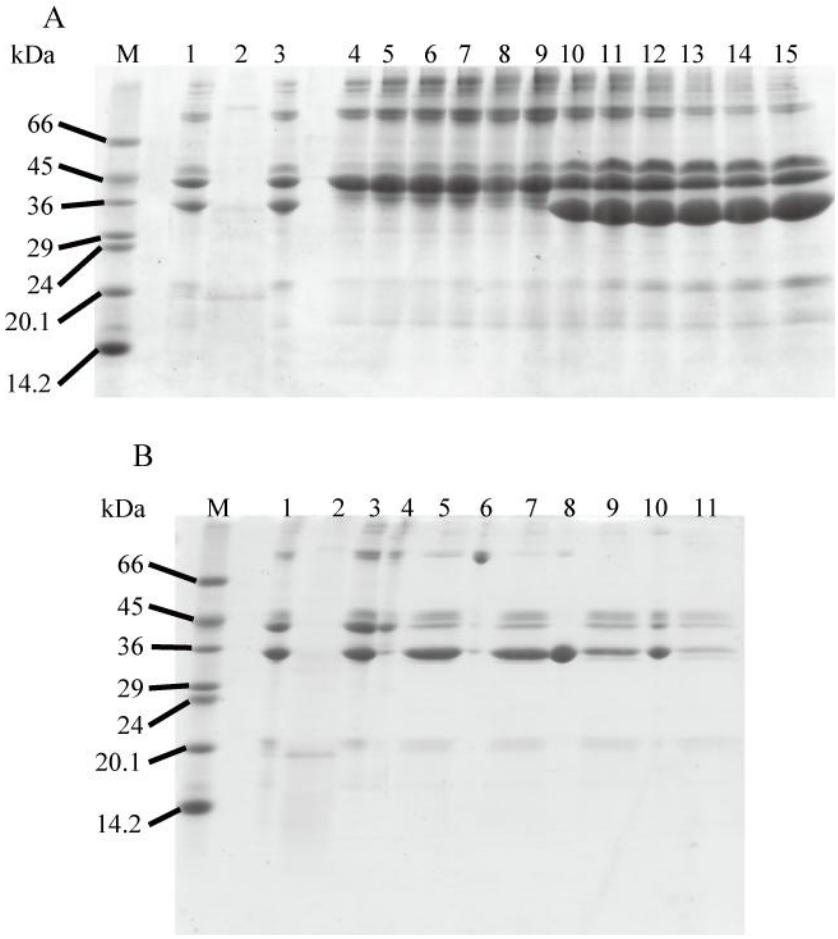

Fig. 1-8. (A) SDS-PAGE patterns of each step of the scallop striated muscle TM preparation. M, marker (SDS-7); 1, crude extract of acetone powder; 2 and 3, the supernatant and precipitate at pH 4.5; 4, 5, 6, 7, 8, 9, 10, 11, 12, 13, 14, and 15, precipitate at 15%, 20%, 25%, 30%, 35%, 40%, 45%, 50%, 55%, 60%, 65%, and 70% ammonium sulfate saturation. 15% gel. (B) SDS-PAGE patterns of each step of TM preparation. M, marker (SDS-7); 1, crude extract of acetone powder; 2 and 3, the supernatant and precipitate at pH 4.5; 4 and 5, the precipitate and supernatant at 30% saturation of ammonium sulfate; 6 and 7, precipitate and supernatant at 40% saturation of ammonium sulfate; 8 and 9, precipitate and supernatant at 45% saturation of ammonium sulfate; 10 and 11, precipitate and supernatant at 45% saturation of ammonium sulfate. 15% gel.

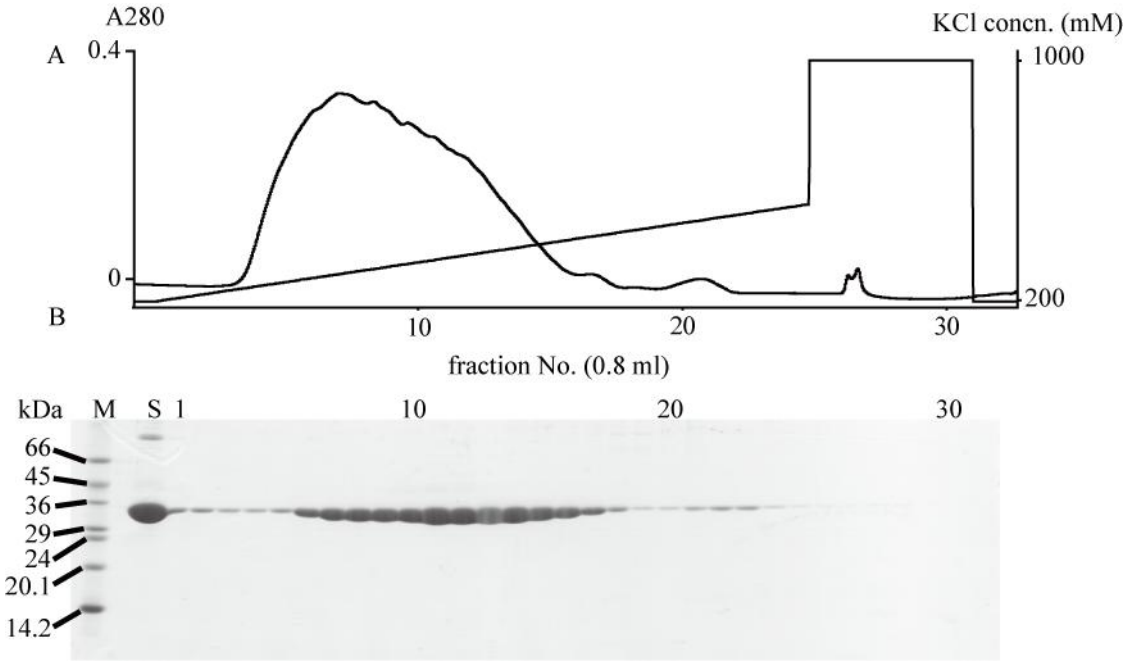

Fig. 1-9. Elution pattern of 40-45% ammonium sulfate saturation fraction of the scallop striated muscle from a Mono Q^{TM} 5/50 GL column (0.5 × 5 cm) (A). The proteins were eluted by the linear gradient from 200 mM to 520 mM KCl (pH 7.0) in the presence of 10 mM KPB (pH 7.0) and 1 mM DTT. (B) SDS-PAGE patterns of the fractions obtained by the chromatography in (A). M, marker (SDS-7); S, the loaded sample. Each number on the top of the gel corresponds to the fraction number in (A). The fractions 1 and 2 are the flow through fractions. 15% gel. TM was eluted at 240-330 mM KCl by AEX (Fig. 3-8). In AEX, TM was detected by SDS-PAGE in the flow through fractions because too much protein was loaded.

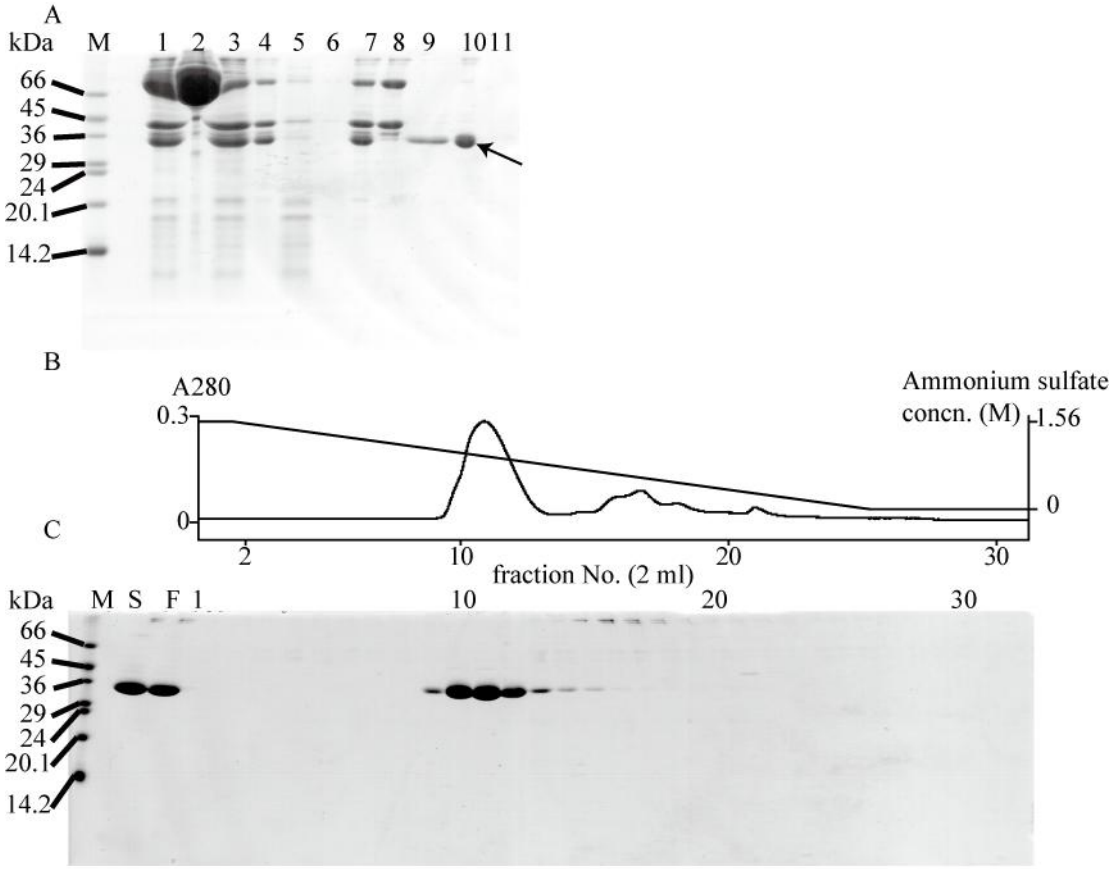

Fig. 1-10. (A) SDS-PAGE patterns of each step of smooth muscle TM of the scallop smooth muscle preparation. M, marker (SDS-7); 1, crude extract of acetone powder; 2 and 3, the precipitate and supernatant at 0.1 M KCl; 4 and 5, the precipitate and supernatant at pH 4.5; 6 and 7, the precipitate and supernatant at pH 7.6; 8 and 9, the precipitate and supernatant at 35% ammonium sulfate saturation; 10 and 11, the precipitate and supernatant at 50% saturation. 15% gel. The arrow indicates TM. (B, C) Elution pattern of smooth muscle of the scallop TM from a TSKgel BioAssist Phenyl column (0.78 × 5 cm) and SDS-PAGE patterns of the fractions obtained by chromatography. The proteins were eluted by the linear gradient from 1.56 M to 0 M ammonium sulfate in the presence of 20 mM potassium phosphate buffer (pH 7.0) (B). M, marker (SDS-7); S, the sample before filtration; F, the loaded sample. Each number on the top of gel corresponds to the fraction number in (B). The fraction 1 is the flow through fraction. 15% gel. TM was eluted at 1.3-1.1 M ammonium sulfate by HIC. Filtration with the filter cartridge (Minisart RC 15, pore size 0.20 μm, Sartorius) before chromatography did not affect the purity of TM.

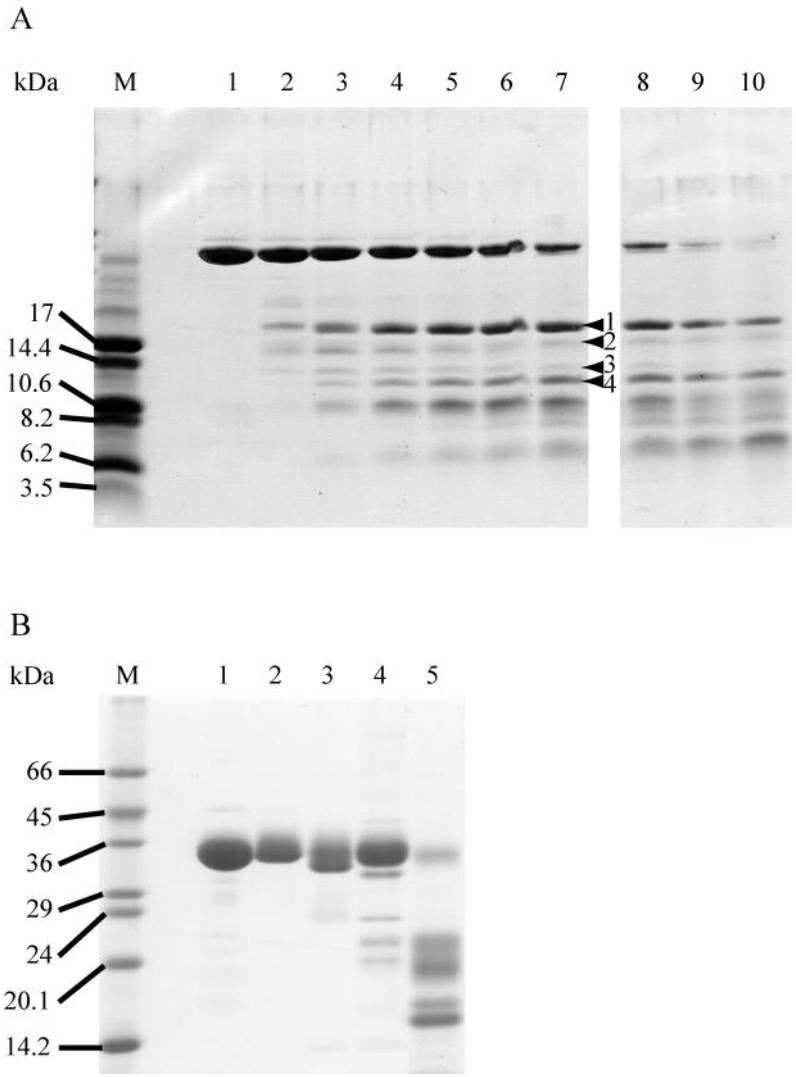

Fig. 1-11. (A) Tris-Tricine PAGE patterns of the endoproteinase Arg-C digest of the scallop smooth adductor muscle TM. TM at a concentration of 2 mg/ml was dissolved in 8.5 mM $CaCl_2$, 5 mM DTT, 0.5 mM EDTA and 90 mM Tris-HCl (pH 7.6) with 5 μg/ml endoproteinase Arg-C and digested at 30°C. M, marker (SDS-17S); 1, undigested TM. Digestion time; 2, 5 min; 3, 15 min; 4, 30 min; 5, 45 min; 6, 60 min; 7, 1.5 hours; 8, 2 hours; 9, 3 hours; 10, 4 hours. 16% gel. The arrowheads indicate the bands 1 through 4 analyzed by Edman method. (B) SDS-PAGE patterns of CNBr-treated TMs. M, marker (SDS-7); 1, smooth muscle TM before CNBr treatment; 2, smooth muscle TM treated with 0.1M HCl and 7M urea; 3, smooth muscle TM after CNBr treatment; 4, white croaker TM treated by 0.1M HCl and 7M urea; 5, white croaker TM after CNBr treatment. White croaker TM was used as a positive control. 15% gel.

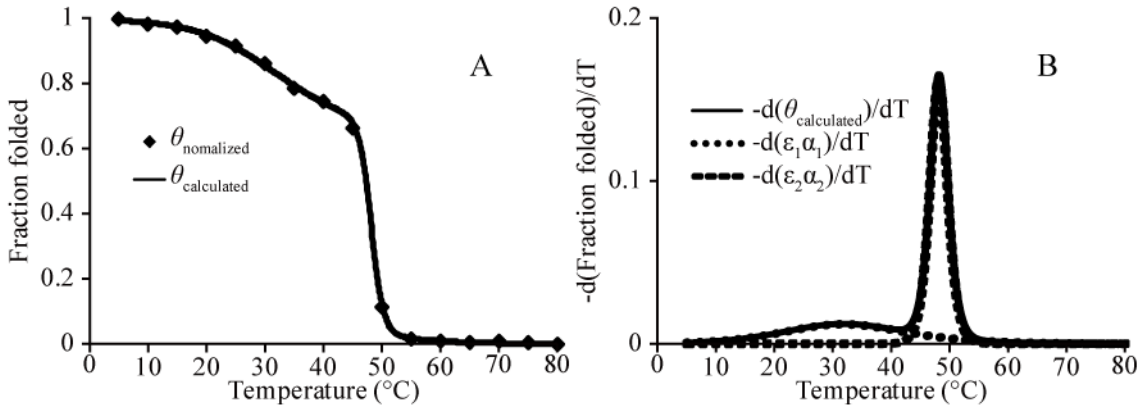

Fig. 1-12. CD analysis on the temperature dependent unfolding of the prawn TM. (A) $[\theta]_{normalized}$ (dot) was obtained by normalizing CD data and $[\theta]_{calculated}$ (line) based on the analysis. (B) Two independent helix-coil transitions.

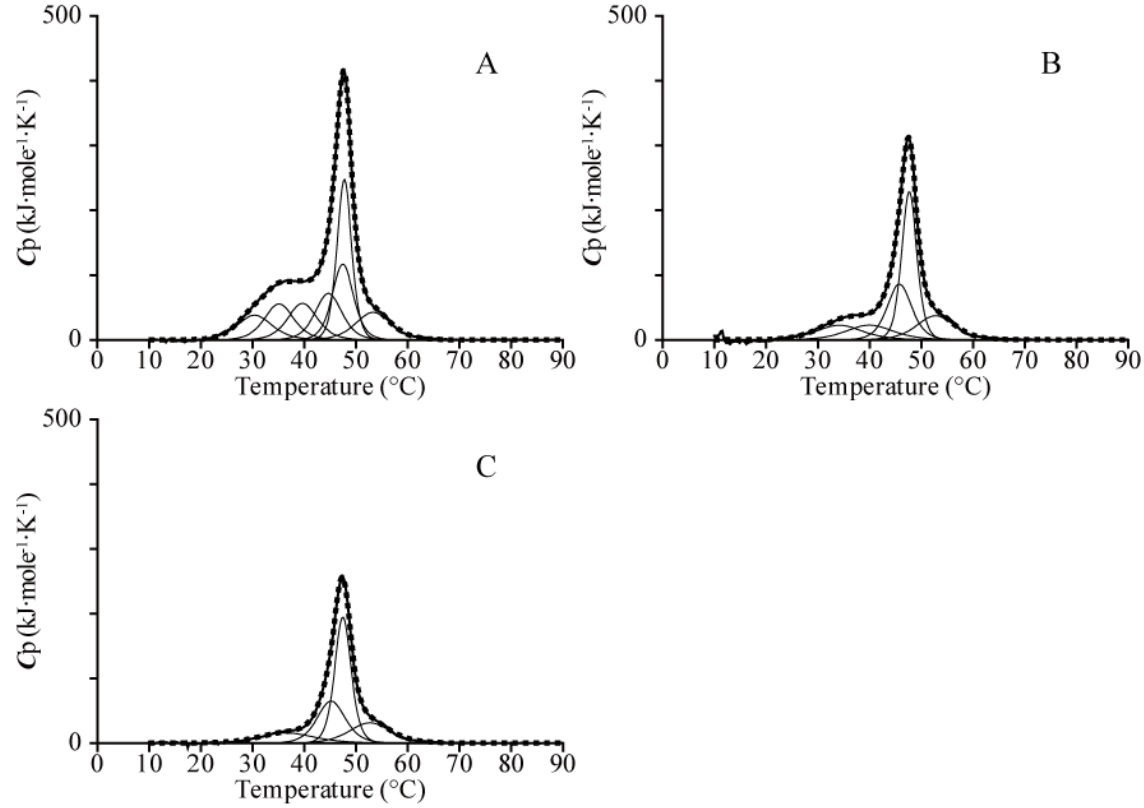

Fig. 1-13. DSC scans of the prawn TM. The observed DSC pattern and the sum of subsequent deconvolution analysis are shown with solid and dotted lines and the subsequent analysis is shown with thin line. The DSC data were subtracted with a progress baseline, and analyzed as a dimer. A, 1st scan; B, 2nd scan; C, 3rd scan.

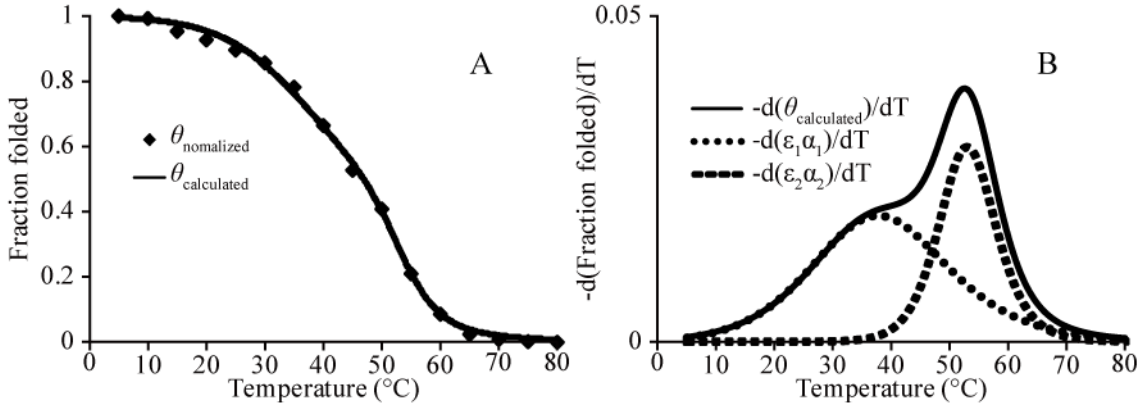

Fig. 1-14. CD analysis on the temperature dependent unfolding of the squid TM. (A) $[\theta]_{normalized}$ (dot) was obtained by normalizing CD data and $[\theta]_{calculated}$ (line) based on the analysis. (B) Two independent helix-coil transitions.

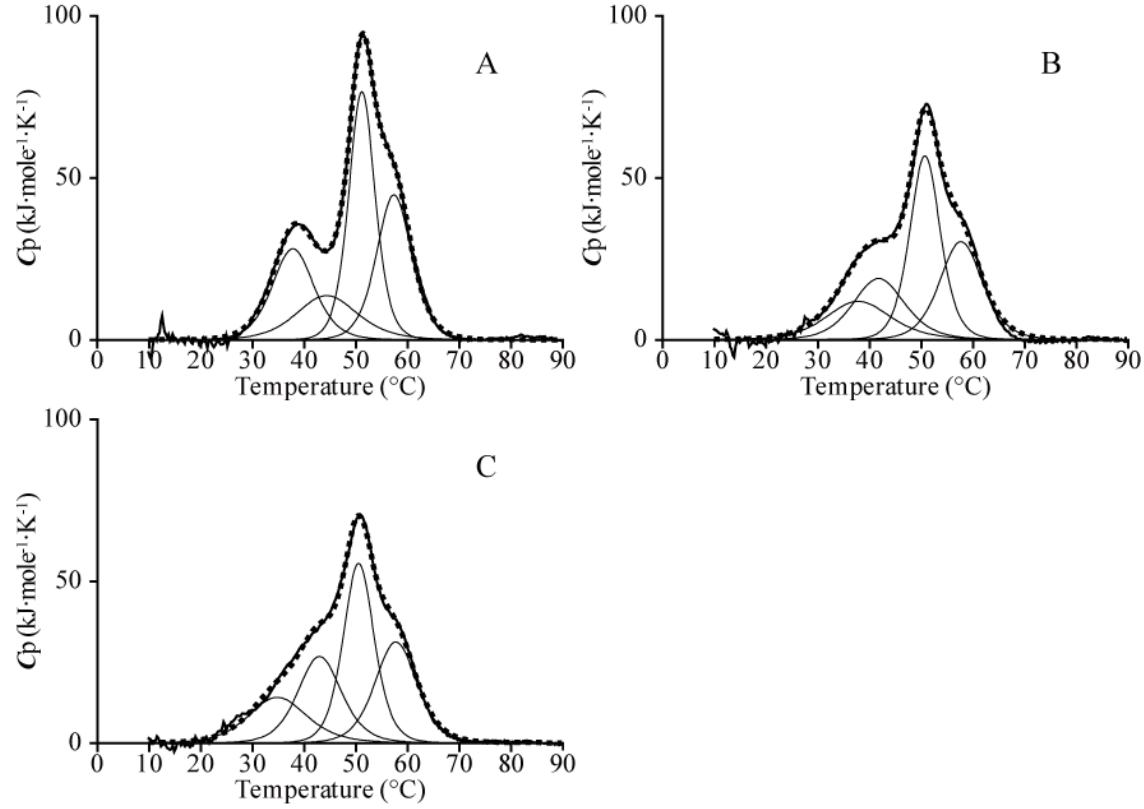

Fig. 1-15. DSC scans of the squid TM. The observed DSC pattern and the sum of subsequent deconvolution analysis are shown with solid and dotted lines and the subsequent analysis is shown with thin line. The DSC data were subtracted with a progress baseline, and analyzed as a dimer. A, 1st scan; B, 2nd scan; C, 3rd scan.

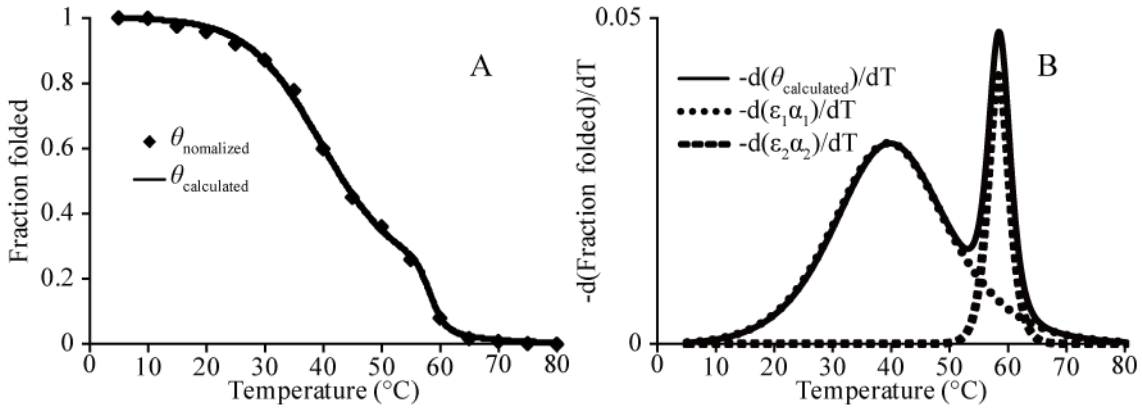

Fig. 1-16. CD analysis on the temperature dependent unfolding of the abalone TM. (A) $[\theta]_{normalized}$ (dot) was obtained by normalizing CD data and $[\theta]_{calculated}$ (line) based on the analysis. (B) Two independent helix-coil transitions.

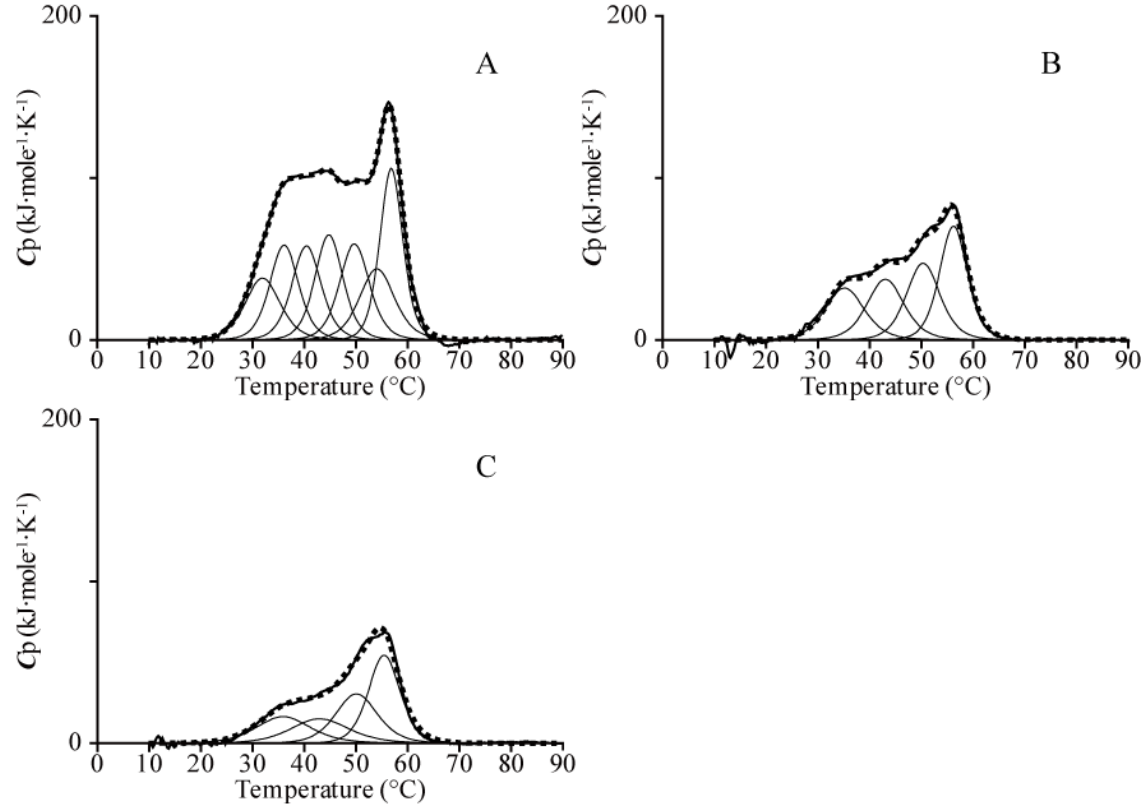

Fig. 1-17. DSC scans of the abalone TM. The observed DSC pattern and the sum of subsequent deconvolution analysis are shown with solid and dotted lines and the subsequent analysis is shown with thin line. The DSC data were subtracted with a progress baseline, and analyzed as a dimer. A, 1st scan; B, 2nd scan; C, 3rd scan.

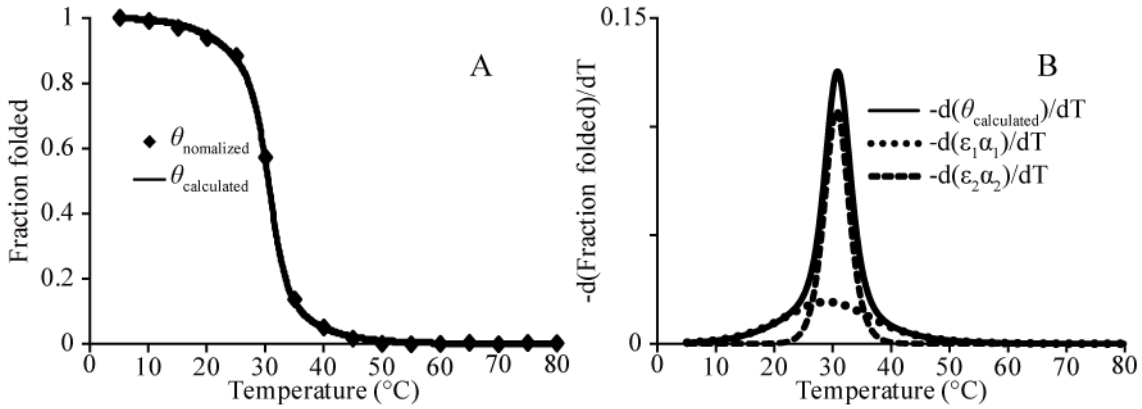

Fig. 1-18. CD analysis on the temperature dependent unfolding of the scallop striated adductor muscle TM. (A) $[\theta]_{normalized}$ (dots) was obtained by normalizing CD data and $[\theta]_{calculated}$ (line) based on the analysis. (B) Two independent helix-coil transitions.

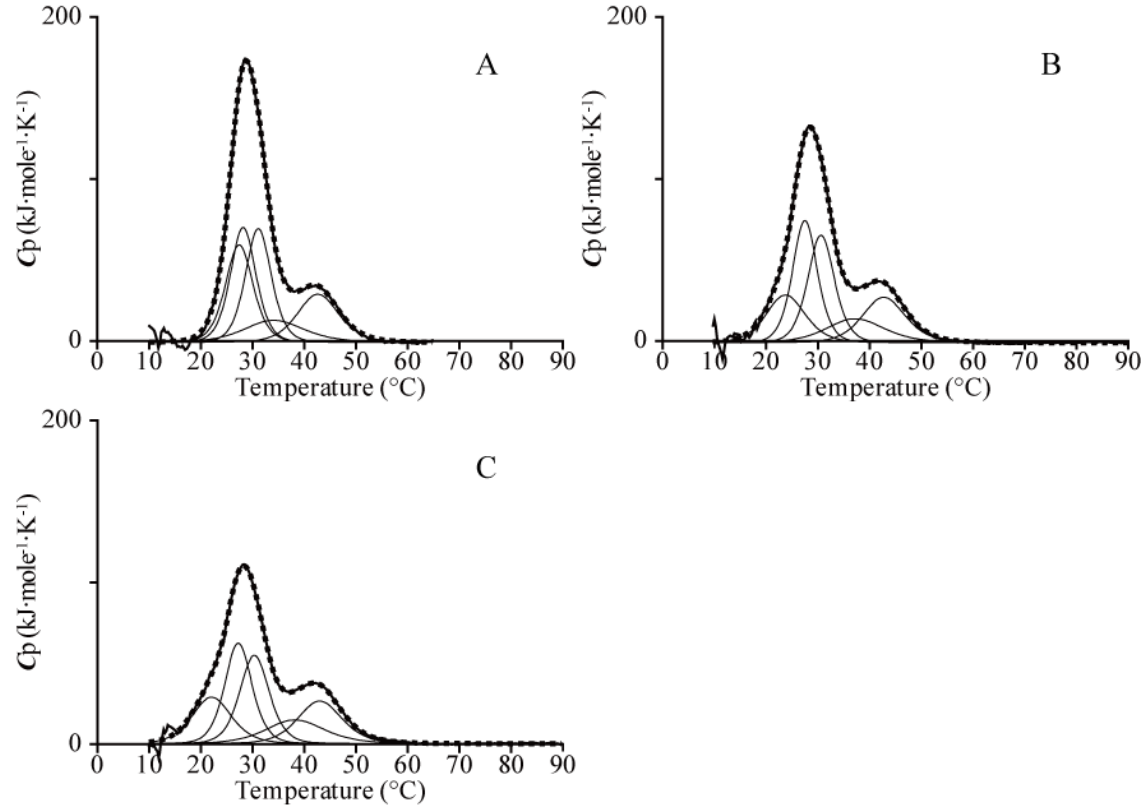

Fig. 1-19 DSC scans of the scallop striated adductor muscle TM. The observed DSC pattern and the sum of subsequent deconvolution analysis are shown with solid and dotted lines and the subsequent analysis is shown with a thin line. The DSC data were subtracted with a progress baseline, and analyzed as a dimer. A, 1st scan; B, 2nd scan; C, 3rd scan.

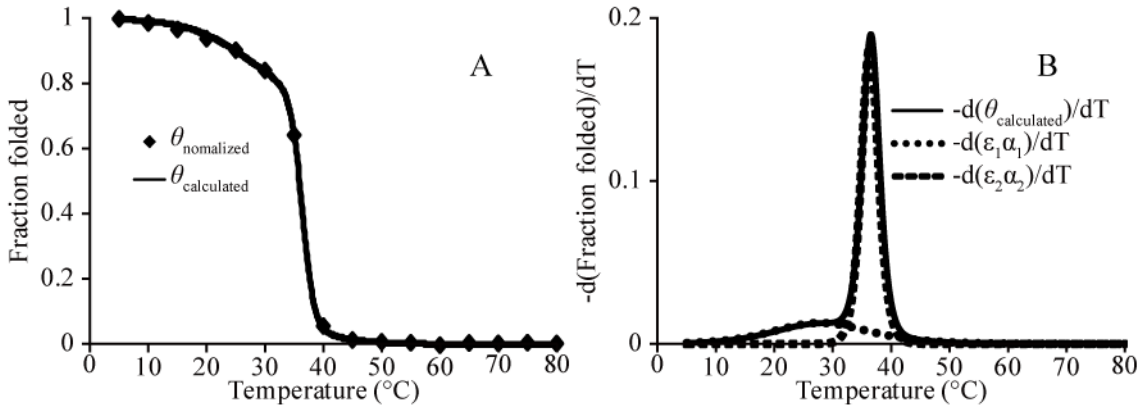

Fig. 1-20. CD analysis on the temperature dependent unfolding of the scallop smooth muscle TM. (A) $[\theta]_{normalized}$ (dots) was obtained by normalizing CD data and $[\theta]_{calculated}$ (line) based on the analysis. (B) Two independent helix-coil transitions.

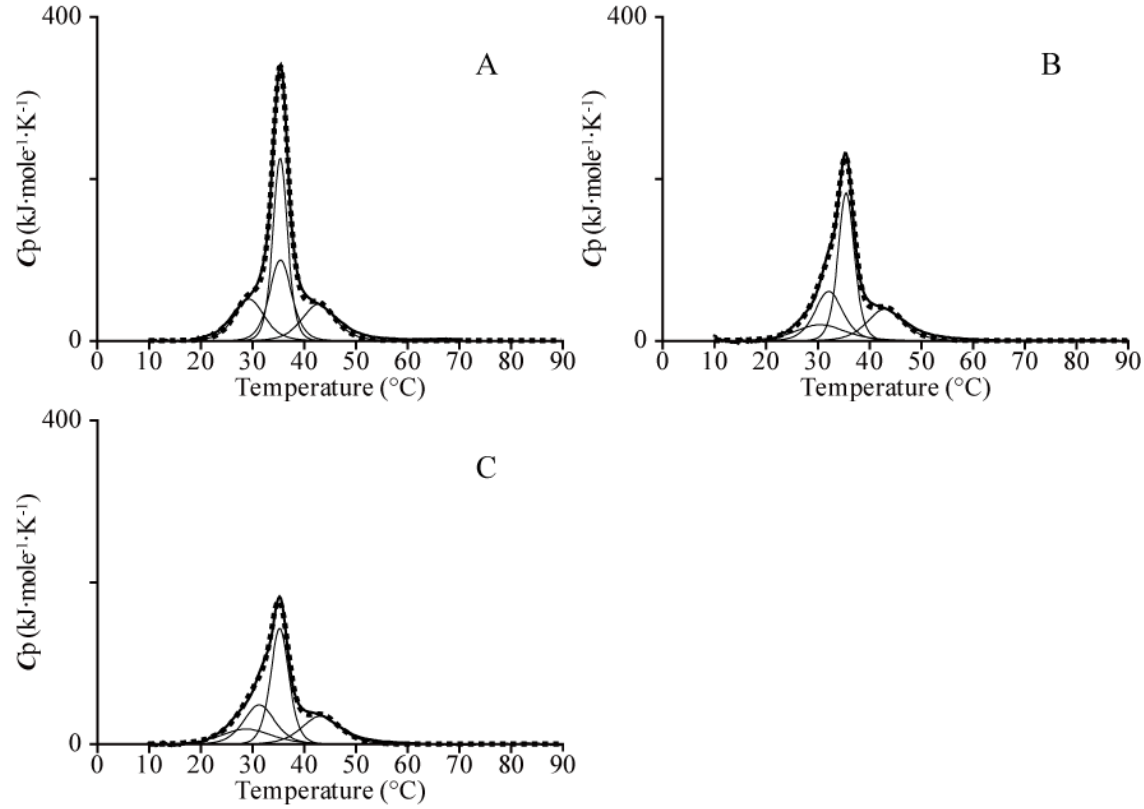

Fig. 1-21. DSC scans of the scallop smooth muscle TM. The observed DSC pattern and the sum of subsequent deconvolution analysis are shown with solid and dotted lines and the subsequent analysis is shown with a thin line. The DSC data were subtracted with a progress baseline, and analyzed as a dimer. A, 1st scan; B, 2nd scan; C, 3rd scan.

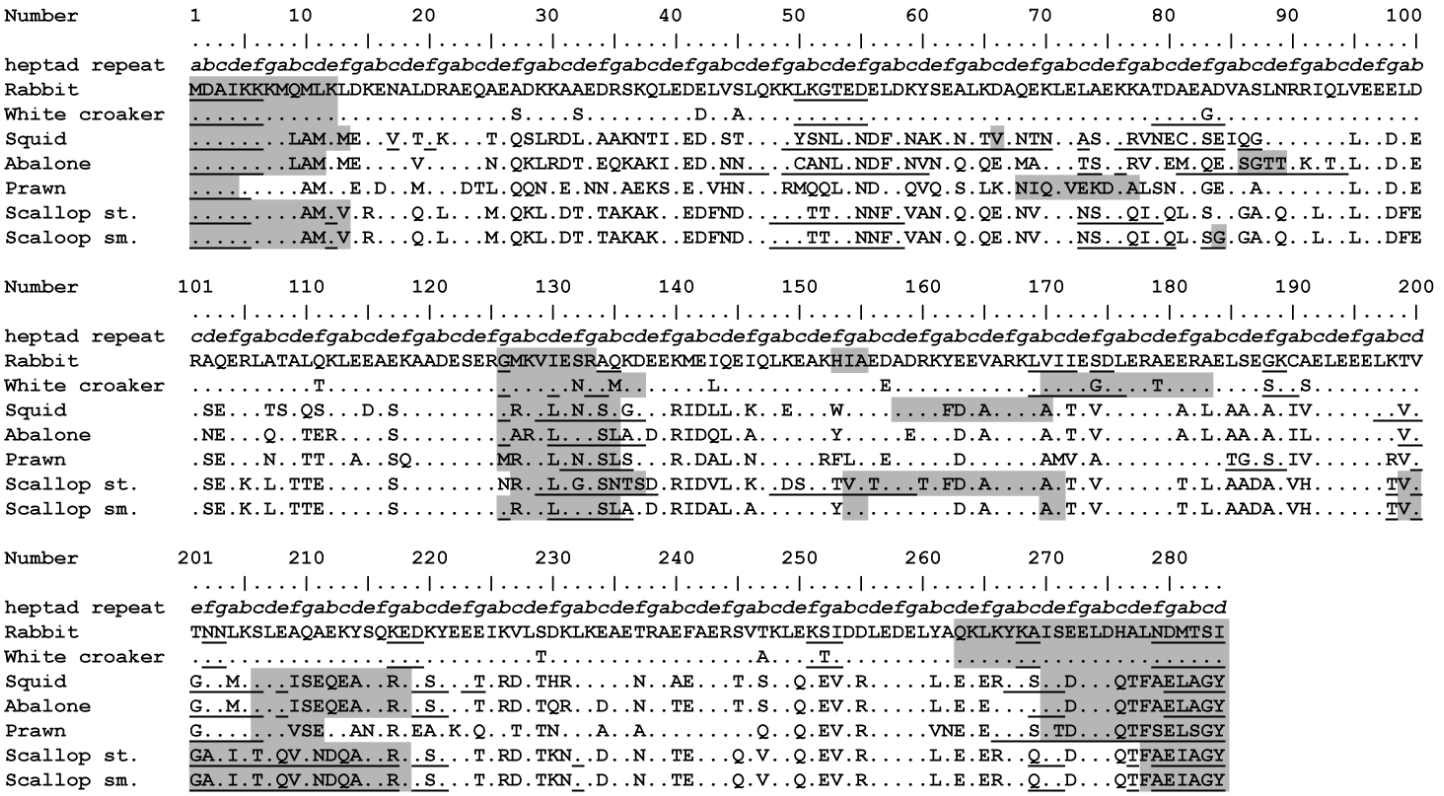

Fig. 1-22. Amino acid sequence alignment of TM. Accession numbers are: rabbit (AAB34957), white croaker (BAB20881), Japanese common squid (BAE54431), tokobushi abalone (AAG08987), kuruma prawn (BAF47263), Yesso scallop *Mizuhopecten yessoensis* striated muscle (BAA20455) and smooth muscle (BAB17857) TMs. The positions where the helical score by GOR IV are lower than 0.6 are underlined. The positions where the coiled-coil score by COILS are lower than 0.8 are shaded. The heptad repeats (*abcdefg*) are indicated in the first lines. Abbreviations: st, striated muscle; sm, smooth muscle. Identical residues with that of rabbit TM are indicated by dots.

Fig. 2-1. The sequence of walleye pollack TM and the location of five synthetic peptides. Peptide Nterm corresponds to Met1-Lys30, Peptide Var to Asp84-Leu113, Peptide Mid to Val128-Ala157, Peptide Cys to Leu176-Lys205, and Peptide Cterm to Asp255-Ile284. At the top of each row is shown the positions of heptad repeat (*a-g*).

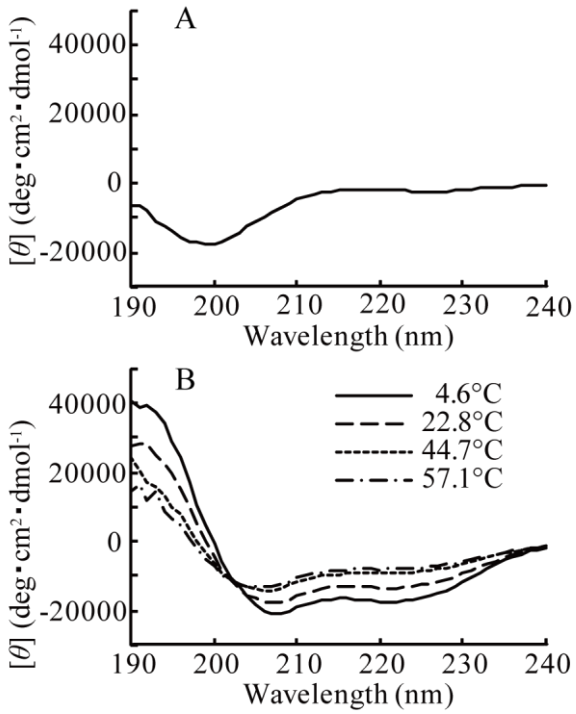

Fig. 2-2. CD spectra of Peptide Nterm. (A) The CD spectrometry of Peptide Nterm in the absence of TFE at 5.7°C. (B) CD spectra of Peptide Nterm in the presence of 40 % TFE at respective temperatures.

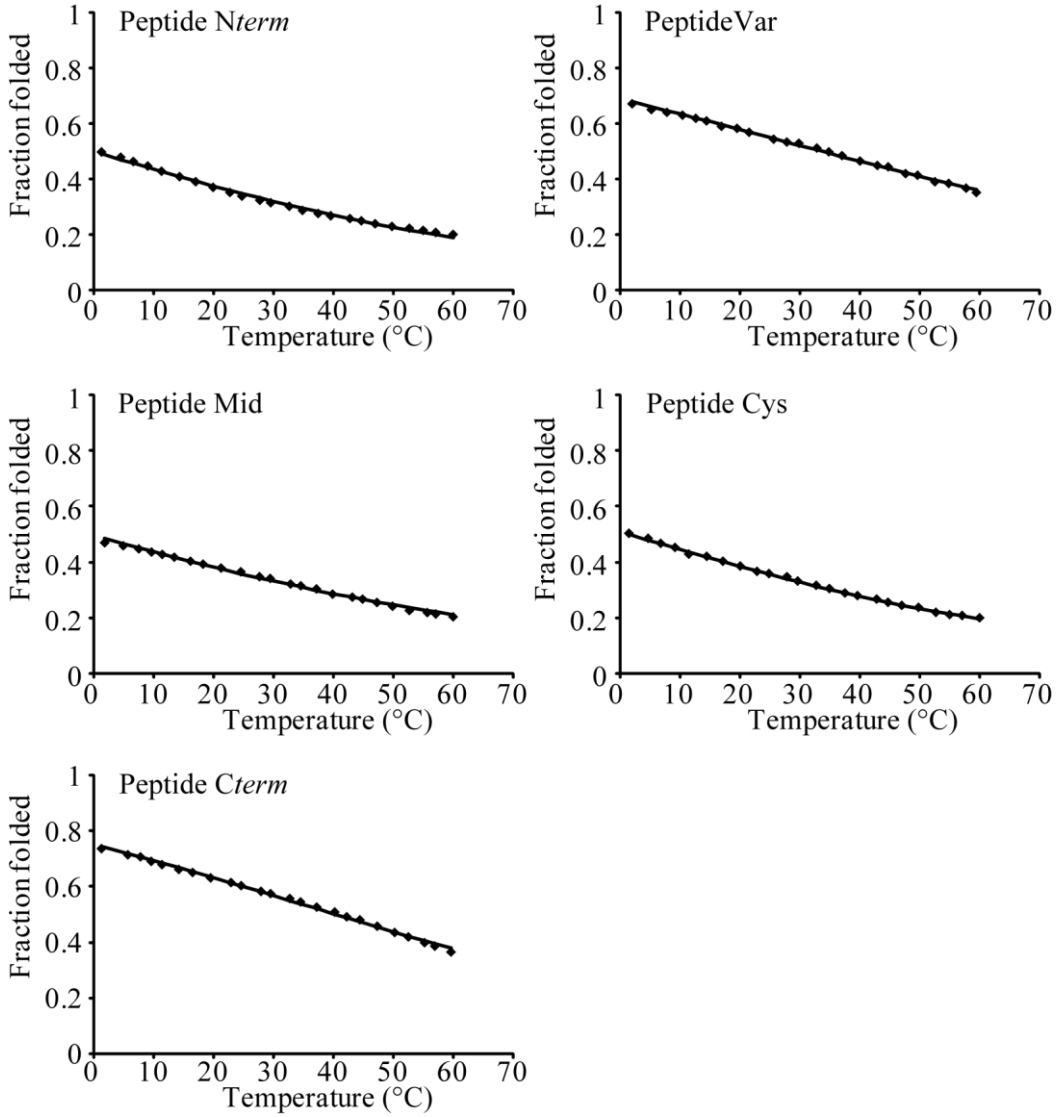

Fig. 2-3. The α-helical value of fraction folded for synthetic peptides in 10 mM sodium phosphate (pH 7.0) containing 0.1 M KCl, 1 mM DTT, 0.01% NaN_3, and 40% TFE. Peptide concentration was 1.0 mg/ml.

.

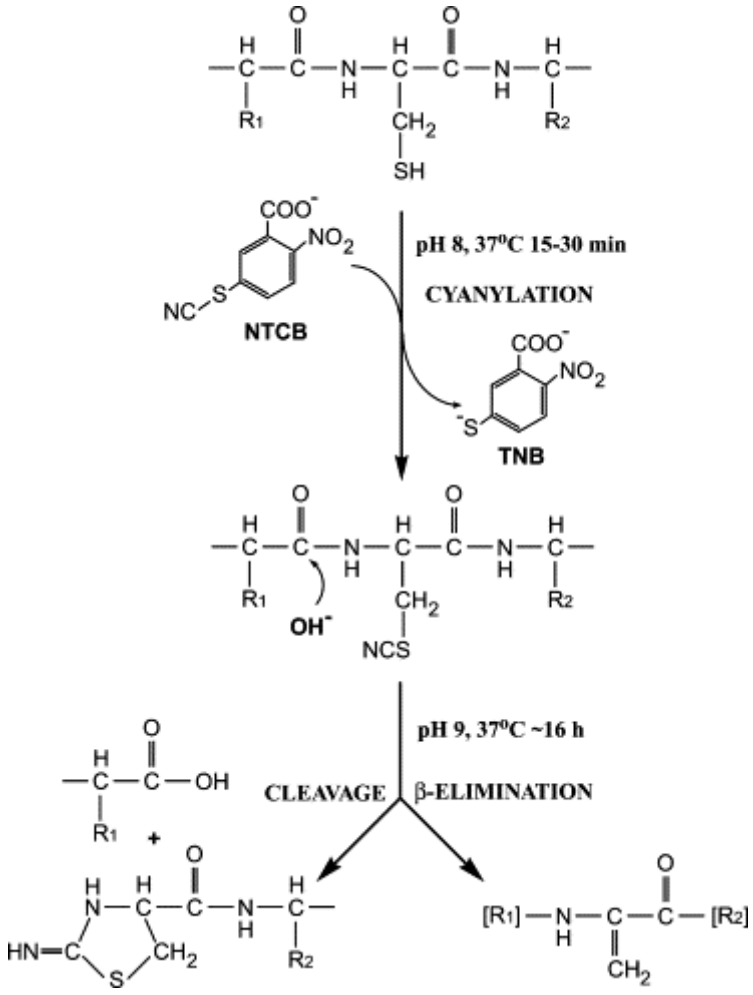

Fig. 3-1. Mechanism of NTCB reaction. The NTCB cleavage is performed in two distinct steps. At the cyanylation (NC-), releasing thionitrobenzoate (TNB), and base-catalyzed cleavage, producing an N-terminal peptide and peptides with cyclized, modified N-terminal Cys. The major competing reaction was previously thought to be β-elimination of the thiocyanato group to produce dehydroalanine as illustrated, but carbamylation of lysine residue was identified as a major side reaction. Cited from Tang and Speicher (2004).

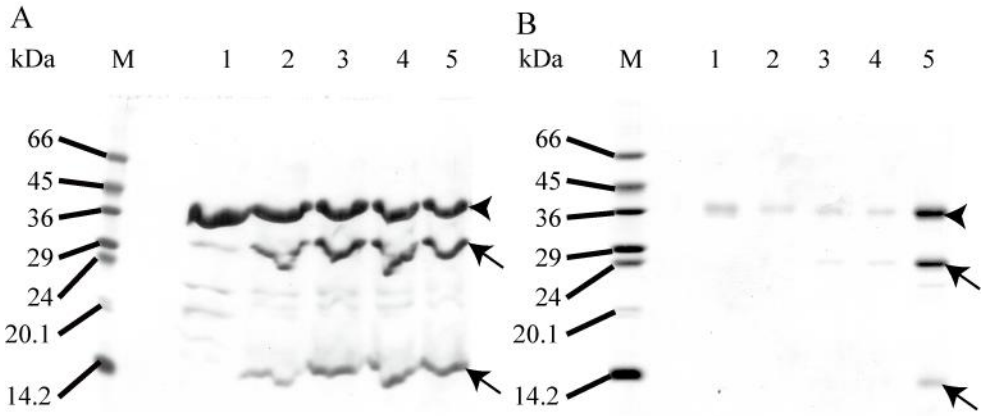

Fig. 3-2. SDS-PAGE patterns of the NTCB cleavage fragments of croaker TM in 1 M glycine containing 6 M guanidine-HCl (pH 9.0). M, marker (SDS-7); 1, uncleaved TM; 2-5, preliminary trial cleavage of TM with NTCB. Reaction time; lane 2, 1 hour; 3, 2 hours; 4, 3 hours; 5, 4 hours. A is before desalting and B is after desalting. 15 % gels. The arrowhead and arrows indicate TM and its fragments, respectively.

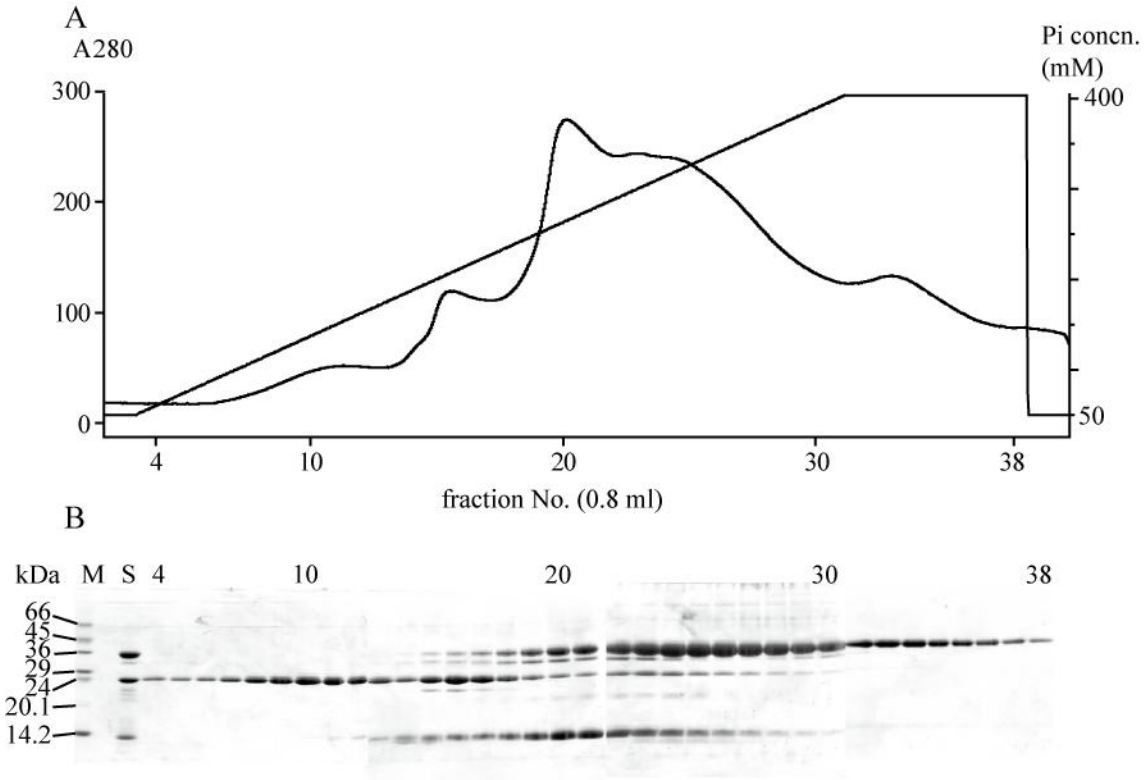

Fig. 3-3. Elution pattern of the NTCB fragments of croaker TM from a Mono Q^{TM} 5/50 GL column (0.5 × 5 cm). (A) The proteins were eluted by the linear gradient from 50 mM to 400 mM potassium phosphate buffer (pH 7.0) in the presence of 4 M urea. (B) SDS-PAGE patterns of the fractions obtained by chromatography in (A). M, marker (SDS-7); S, the loaded sample. Each number on the top of gel corresponds to the fraction number in (A). The fractions 1-3 are the flow through fractions. Fractions (19-22) were further applied to the next chromatography. 15% gels.

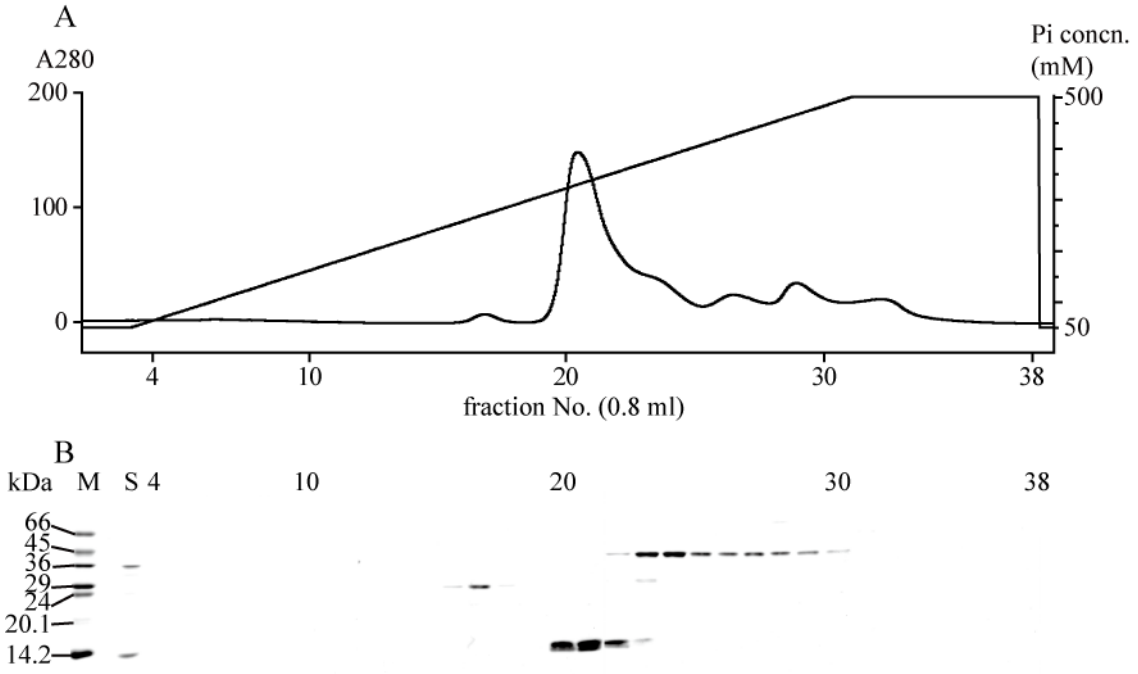

Fig. 3-4. Elution pattern of the NTCB fragments of croaker TM from a Mono Q^{TM} 5/50 GL column (0.5 × 5 cm). (A)The proteins were eluted by the linear gradient from 50 mM to 500 mM potassium phosphate buffer (pH 7.0) in the absence of urea. (B) SDS-PAGE patterns of the fractions obtained by the chromatography in (A). M, marker (SDS-7); S, the loaded sample. Each number corresponds to the fraction number in (A). The fractions 1-3 are the flow through fractions. 15% gels.

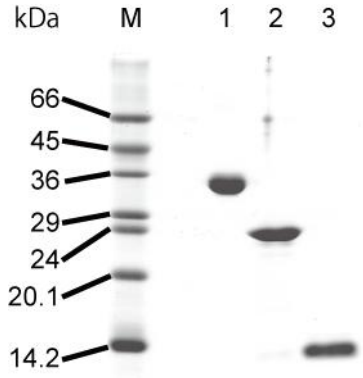

Fig. 3-5. SDS-PAGE patterns of white croaker TM and NTCB fragments. 1, TM without cleavage; 2, the TM fragment including Met1-Lys189; 3, the TM fragment including Cys190-Ile284. 15 % gel.

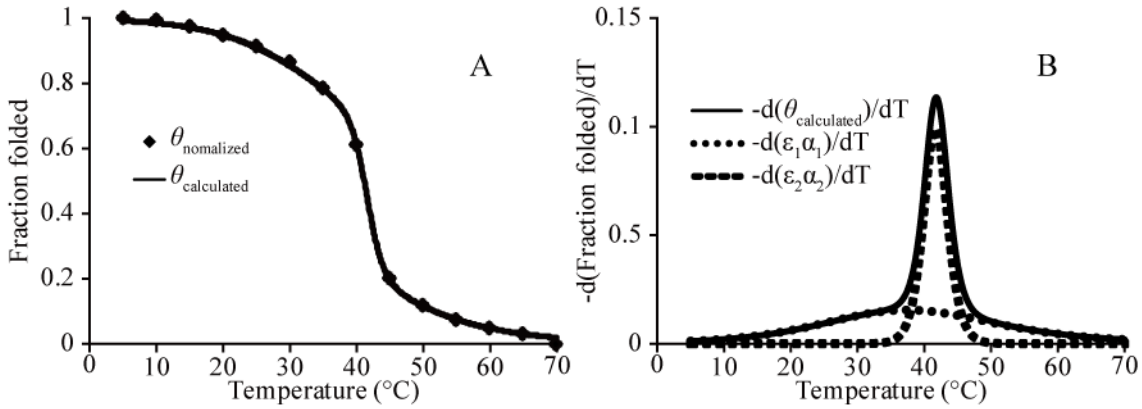

Fig. 3-6. CD analysis of white croaker TM. (A) The temperature dependence of unfolding of TM. $[\theta]_{normalized}$ was obtained by normalizing CD data and $[\theta]_{calculated}$ came from the equation. (B) Derivative of $[\theta]$. Two independent helix-coil transitions had clearly different contribution.

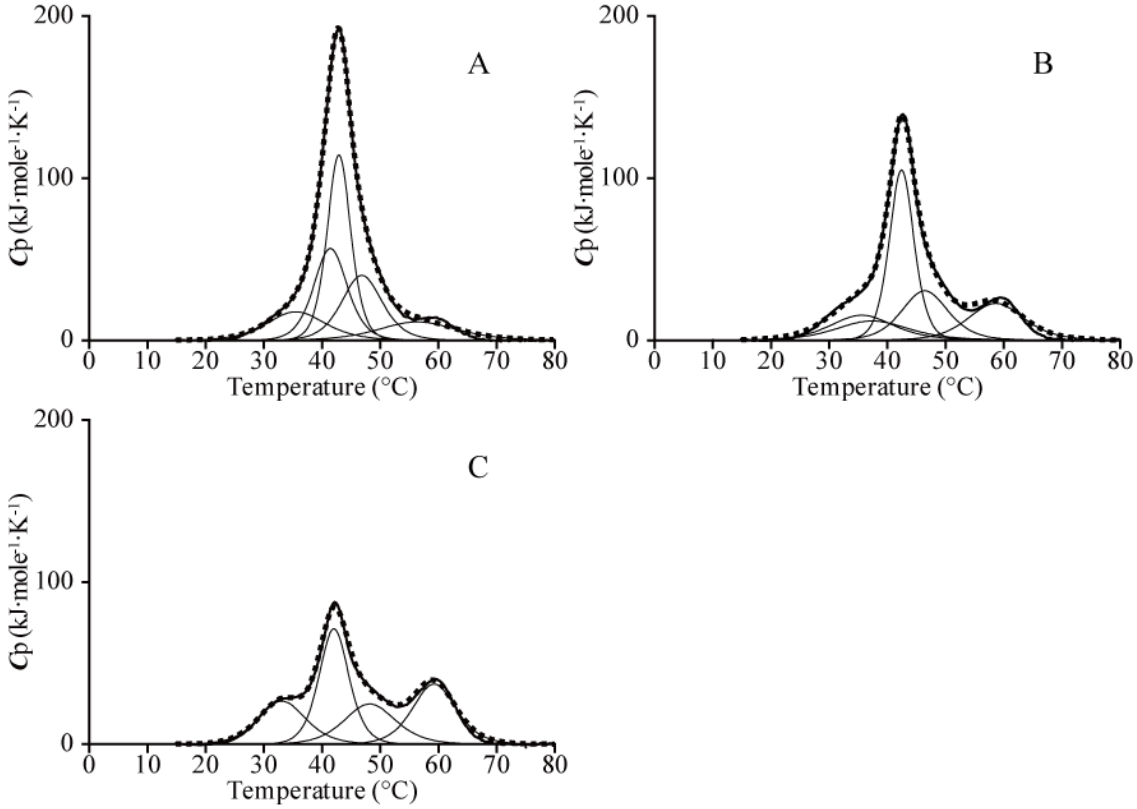

Fig. 3-7. DSC scans of white croaker TM. The observed DSC pattern and the sum of subsequent deconvolution analysis are shown with solid and dotted lines and the subsequent analysis is shown with thin line. The DSC data were subtracted with a progress baseline, and analyzed as a dimer. A, 1st scan; B, 2nd scan; C, 3rd scan. In A, B and C, the number of peaks were 5, 4 and 4, respectively. The scanning was performed in 10 mM sodium phosphate (pH 7.0) containing 0.1 M KCl, 0.1 mM DTT, and 0.001% NaN_3. The raising speed of temperature was 1°C/min.

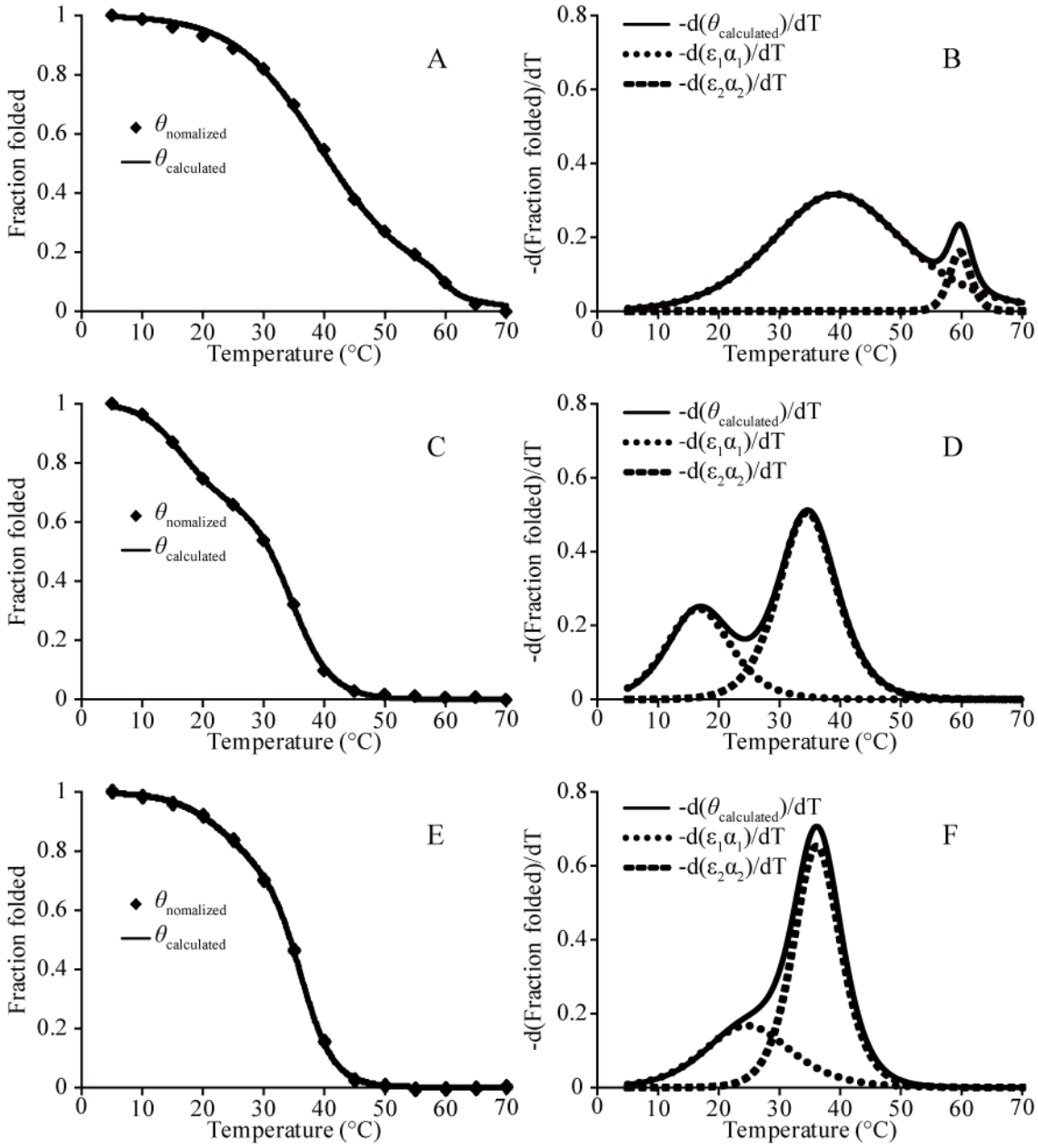

Fig. 3-8. CD analysis on the temperature dependent unfolding of the TM treated with 1 M glycine containing 6 M guanidine-HCl (pH 9.0) for 4 hours (A, B) and its fragments including Met1-Lys189 (C, D) and Cys190-Ile284 (E, F). (A), (C), (E). $[\theta]_{normalized}$ was obtained by normalizing CD data and $[\theta]_{calculated}$ came from the analysis. (B), (D), (E) Two independent helix-coil transitions.

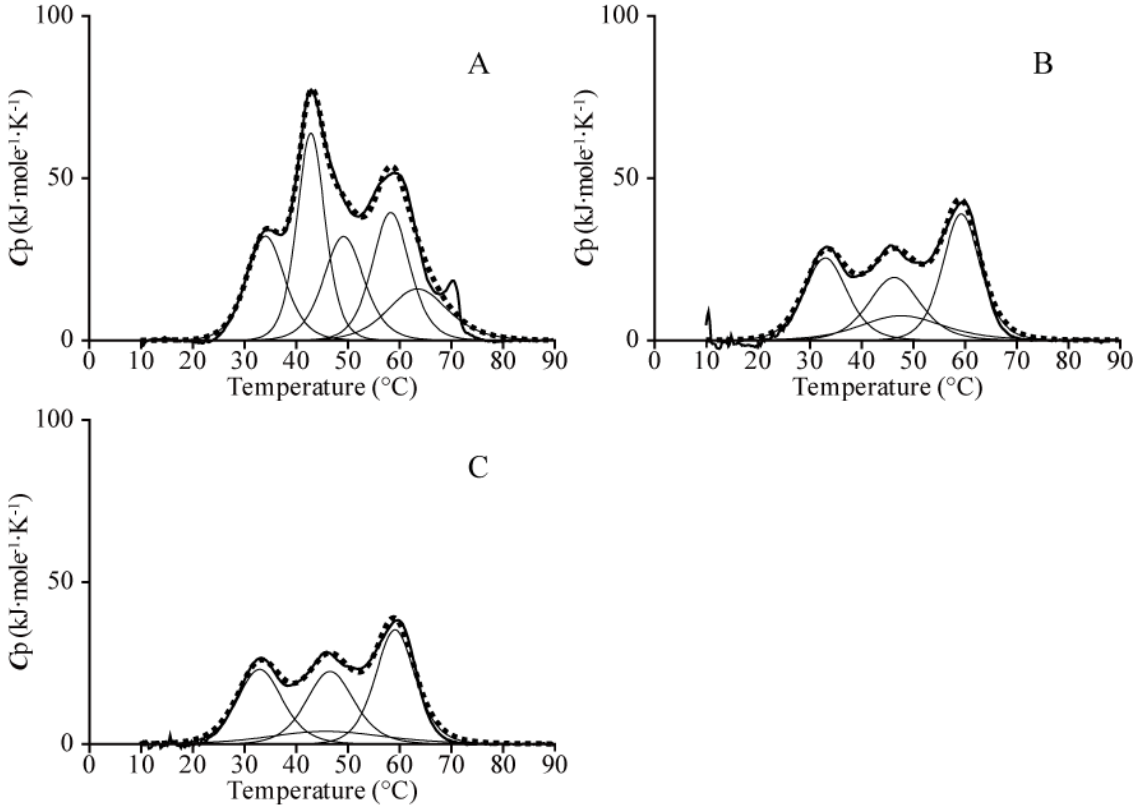

Fig. 3-9. DSC scans of white croaker TM treated by guanidine-HCl. The observed DSC pattern and the sum of subsequent deconvolution analysis are shown with solid and dotted lines and the subsequent analysis is shown with thin line. The DSC data were subtracted with a progress baseline, and analyzed as a dimer. A, 1st scan; B, 2nd scan; C, 3rd scan. In A, B and C, the numbers of peaks were 5, 4 and 4, respectively. The scanning was performed in 10 mM sodium phosphate (pH 7.0) containing 0.1 M KCl, 0.1 mM DTT, and 0.001% NaN_3. The raising speed of temperature was 1°C/min.

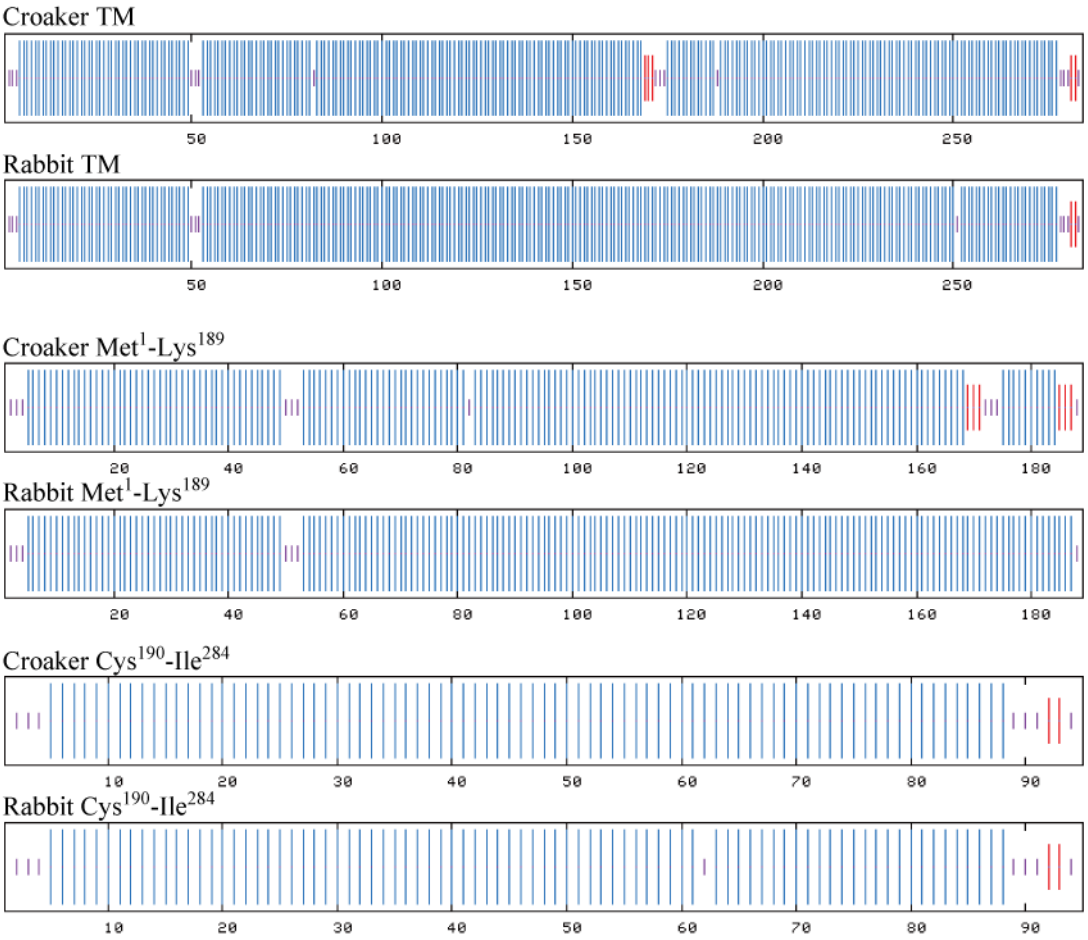

Fig. 3-10. Secondary structure prediction of white croaker and rabbit TMs by GOR IV (Garnier et al., 1996). Location of secondary structures. α-Helix is indicated by long vertical line in blue, whereas random coil and extended strand are short line in purple and middle line in red.

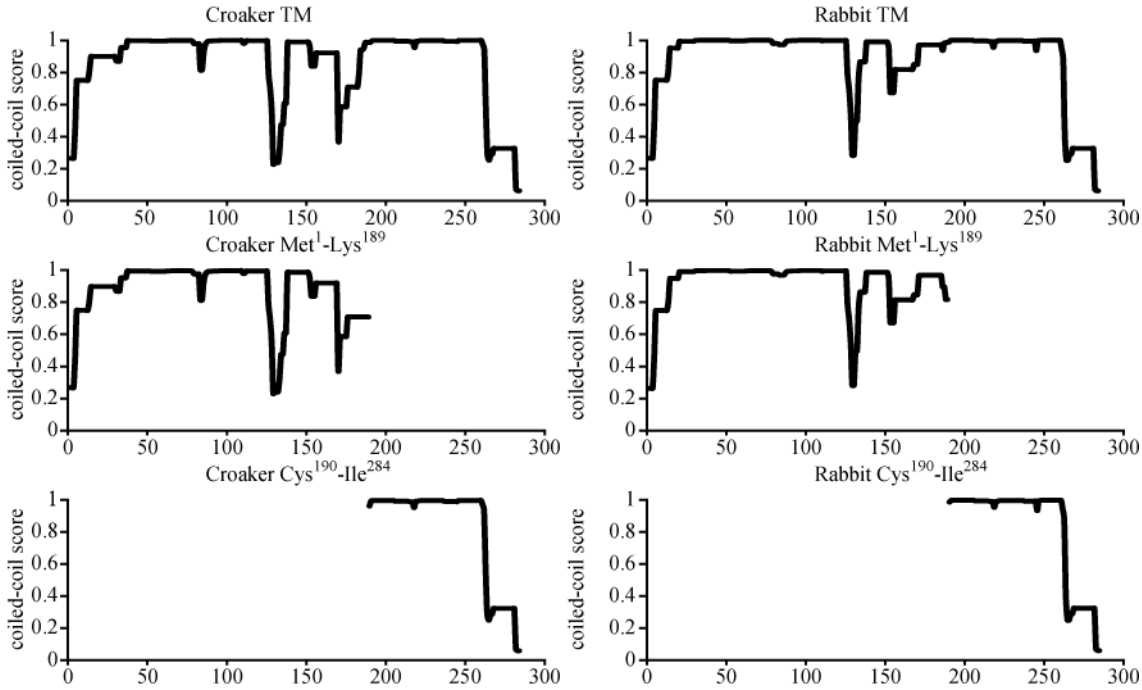

Fig. 3-11. Coiled-coil score was calculated by coiled-coil prediction software COILS http://www.ch.embnet.org/.

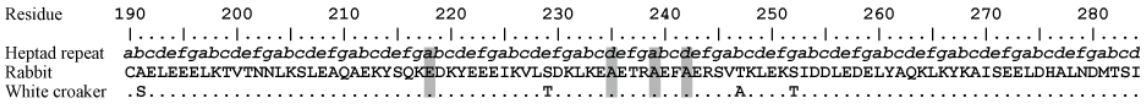

Fig. 4-1. The amino acid sequences of the rabbit and white croaker TM C-terminal fragments [Cys190(*a*)-Ile284(*d*)]. Acidic core [Glu218(*a*)] and alanine cluster [Ala235(*d*)-Ala239(*a*)-Ala242(*d*)] are shown in gray.

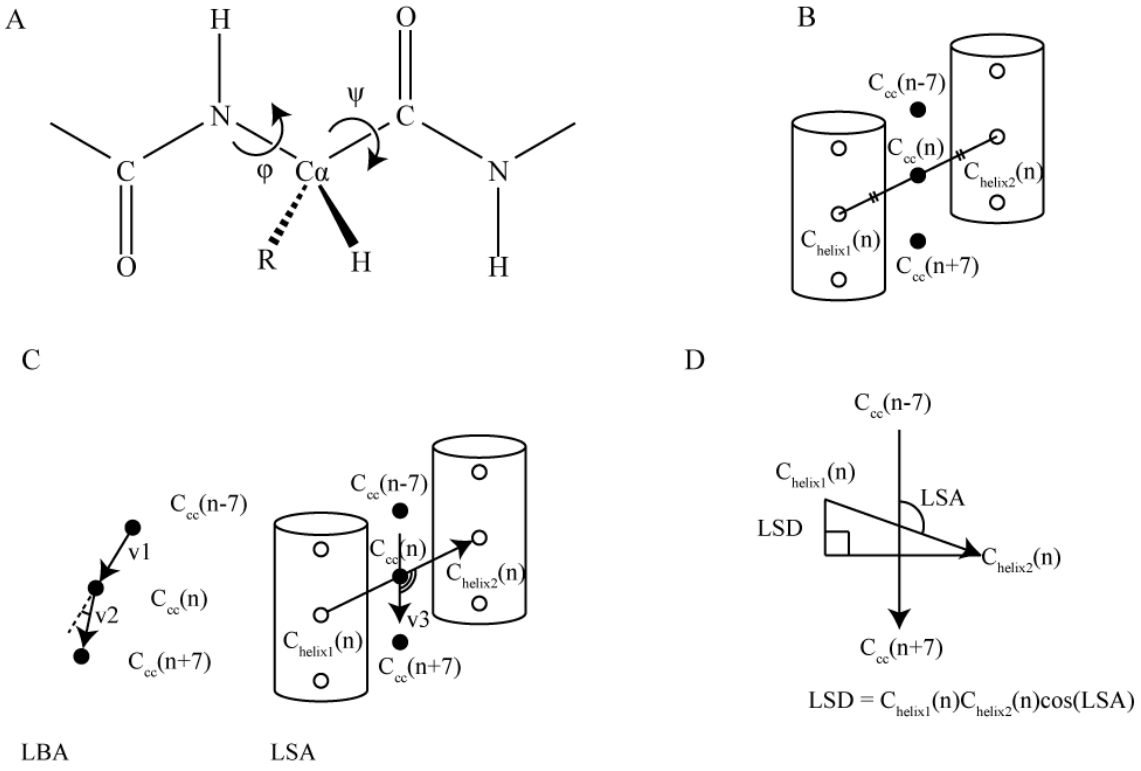

Fig. 4-2. (A) The dihedral angles of back bone, φ and ψ. (B) The centers of α-helices [$C_{helix1}(n)$ and $C_{helix2}(n)$] and coiled-coil [$C_{cc}(n)$]. (C) Local bending angle (LBA) and local staggering angle (LTA). (D) Local staggering distance (LSD).

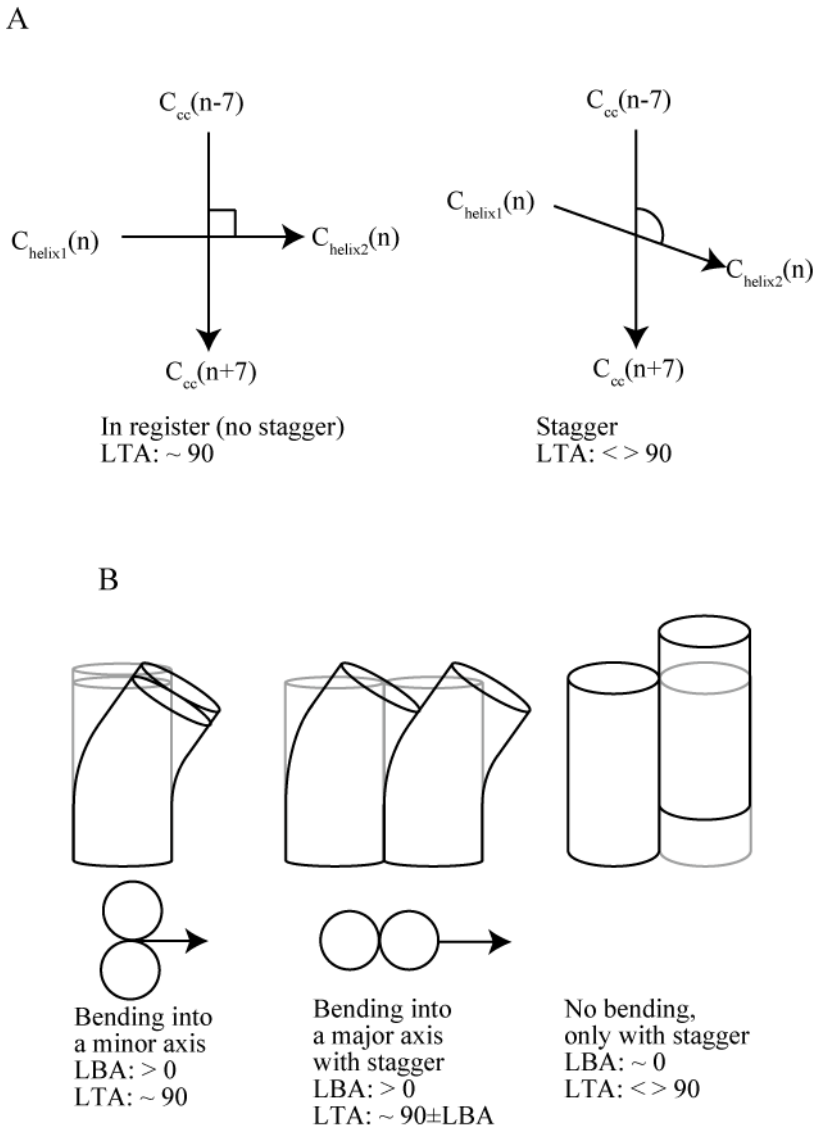

Fig. 4-3. (A) In register and stagger. (B) The bending pattern.

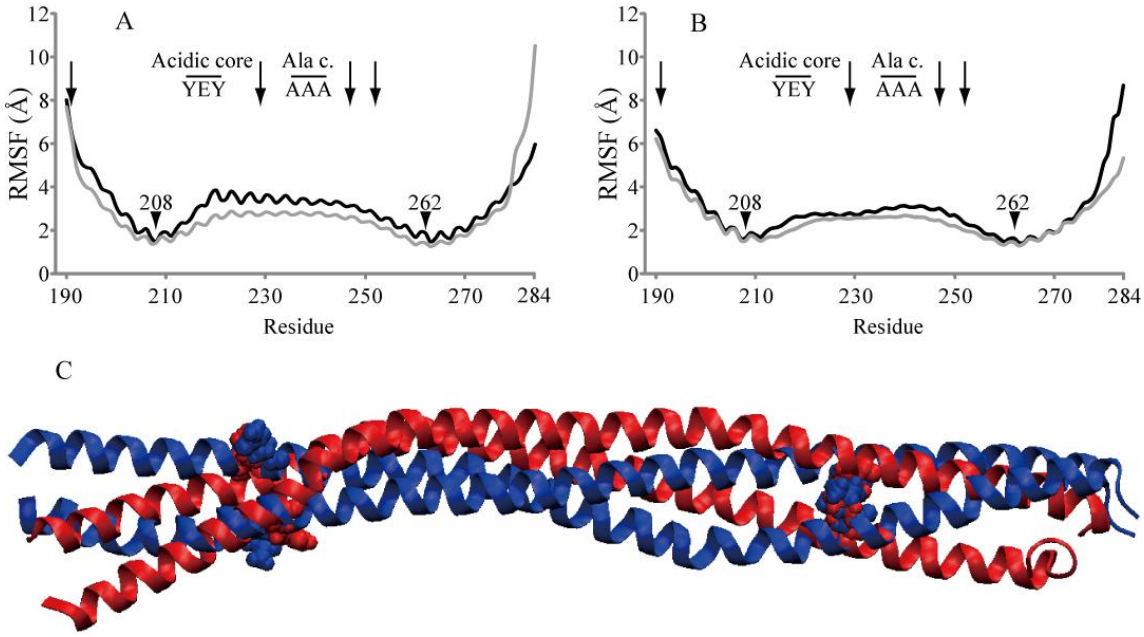

Fig. 4-4. Root mean square fluctuation (RMSF) and root mean square fitting. Rabbit and white croaker TM fragments are shown in black and gray lines, respectively. (A) RMSF for A chain. (B) RMSF for B chain. (C) After 20 ns of the simulation of rabbit TM fragment (red), RMS fitting was performed by aligning to the energy minimized structure (blue). TM fragment is shown as NewCartoon model and Gln210(*g*) and Leu260(*a*) are shown as Van der Waals model. Ala c. stands for alanine cluster [Ala235(*d*)-Ala239(*a*)-Ala242(*d*)]. Acidic core represents glutamic acid at the core and neighboring core Tyr [Tyr214(*d*)-Glu218(*a*)-Tyr221(*d*), and Gln263(*d*)-Tyr267(*a*)]. Arrows indicate the amino acid substitutions between the rabbit and white croaker TM C-terminal fragments; Ala191(*b*)Ser, Ser229(*e*)Thr, Thr247(*b*)Ala, and Ser252(*g*)Thr. Glu208(*e*) and Ala262(*c*) were indicated by arrowheads in A and B.

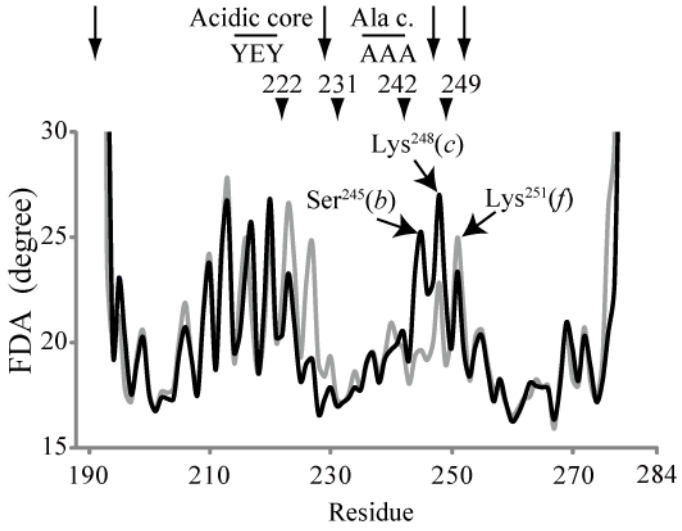

Fig. 4-5. FDA for the rabbit (black line) and white croaker (gray line) TM fragments [Cys190(*a*)-Ile284(*d*)]. Refer to the legend of Fig. 4-4 for acidic core, Ala c. and arrows. The Glu222(*e*), Lys231(*g*), Phe242(*c*), and Leu249(*d*) were indicated by arrowheads.

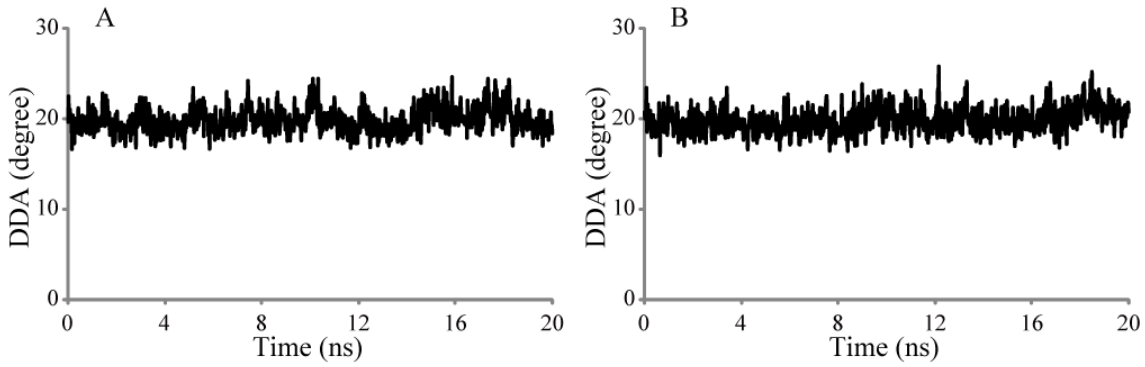

Fig. 4-6. Deviation of dihedral angle (DDA) for rabbit (A) and white croaker (B) TM fragments [Cys190(*a*)-Ile284(*d*)]. To calculate DDA, the data between the Cys190(*a*) and Leu193(*d*) and between His276(*c*) and Ile284(*d*) were omitted.

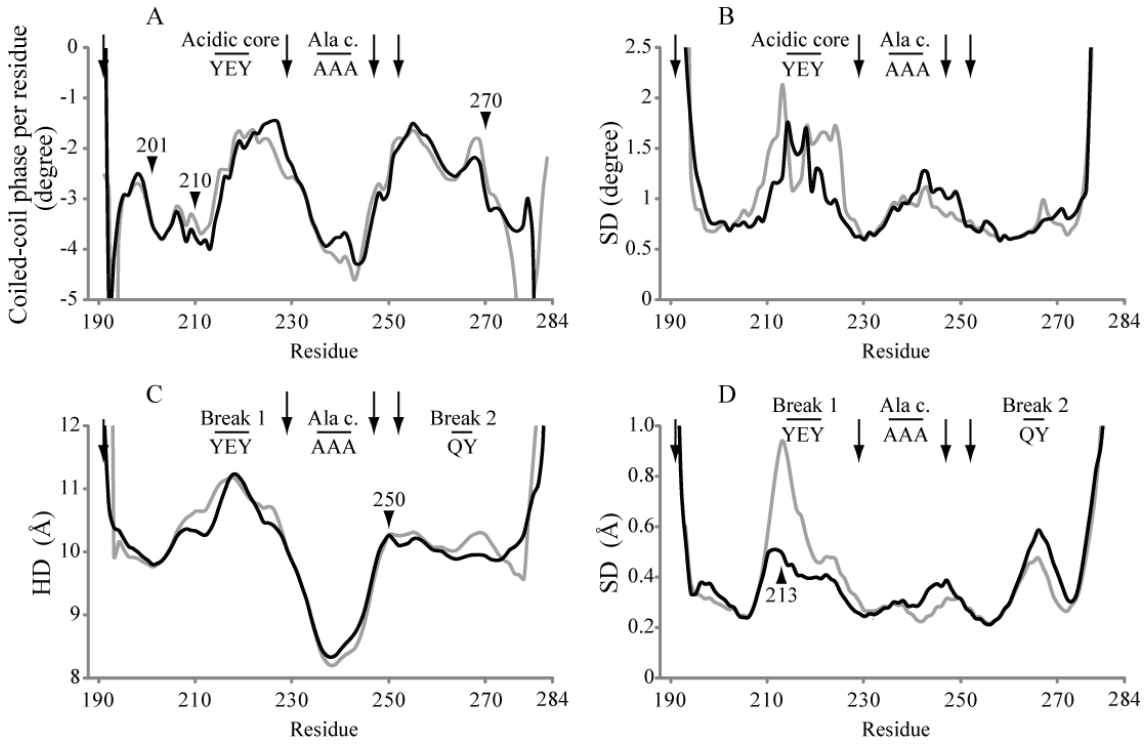

Fig. 4-7. Increment of coiled-coil phase per residue and its SD (A, B). Interhelical distance (HD) and its SD (C, D). Black and gray lines indicate rabbit and white croaker TM fragments, respectively. Refer to the legend of Fig. 4-4 for acidic core, Ala c. and arrows. Thr201(*e*), Gln210(*g*), and Ile270(*d*) were indicated by arrowheads in A. Gle250(*e*) and Lys213(*c*) were indicated by arrowheads in C and D respectively.

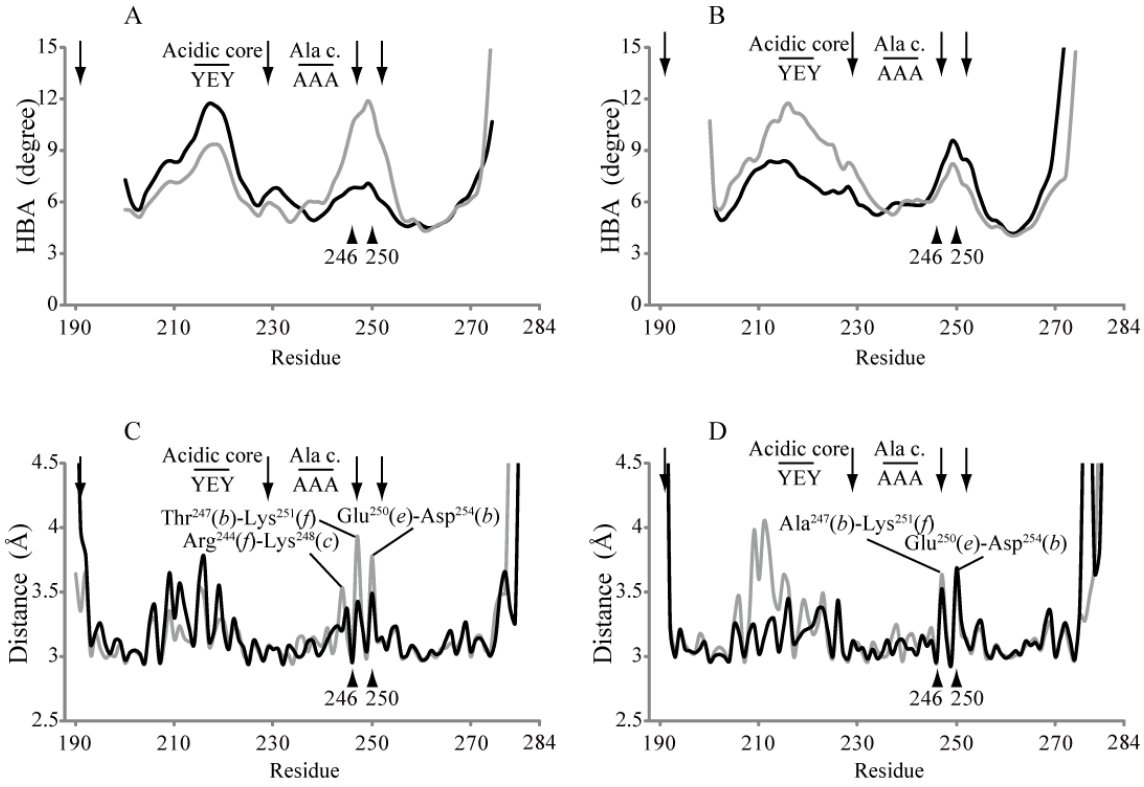

Fig. 4-8. α-Helix bending angle (HBA) for rabbit (A) and white croaker (B) TM fragment. The α-helical hydrogen bond distance of "n"th residue, which was measured as the distance between carbonyl oxygen of "n"th residue and nitrogen of "n+4"th residue for rabbit (C) and white croaker (D) TM fragment. Refer to the legend of Fig. 4-4 for acidic core, Ala c. and arrows. Val246(*a*) and Glu250(*e*) were indicated by arrowheads.

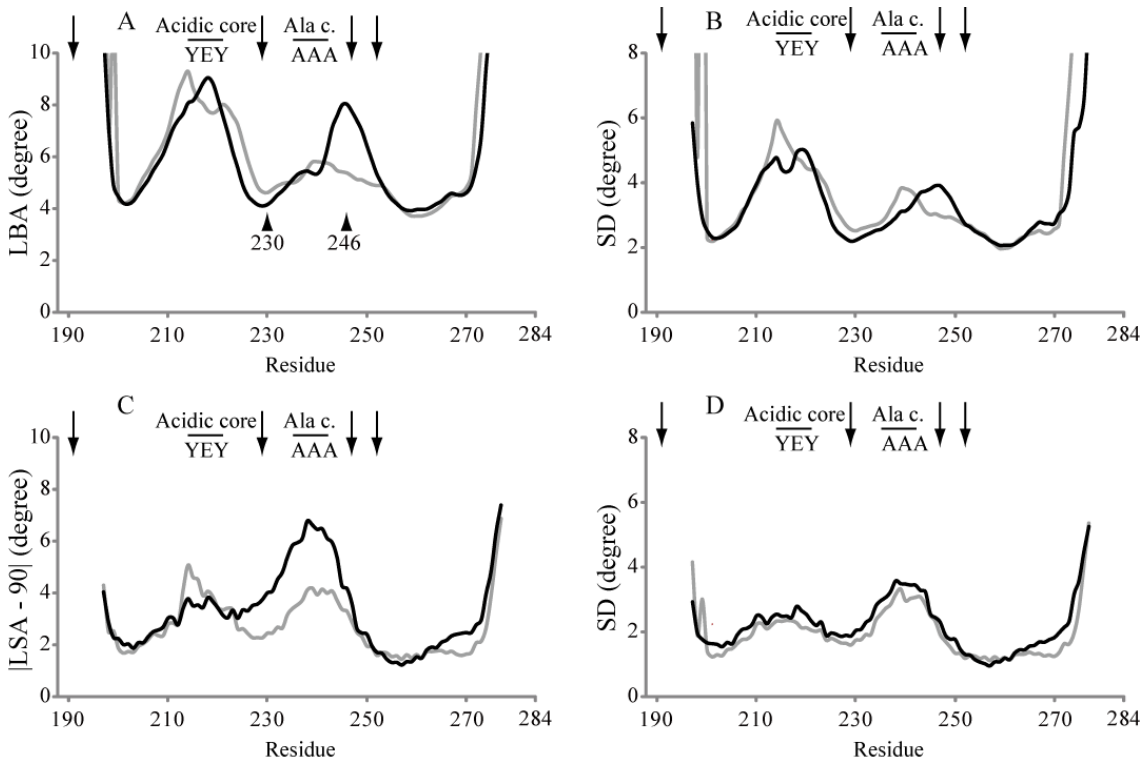

Fig. 4-9. Local bending angle (LBA) and its SD (A, B). |90° - local staggering angle(LSA)| and its SD (C, D). Black and gray lines indicate rabbit and white croaker TM fragments, respectively. Refer to the legend of Fig. 4-4 for acidic core, Ala c. and arrows. The Asp230(*f*) and Val246(*e*) were indicated by arrowheads in A.

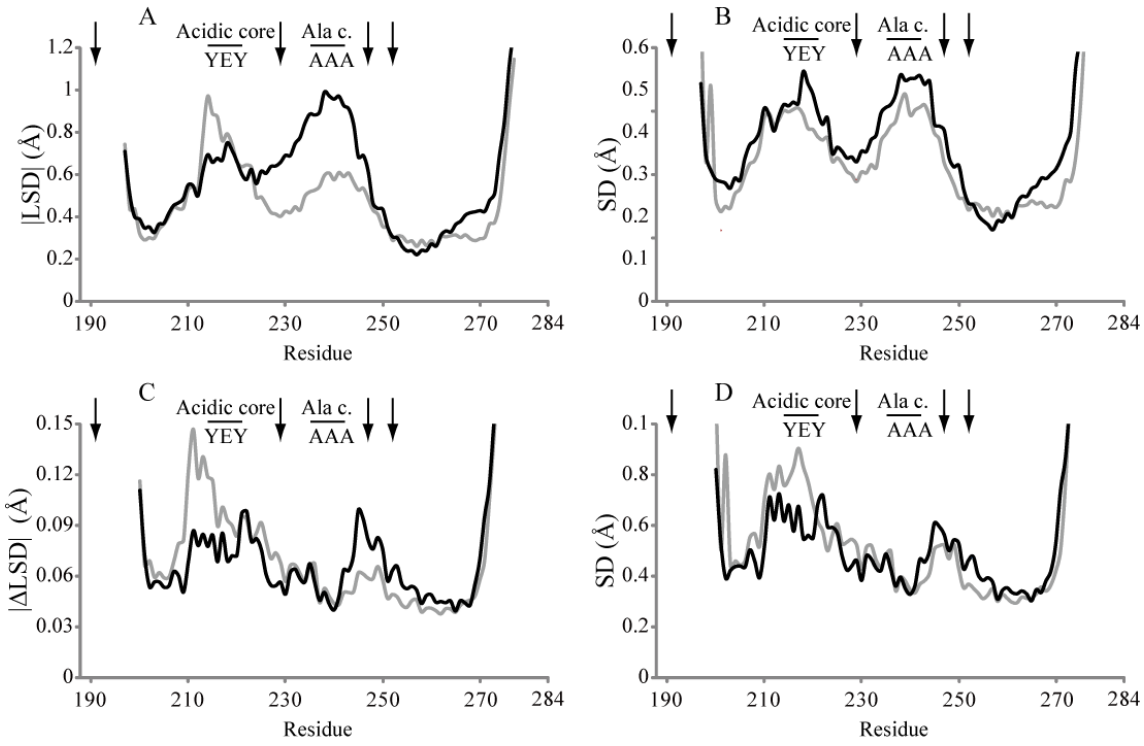

Fig. 4-10. Local staggering distance (LSD) and its SD (A, B). Change of the LSD and its SD (C, D). Black and gray lines indicate rabbit and white croaker TM fragments, respectively. Refer to the legend of Fig. 4-4 for acidic core, Ala c. and arrows.

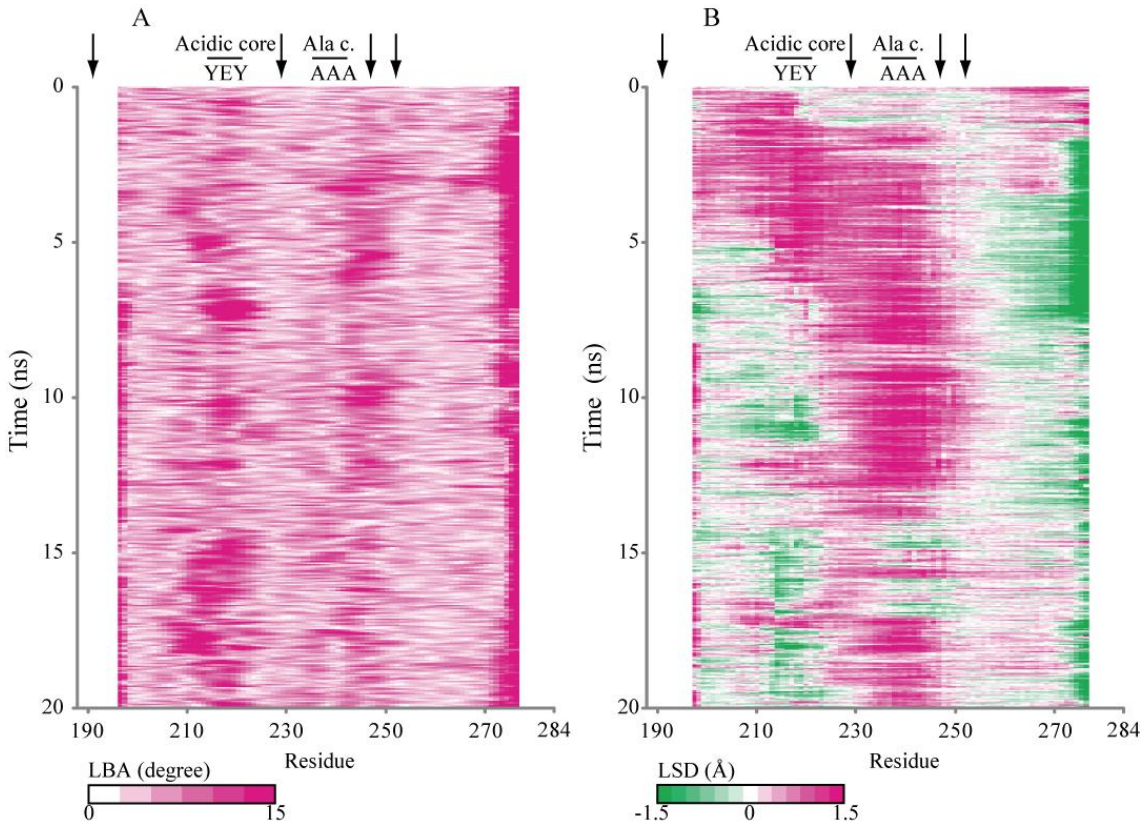

Fig. 4-11. The time-dependency of LBA (A) and LSD (B) of rabbit TM fragment. In A, red region indicates the curvature of coiled-coil. In B, red and green regions indicate the stagger, but these directions are opposite. Refer to the legend of Fig. 4-4 for acidic core, Ala c. and arrows.

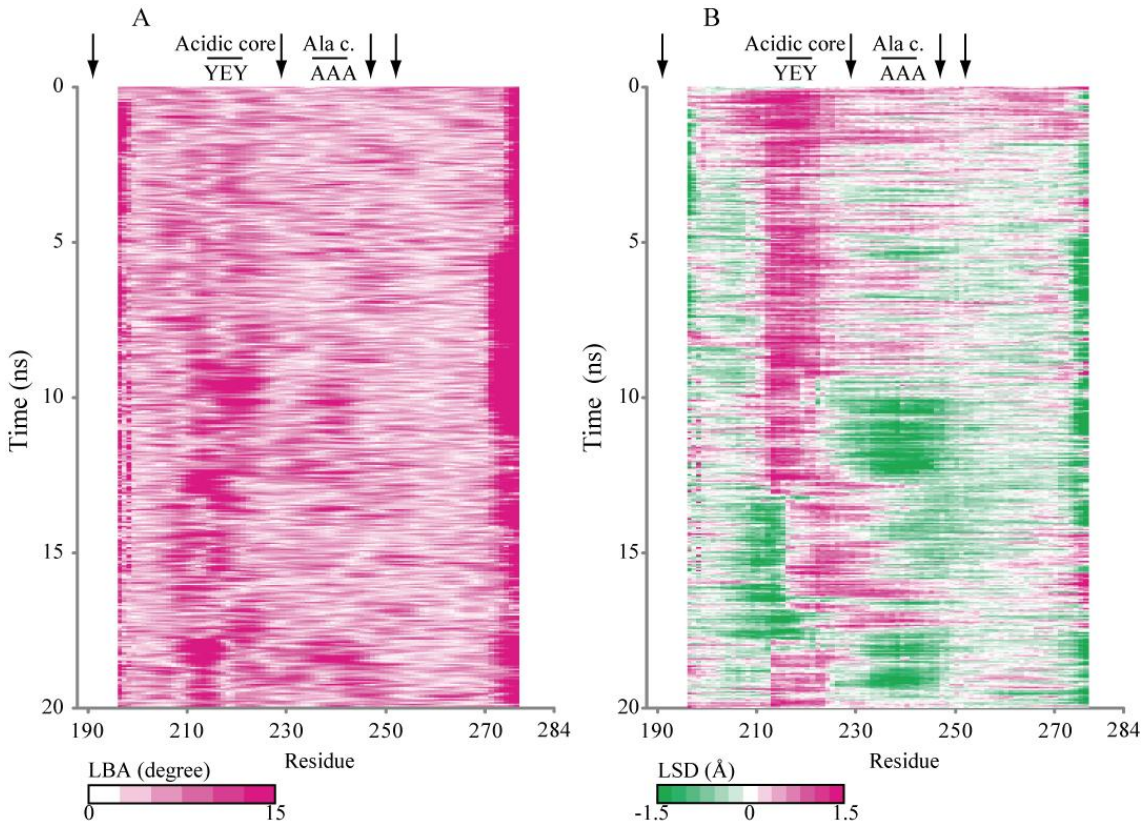

Fig. 4-12. The time-dependency of LBA (A) and LSD (B) of white croaker TM fragment. In A, red region indicates the curvature of coiled-coil. In B, red and green regions indicate the stagger, but these directions are opposite. Refer to the legend of Fig. 4-4 for acidic core, Ala c. and arrows.